Photocopy and Use Authorization

In presenting this thesis in partial fulfillment of the requirements for an advanced degree at Idaho State University, I agree that the library shall make it freely available for inspection. I further state that permission for extensive copying of my thesis for scholarly purposes may be granted by the Dean of the Graduate School, Dean of my academic division, or by the University Librarian. It is understood that any copying or publication of this thesis for financial gain shall not be allowed without my written permission.

Signature:

Date:

Fine-scale Spatial Structure of Saturated Hydraulic Conductivity Controls Intermittent Flow Patterns in Headwater Stream in the Northern Rocky Mountains, Idaho, USA

By

Michael J. Ferraro

A thesis

Submitted in partial fulfillment

of the requirements for the degree of

Master of Science in the Department of Geosciences

Idaho State University

Fall 2021

To the Graduate Faculty: The members of the committee appointed to examine the thesis of Michael J. Ferraro find it satisfactory and recommend that it be accepted.

Dr. Sarah E. Godsey

Major Advisor

Dr. Paul K. Link

Committee Member

Dr. Colden V. Baxter

Graduate Faculty Representative

Dedication

To my dad, may you rest in peace old man.

Acknowledgments

A watershed is "that area of land, a bounded hydrologic system, within which all living things are inextricably linked by their common water course and where, as humans settled, simple logic demanded that they become part of a community."

-John Wesley Powell-

I am indebted to Dr. Godsey for her encouragement and support while navigating the frightening process of obtaining a graduate degree during a global pandemic. I also would like to acknowledge my close friend Josh Oldroyd for his beautiful welds and brilliant backyard engineering skills, and thank you, Athena Perkins, for graciously allowing me to hang out with Josh so much all these years. Special appreciation to Douglass McGregor, Kade Lewis, and Ryan Braum, who provided supple spines, soft hands, and great company during individual portions of my field campaign. I am indebted to my department and the greater ISU community; thank you. Without your encouragement and compassionate support, I likely would not have survived the madness of 2020-2021, let alone obtained a graduate degree. Most importantly, I want to express thanks to my daughter Aislinn for being such a great kid and putting up with me during this process; I'm wicked proud of you dude.

Table of Contents

List of Figures

List of Tables

Fine-scale Spatial Structure of Saturated Hydraulic Conductivity Controls Intermittent Flow Patterns in Headwater Stream in the Northern Rocky Mountains, Idaho, USA

Thesis Abstract—Idaho State University (2021)

Over 50% of the global stream network currently dries each year and drying is expected to increase. Climatic, land use, and geologic controls on drying vary spatiotemporally, but geologic controls remain poorly understood because practical constraints limit subsurface data collection. I measured subsurface saturated hydraulic conductivity (Ksat), a key geological control on stream drying, throughout the ~16-km^2 Gibson Jack Creek, Idaho. I characterized the spatial structure of Ksat along both Euclidean and hydrologic distances along the stream network based on 194 measurements following an unbalanced nested sampling design at 50-70cm below the channel surface. Ksat varied by ~1000x and was autocorrelated over single-meter distances; it was significantly higher in perennial than non-perennial reaches (p-value = $3e^{-6}$) and varied significantly with underlying lithologic or soil textural class (p-value = 0.001, 0.03), but not other landscape metrics. Thus, accurate predictions of fine-scale drying patterns may require detailed Ksat measurements.

Keywords: Saturated hydraulic conductivity, subsurface controls, flow permanence, regulation, Clean Water Rule, intermittency, stream drying, intermittent streams, headwater stream networks, hydrology, Idaho

Chapter 1: The Current State of Intermittent Stream Science: Water Quality Protections, Drivers of Drying Patterns, Hydraulic Conductivity and Spatial Analysis along Stream Corridors

Overview

This thesis is comprised of three chapters. The first chapter provides a critical literature review of key aspects of intermittent stream science. Technical terms are defined in depth to give the reader the necessary background knowledge to better understand the motivation of this work. My novel contributions are then presented in Chapter 2; this chapter has been written for peer-reviewed publication. Lastly, Chapter 3 contains recommendations for future work. The appendices of this thesis include advice to future graduate students, schematics for the well-drive equipment built for this project, and data collection and analysis summaries as well as compiled site details.

This first chapter is grouped into four main sections: first, I present an overview of intermittent stream science and the motivation for studying these dynamic systems, including a review of the U.S. Clean Water Act and revisions to the Clean Water Rule that are critical in defining Waters of the United States. Alongside this overview, I also review the hypothesized drivers of drying, including current state-of-the-art modeling and potential geological controls on drying patterns. Then I dive more deeply into one of those drivers, reviewing current knowledge of saturated hydraulic conductivity (Ksat) and how it is measured. Ksat is the focus of much of my research in intermittent stream corridors, and I also outline what is currently known about how it varies spatially. Then I review spatial analysis techniques, including correlation, semivariograms, kriging, and adaptations required to apply these techniques in stream corridors. Finally, I present the natural and human history of the Gibson Jack watershed, where I completed my research, to provide as much context as possible for how to interpret my findings.

1. Overview of Intermittent Stream Science and Policy

1.1 Definitions and Ecosystem Services of Intermittent Streams

A photograph of a stream in the Rocky Mountain region often includes a clear babbling brook cascading over moss-covered boulders in a lush riparian corridor full of willows, aspen, and pine. As beautiful as this image can be, it fails to capture the fact that the majority of headwater streams, regardless of geography, seasonally cease to babble because they are non-perennial (Nadeau and Rains, 2007; Datry et al., 2014; Busch et al., 2020; Messager et al., 2021). Also known as seasonal, temporary, episodic, and ephemeral, these non-perennial stream systems are defined by having flow phases that include both wet and dry periods. If flow persists between at least some storms, these systems are referred to as “intermittent” streams (Leigh et al., 2016). More specifically, *ephemeral* streams contain water only during or after a precipitation event or snowmelt. In contrast, *intermittent* streams have surface water flowing during specified times during the year or discharge that persists beyond the direct responses to precipitation events. *Perennial* streams have surface water flowing throughout the year (Department of Defense, 2020; Fesenmyer et al., 2021).

Intermittency is common: over 50% of the global stream network, regardless of climate or biome, experiences some degree of annual stream drying (Tooth, 2000; Nadeau and Rains, 2007; Costigan et al., 2016; Busch et al., 2020; Messager et al., 2021). Drier conditions and shifts in intermittency are already occurring (Zipper et al., 2021) and predicted changes in climate and increased human water use are expected to cause increased stream intermittency, both spatially and temporally (Steward et al., 2012; Jaeger et al., 2014; Eng et al., 2019).
Early research summarized in Leigh et al. (2016) focused on the ecological effects of stream drying, and more recent work includes perspectives from geomorphology (Lapides et al., 2021),

hydrology (Botter and Durighetto, 2020; Ward et al., 2020), geochemistry (Floriancic et al., 2019; MacNeille et al., 2020), and statistics (Ward et al., 2018; Jaeger et al., 2019) to better model, protect, and manage these water resources (Department of Defense, 2020; Fesenmyer et al., 2021). Because intermittent streams are common and predicted to expand, a growing body of interdisciplinary research on their dynamics and impacts is emerging.

Intermittent streams provide many of the same ecological services as their perennial counterparts (Steward et al., 2012; Datry et al., 2016; Leigh et al., 2016). These services include increased biodiversity and habitat in the adjacent stream corridor, carbon storage, high rates of nutrient cycling, and groundwater recharge areas (Steward et al., 2012; Datry et al., 2016; Dohman et al., 2021). Increased stream drying can directly affect sediment load, and lead to declines in water quality, increased stream temperatures, and decreased dissolved oxygen (Steward et al., 2012; Stewardson et al., 2016; Obedzinski et al., 2018; Gendaszek et al., 2020). Furthermore, many organisms have evolved in response to annual fluctuations in flow permanence and depend on perennial reaches of headwater streams for spawning/hatching ground, making the understanding of patterns in stream drying important to the management streams for ecological purposes (Vaux, 1968; Baxter and Hauer, 2000; Jaeger et al., 2014). Indeed survival rates of juvenile salmonids are negatively correlated with days of disconnection or drought conditions in headwater portions of stream networks (Fleckenstein et al., 2006; Steward et al., 2012; Obedzinski et al., 2018).

1.2 Regulation of Water Quality: A Brief History of the U.S. Clean Water Act and its Relationship with Intermittent Streams

Because non-perennial flow status affects ecological services, including water quality and the health and habitat of aquatic organisms, their protection under different regulatory statutes, like the U.S. Clean Water Act, can be scientifically justified. Still, such regulation has been controversial because these systems are often undervalued (Steward et al., 2012). Here I summarize the evolution of regulatory guidelines for water pollution in the United States with particular attention to non-perennial systems. The birth of regulatory processes for water quality standards in the United States was in 1899 with the Congressional passage of the Rivers and Harbors Act (RHA); this legislation first used the term "navigable waters of the United States." Federal enforcement of water quality protection standards passed under the RHA fell solely upon the Department of the Army, also known as the U.S. Army Corps of Engineers or USACE (Department of Defense, 2020). Later, in 1948, the Federal Water Pollution Control Act (FWPC) was enacted by Congress to address water contamination and interstate pollution. This act was amended three times in 1956, 1961, and 1965 to better develop water quality standards for individual states, promote pollution reduction programs, and permit the federal regulation of water quality standards (Department of Defense, 2020).

In 1972, the FWPC was significantly amended and restructured to become the now well-known US Clean Water Act (CWA). The 1972 CWA established the basic structure of our current water regulation. It gave the newly founded US Environmental Protection Agency (USEPA) authority to regulate programs designed to "restore and maintain the chemical, physical, and biological integrity of the Nation's waters" (Department of Defense, 2020). The CWA also contained a statute requiring individual states to establish their water quality standards and report to the USEPA every two years. It was also at this time that Congress outlined the framework for the USEPA to grant financial and technical assistance to individual states or municipalities for the development of:

> "…any project which will demonstrate a new or improved method of preventing, reducing, and eliminating the discharge into any waters of pollutants from sewers which stormwater or stormwater and pollutants […or for state agencies to] demonstrate in river basins or portions thereof, advanced treatment and environmental enhancement techniques to control pollution from all sources […and for] demonstration projects for prevention of pollution of any waters by industry including, but not limited to, the prevention, reduction, and elimination of the discharge of pollutants" (Department of Defense, 2020).

With the passage of the CWA, Congress declared two clean water goals. First, the CWA sought to eliminate the discharge of non-point source pollutants into U.S. waterways by 1985 (United States Congress, 2018; Department of Defense, 2020). Second, the CWA aimed to provide water quality protection status to ensure the successful propagation of fish, shellfish, wildlife, and recreational purposes, both in and out of the water (United States Congress, 2018; Department of Defense, 2020).

Since 1972, two federal agencies, the USACE and the USEPA have administered regulatory programs regarding water quality. Curiously, between 1974 and 1986, each agency had its own definition of WOTUS that persisted for over a decade before an initial attempt at reconciliation. The USEPA definition arose from the first National Pollutant Discharge Elimination System (NPDES), issued in 1973, where the phrase "navigable waters" was first defined for regulatory purposes. The EPA then determined navigable waters to include "all navigable waters, all interstate waters, intrastate waters utilized by interstate travelers for recreational purposes, intrastate waters which supply interstate commerce of fish or shellfish, and intrastate waters that are used for interstate commerce" (Department of Defense, 2020). Shortly after that, in 1974, the USACE defined waters of the United States as being "subject to the ebb and flow of the tide and/or are presently, or may be in the future, susceptible for use for purposes of interstate or foreign commerce," and then further broadened to include "periodically inundated" coastal and freshwater wetlands that lie adjacent to traditionally defined navigable waters. In 1977, the USACE definition was revised to include traditionally defined navigable, interstate waters, adjacent wetlands or tributaries, and all other waters the "degradation or destruction of which could affect interstate commerce" (Department of Defense, 2020).

In 1985, the Supreme Court was called upon to interpret the definition of "waters of the United States" in the United States v. Riverside Bayview Homes. In these proceedings, the court deferred to the USACE jurisdiction over wetlands adjacent to traditional navigable waters because they are "inseparably bound up" and have "significant effects on water quality and the aquatic system." At this time, water pollution was defined as being a "man-made or man-induced alteration of the chemical, physical, biological, and radiological integrity of water" (Department of Defense, 2020). The Supreme Court acknowledged the difficulties of delineating wetlands, but decided that the close ecological relationship between a regulated water body and a wetland justified federal regulation (Department of Defense, 2020). In 1986, the USACE reclassified their regulations to parallel the USEPA's with two key additions: the preamble known as the Migratory Bird Rule (MBR) and a provision for waters used in interstate agricultural commerce. The MBR claimed jurisdiction over any waters that have the potential to serve as migratory bird habitat, which was a common designating factor for jurisdictional WOTUS under the CWA, resulting in stakeholder agencies recognizing nearly all delineated wetlands as jurisdictional until 2001 (Leibowitz et al., 2008). The MBR stated that any water body that is, or may be, used as habitat for endangered species and/or birds that migrate over state lines would also fall under federal jurisdiction (Department of Defense, 2020). Furthermore, the USACE found that any waters used in agricultural processes where goods were sold in interstate commerce also fell under federal jurisdiction (United States Congress, 2018; Department of Defense, 2020).

The Supreme Court was later called upon to address the definition of WOTUS under the CWA in Solid Waste Agency of Northern Cook County v. U.S. Army Corps of Engineers (SWANCC) in 2001. This case considered the delineation of wetlands and wetlands regulation for areas not significantly connected to jurisdictional WOTUS and pertained to non-navigable intrastate waters and artificial features. In response, a joint interpretation of WOTUS was issued by the USACE and USEPA in 2003 (Walsh and Ward, 2019; Department of Defense, 2020). This guidance called for coordination with respective agencies that preside over jurisdictional waters to determine the extent of the regulated area as defined under the CWA/MBR and asserted jurisdiction over relatively permanent non-navigable tributaries and connected wetlands (Leibowitz et al., 2008; Department of Defense, 2020).

Two cases arose over the next five years (*Rapanos v. the United States* and *Carabell v. the United States)* that challenged federal authority to enforce regulations on intrastate wetlands near manufactured ditches that flowed into traditionally navigable waterways (Leibowitz et al., 2008; Department of Defense, 2020). These cases were consolidated under one decision *Rapanos v. the United States* in 2006 and led to two new standards introduced by Justices Antonin Scalia and Anthony Kennedy (Leibowitz et al., 2008). Scalia opined that WOTUS regulation extended past the boundaries of traditionally navigable waterways to include “relatively permanent” bodies of water and “seasonal rivers.” Kennedy concluded that jurisdictional waters have a “significant nexus” with traditionally regulated water bodies, regardless of permanency or duration (Leibowitz et al., 2008). According to Kennedy, a significant nexus exists between a wetland/non-navigable waterbody and traditional navigable water if it significantly affects the “chemical, physical, or biological integrity” of a nearby traditionally navigable waterway or other federally protected water body (Leibowitz et al., 2008; Department of Defense, 2020). As a result, the USACE and USEPA issued a joint protocol for regulating waters that fell under either the Scalia or Kennedy standards (Leibowitz et al., 2008; Walsh and Ward, 2019; Department of Defense, 2020).

In 2015, the USEPA introduced a new Clean Water Rule (CWR) to clarify the application of the CWA by categorizing water bodies into the following six types following the significant nexus test:

> “Waters considered jurisdictional by rule included (1) waters which are currently used, were used in the past or may be susceptible to use, for interstate or foreign commerce, including all waters which are subject to the ebb and flow of the tide; (2) interstate waters, including interstate wetlands; (3) the territorial seas; (4) impoundments of waters otherwise identified as jurisdictional; (5) tributaries of the first three categories of ‘jurisdictional by rule’ waters; and (6) waters adjacent to a water identified in the first five categories of ‘jurisdictional by rule’ waters, including wetlands, ponds, lakes, oxbows, impoundments, and similar waters’’ (Department of Defense, 2020).

However, this rule specified that “for a nexus to be significant, it must be more than speculative or insubstantial” (Department of Defense, 2020), and this legislation relied upon a scientific literature review colloquially known as the connectivity report (United States Environmental

Protection Agency, 2015) to expressly define terms such as “tributary” and “adjacent”. For example, “tributary” was defined as a waterway contributing discharge to jurisdictional water that contains physical indicators such as a bed, banks, and a high watermark. The term “adjacent” was formally defined as any waters within 100 ft. of the 100-year floodplain or within 1500 ft. of the high tide mark of traditionally navigable waterways (Department of Defense, 2020).

The 2015 CWR continued to be challenged in courts, and by 2019, 24 states had reverted to enforcing prior versions of the CWA. These judicial proceedings resulted in the USACE/USEPA releasing a revision called the Navigable Waters Protection Rule (NWPR) in April 2020. This April 2020 rule effectively redefined the application of federal protection status by shifting from the “significant nexus” test to standards based on stream permanence (Fesenmyer et al., 2021). This iteration of the CWA jurisdictionally defined the terms ephemeral, intermittent, and perennial as classifications of flow permanency. Under the April 2020 rule, a non-perennial tributary must be defined as intermittent in a typical year to receive federal protection. Because ephemeral streams constitute approximately 48% of the total length of the U.S. stream network (Fesenmyer et al., 2021), their removal from federal protection raised concerns that the 2020 definitions of WOTUS under the NWPR do not fulfill the primary CWA objectives of maintaining the “chemical, physical and biological integrity” of the waters of the United States (Busch et al., 2020; Fesenmyer et al., 2021).

1.3 Controls on Intermittency

Headwater streams – whether perennial or non-perennial – comprise up to 80% of the global stream network (Nadeau and Rains, 2007; Downing et al., 2012; Wohl, 2017), and coincidentally are also where most intermittent sections are found (Leopold and Langbein, 1962; Nadeau and Rains, 2007; Pate et al., 2020; Jaeger, 2021; Messager et al., 2021). Intermittent headwater streams directly impact downstream waters' ecological health and water quality (Ward et al., 2018; Hale and Godsey, 2019; Jaeger, 2021) and are typically dynamic in spatial extent. Many factors contribute to their heterogeneity in both space and time, including climate, human impact/land use, and geological controls (Costigan et al., 2016; Zipper et al., 2021). These factors can also interact: for example, reaches with limited subsurface contributions are more likely to expand and retract in response to seasonal weather fluctuations and precipitation events (Whiting and Godsey, 2016; Ward et al., 2018; Van Meerveld et al., 2019). Here I briefly review climatic and land use controls before more thoroughly exploring geologic controls in section 1.3.3.

1.3.1 Climatic Controls:

Climatic shifts affect the spatial patterns, intensity, frequency, magnitude, and phase (e.g., rain v. snow) of precipitation events, and these controls can drastically alter flow permanence within a stream network (Costigan et al., 2016; Eng et al., 2019; Hammond et al., 2021). In mountainous headwater catchments, accumulated snowmelt moderated by the storativity of saturated valley-fill deposits or hillslope colluvium and aeolian deposits can impact drying patterns (Whiting and Godsey, 2016). Climate also affects vegetation type and overall biomass and, in turn, drives evapotranspiration rates that contribute to atmospheric losses within the stream network (Ward et al., 2018). Predicted shifts toward a warmer and more arid climate will affect precipitation amounts, phase, and timing, resulting in less water being stored in the form of snow during winter months. These changes are predicted to increase the duration and magnitude of stream intermittency and affect the viability of current water resources (Costigan et al., 2016; Zipper et al., 2021).

1.3.2 Human Use and Land Cover Controls:

Urbanization, water withdrawals, and agricultural practices can have variable impacts on stream drying patterns, both extending or contracting periods of intermittency (Hammond et al., 2021; Zipper et al., 2021). For instance, urbanization increases impervious area fractions within watersheds, which negatively correlates with peak-to-no-flow duration, suggesting that urbanization leads to flashier drought responses (Hammond et al., 2021). Damming practices and diversionary structures can restrict flow to downstream sections or extend stream permanence because of low flow requirements (Costigan et al., 2016; Hammond et al., 2021). Regionalized groundwater withdrawal for both municipal and agricultural purposes has already altered the surface expression of rivers, lakes, and wetlands, severely impacting traditionally perennial water bodies, sometimes causing them to dry periodically during summer months (Costigan et al., 2016; Eng et al., 2019; Hammond et al., 2021). In the last 50 years, many historically perennial rivers such as Colorado, the Rio Grande, the Yellow, and the Nile have been heavily affected by urbanization, industrialization, and agricultural practices, and thus shifted to seasonally or episodically intermittent (Datry et al., 2016). These scenarios will become more frequent as global intermittency is expected due to predicted shifts in climate and high human needs (Lapides et al., 2021; Zipper et al., 2021).

1.3.3 Geological Controls

Although surface and subsurface waters interact, they have characteristically different flow patterns and react to wetting or drying conditions differently. Surface flow velocities fluctuate more readily and exceed subsurface flow velocities by up to five orders of magnitude (Ward et al., 2018; Van Meerveld et al., 2019). Stream corridor sediments can often remain wet even when channels run dry (Ward et al., 2018). These differences in velocity and storage explain why surface flows usually garner more attention than subsurface water when assessing storm responses and contaminant transport. However, neither surface nor subsurface flow paths can be ignored in intermittent streams because both are crucial to predicting extent and travel time distributions. Because approximately two-thirds of the United States' stream network are located in losing reaches (Jasechko et al., 2021), quantifying geologic controls can help assess where and how quickly such losses might occur.

One common way that geological controls have been quantified is through their geomorphologic expressions such as slope angle, aspect, sinuosity, and contributing drainage area (Whiting and Godsey, 2016; Ward et al., 2018; Prancevic and Kirchner, 2019). These geomorphic controls can affect the delivery time of precipitation within a catchment because topography often affects where precipitation will accumulate and flow. Convergent flow paths increase fluxes resulting in a more stable flow regime (Whiting and Godsey, 2016; Prancevic and Kirchner, 2019). Nonetheless, the volume of valley-fill deposits and their hydraulic properties will dictate where this flow will be surficially expressed (Prancevic and Kirchner, 2019). Stream drying often occurs in areas where the stream corridor is disconnected from the underlying water table or in areas where subsurface accommodation space exceeds the volume of accumulated precipitation (Godsey and Kirchner, 2014; Ward et al., 2018). Shallower slopes also reduce substrate transmissivity (Prancevic and Kirchner, 2019), restricting subsurface flow and forcing water to the surface (Powell, 1998; Krause et al., 2010; Ward et al., 2018). Thus, geomorphic metrics are often used as proxies for subsurface storage and fluxes because they are easier to characterize (often from LIDAR-derived digital elevation models) than direct subsurface measurements.

However, geomorphic scaling relationships may not fully capture spatial and temporal variations in valley width, depth to bedrock, and the hydrogeological properties of valley-fill deposits (Wondzell, 2011; Godsey and Kirchner, 2014; Prancevic and Kirchner, 2019). These variations affect transport capacity in the stream corridor which also depend on spatial patterns of hydraulic gradients and the size and sorting of stream corridor sediments (Wondzell, 2011; Godsey and Kirchner, 2014; Warix et al., 2021). Intermittent stream networks are dynamically connected to their watersheds in three dimensions with surface flow networks that expand and contract with changes in flow. Small events such as tree fall, beaver damming, sediment pulses, or high discharge precipitation events can induce changes in channel morphology, affecting surface-subsurface exchange at the reach scale. In contrast, more significant events such as landslides, erosion, water withdrawals, and other human-caused disturbances can change the spatial structure of entire stream networks (Powell, 1998; Kondolf et al., 2005). Alternating patterns of incision and aggradation can combine with channel migration events to produce complex sedimentary structures within fluvial deposits (Powell, 1998; Krause et al., 2010). These structures govern longitudinal, lateral, and vertical flow paths within the subsurface, and the magnitude of subsurface exchange is related to the size and sorting of the stream bed sediments and valley fill deposits (Vaux, 1968; Powell, 1998; Kondolf et al., 2005).

In addition to erosion/deposition events, the underlying lithology can dramatically affect valley steepness, depth, and composition of valley fill sediments, vegetative cover, and drainage density within a stream network (Whiting and Godsey, 2016; Lovill et al., 2018; Hahm et al., 2019). Permeable lithologic units such as sandstone can act as seasonal to annual reservoirs to sustain flow through seasonal dry periods and episodic droughts. In contrast, areas with impermeable lithology will shed water rapidly, resulting in a more dynamic surface flow network (Hahm et al., 2019). Large submerged blocks of porous weathered bedrock or thick packages of hillslope colluvium in an otherwise low permeability matrix can act as reservoirs of water (Lovill et al., 2018). Fractures and weathering patterns govern flow in both the shallow and deeper subsurface and influence the location of exchanges between surface and subsurface water known as hyporheic flow exchange (Lovill et al., 2018; Hahm et al., 2019) and may not be captured by geomorphic metrics.

Geological structures such as faulting, folding, and dipping/cross-bedded strata can also affect the valley shape, thus concentrating or dispersing flow both on the surface and in the subsurface (Toth, 1962; Whiting and Godsey, 2016; Naganna et al., 2017; Lovill et al., 2018). The characteristics of parent lithology directly affect the hydraulic properties of the overlying substrate through susceptibility to physical and chemical weathering and indirectly through soil and critical zone development processes (Boulton et al., 1998; Lovill et al., 2018). Physical and chemical weathering processes also affect the depth and structure of the weathered bedrock zone, impacting the porosity and storativity of valley-fill deposits and controlling subsurface flow volume and residence time (Lovill et al., 2018; Hahm et al., 2019).

1.4 Existing Models of Stream Intermittency

As discussed in section 1.2, regulatory agencies have shifted from previous definitions of WOTUS based upon evidence of a “significant nexus” to flow permanence classifications (Jaeger et al., 2019; Allen et al., 2020). Thus, a number of recent models have been developed to accurately predict flow permanence focused on the drivers of the spatiotemporal patterns of flow that were summarized in section 1.3. However, developing accurate predictions of changes in stream intermittency in the face of climate change and increased human demands has remained difficult (Durighetto et al., 2020; Messager et al., 2021). Currently, most models rely heavily on observational data and only partially integrate our understanding of drivers of stream intermittency.

The current U.S. National Hydrography Dataset (NHD) High Resolution stream permanence classifications (SPC) dataset is primarily based upon field surveys performed in the mid-1900s, even though it can be updated on a site-specific basis (Hafen et al., 2020b). As a result, misclassification rates for intermittency using the NHD can be as high as 50% (Hafen et al., 2020a). Building from the NHD, the USGS developed the PRObability of Streamflow Permanence (PROSPER) model to predict the annual probability of year-round flow in Washington, Oregon, and Idaho (Jaeger et al., 2019). PROSPER combines wet/dry observations with information about climate conditions, physiological attributes such as vegetative cover, and topography to predict annual stream permanence at a 30-meter resolution scale. Neither surficial geologic nor subsurface hydrologic properties are included as predictor variables, but mechanisms such as interannual variability in regional meteorology are considered. PROSPER can predict stream permanence with 79% accuracy in some regions and extends the percentage of headwater stream sections from those represented by the NHD dataset (Sando et al., 2017;

Jaeger et al., 2019). The PROSPER model is limited by its failure to account for the impact of upstream reservoirs and water withdrawals on downstream segments, nor does it account for local-scale controls such as hyporheic exchanges within a stream network (Jaeger et al., 2019). Another model of stream intermittency that couples field observations with statistical or physical theories to produce network-wide predictions is the recent correlation-ranking model from Botter and Durighetto, 2020 and Durighetto et al., 2020. This model relies on site-specific observations and assumptions about the relationship between flow at pairs of sites within the stream network to generate time series of flow likelihood throughout watershed-scale networks. Both the correlation-ranking and PROSPER models require large data inputs and focus on statistical relationships without additional detailed analysis of in-stream processes. Thus, with these models, it may be difficult to extrapolate from observations to future drying patterns and transfer knowledge to other sites or regions with these models.

By contrast, because topographic information is widely available, the mechanistic model of streamflow drying described by Prancevic and Kirchner (2019) may be relatively easy to apply across broad regions. This topographically-driven model relies on metrics such as upstream accumulation area, cross-sectional area, the average hydraulic conductivity of stream bed sediments, and local topographic gradient to predict stream network dynamics (Prancevic and Kirchner, 2019). However, the model requires an assumption (or measurement) of average Ksat and does not account for the heterogeneity in subsurface properties such as transmissivity or hydraulic conductivity. It is also limited to mountainous catchments in humid to semi-arid environments, and it remains to be validated across many regions (Prancevic and Kirchner, 2019).

In addition to the aforementioned statistical models, patterns of streamflow permanence have also been modeled using a reduced-complexity framework that simplifies a system to its key controlling factors (Bencala and Walters, 1983; Ward et al., 2018), which in this case include both conservation of mass and momentum equations. The reduced-complexity stream permanence model builds off past efforts to model ground and surface water as parts of a single dynamic system that requires accurate measurements and predictions of hydrogeological properties like hydraulic conductivity and storativity of stream corridor sediments (e.g., Pliakas and Petalas, 2011). Reduced-complexity models are computationally efficient, yet limited by the number of controls they can consider; they typically apply at small spatial scales and assume that site-specific processes extend across reach-to-network scales (Bencala and Walters, 1983; Ward et al., 2018). The reduced-complexity model of streamflow permanence also demands large amounts of site-specific information to produce accurate results (e.g., high-quality digital elevation models (DEMs) are necessary to determine slope and channel width). To date this model does not account for the spatial variation in subsurface properties, and its performance at the reach scale is poor despite strong system-wide performance (Ward et al., 2018).

Stream protection depends on flow permanence predictions that vary in space. Flow permanence depends on variation in subsurface properties such as saturated hydraulic conductivity, also known as Ksat, but this variation is ignored in all of these leading models. Moving forward, the growing availability of remote sensing applications and increased computational power, and improved statistical modeling approaches will likely accelerate the understanding of the drivers of intermittency along with site-specific predictions of drying (Jaeger et al., 2019). Furthermore, the consideration of dominant local-scale controls such as storage-discharge relationships (Godsey and Kirchner, 2014; Whiting and Godsey, 2016) and the spatial structure of subsurface properties (Abimbola et al., 2020a; Warix et al., 2021) as well as longer duration field observations will both improve our understanding of the drivers of stream intermittency, and allow us to predict flow permanence on multiple scales more accurately. In particular, the time is ripe to assess how variations in stream corridor Ksat affect flow permanence throughout a stream network.

1.5 Saturated Hydraulic Conductivity (Ksat) to Help Quantify Subsurface Flows

1.5.1 Definition

Saturated hydraulic conductivity (Ksat) of stream corridor sediments is a critical parameter in quantifying hyporheic exchange within fluvial systems (Payn et al., 2012); it can also influence stream intermittency as losses within a network may occur in areas with higher Ksat values (Godsey and Kirchner, 2014; Naganna et al., 2017; Dohman et al., 2021). Ksat is defined as the volume of water that can pass through a unit area of the saturated substrate in unit time, given a head gradient measured perpendicular to the flow direction (Freeze and Cherry, 1979); it is typically presented in units of depth per time. This hydrogeologic property is the proportional coefficient K in Darcy's Law ($Q = -KiA$), which states that discharge (Q) within a cross-sectional area (A) of a stream corridor is proportional to the hydraulic gradient (i), and the hydraulic conductivity (K) of the stream corridor sediments (Freeze and Cherry, 1979). This thesis focuses on saturated hydraulic conductivity because it is the relevant parameter during stream drying processes. Because Ksat is related to the size and sorting of streambed sediments, it can be used to quantify residence time and the advection/dispersion processes that affect groundwater nutrient and contaminant transport (Naganna et al., 2017).

1.5.2 Measuring Ksat

Henry Darcy first introduced the empirical method that carries his name in 1856 (Freeze and Cherry, 1979) after devising a laboratory method to measure hydraulic conductivity, later adapted by others to use in the field (Hvorslev, 1951; Freeze and Cherry, 1979; Landon et al., 2001). Field techniques include *in situ* parameter tests, seepage flux measurements, and induced slug, *aka* falling head tests (Hvorslev, 1951). Lab-based methods such as grain size analyses are typically performed on sediments that have been sampled in the field using a coring tool or with hollow sampling tubes driven into sedimentary assemblages (Freeze and Cherry, 1979; Landon et al., 2001). Calculated Ksat estimates typically rely on empirical relationships based upon sediment size distributions (Pliakas and Petalas, 2011; Naganna et al., 2017). Laboratory techniques are less expensive than field techniques (Pliakas and Petalas, 2011), but typically disturb structure in heterogeneous sediments and are subject to incomplete core recovery, sometimes producing unreliable results (Landon et al., 2001). Ksat values derived from field techniques are typically more reliable than those used in laboratory settings (Landon et al., 2001); however, collecting large field-based Ksat datasets is challenging. Here I review the most common *in situ* field methods for estimating Ksat in a stream corridor.

In situ Ksat measurements usually rely on one of two methods. First, the Hvorslev method utilizes point piezometers to measure Ksat over a pre-defined interval in unconfined aquifer conditions (Hvorslev, 1951). Second, the Cooper method uses piezometers screened over the entire thickness of an aquifer (Cooper et al., 1967) to measure the Ksat over the aquifer. Although designed for different applications, both types of tests rely upon an initial head displacement caused by adding or removing a predetermined volume of water (or "slug") and measuring the head recovery inside the well over time as water flows through the portion of the well that permits flow (either at a point, or over an open or screened interval) as the water level returns to static conditions (Freeze and Cherry, 1979).

Here I expand on the Hvorslev method for obtaining *in situ* Ksat values in unconfined aquifer conditions. This method relies on several key assumptions: first, the method assumes an infinite areal extent with isotropic and homogenous conditions. Second, the method assumes the “slug” or added volume of water is injected or discharged instantaneously. Third, the potentiometric surface is initially considered horizontal, and fourth, both the medium and water are assumed to be incompressible (Hvorslev, 1951). Finally, the discharge rate through the well screen is considered to be comparable to the hydraulic conductivity of the saturated sediments. If these assumptions are met, the difference between the head at the beginning of the test and any given time (H-h) reflects the unrecovered head as it returns to static conditions (Hvorslev, 1951). Although these assumptions are rarely fully met, the influence of these sources of error is usually considered negligible if deviations from the assumptions are minor.

Uncertainties in Ksat values derived using the Hvorslev method can arise during piezometer installation and subsequent field tests, but there are ways to minimize these potential sources of error. One common concern is that compaction of sediments during piezometer installation, or the formation of a low-K “well-skin”, can be caused by smearing sediments with either the casing or screened interval. This smearing or compaction can artificially lower Ksat estimates (Butler, 1998). In contrast, artificially high estimates can occur due to disturbance of sedimentary structures during installation or improper well development that can cause boundary flow between the outer wall of the piezometer and the surrounding well-bore sediments. In addition, over-development of the screened interval can cause scouring of fine-grained sediments via hyporheic flow and can even lead to the development of macropores or preferential subsurface flow paths caused by excessive head gradients (Butler, 1998). These potential sources of error can be eliminated using proper installation techniques that avoid excessive reaming and wallowing of the well-bore and excessive head pressures during well development. Falling head test results can help confirm that adequate well-development has occurred: data should exponentially decline and asymptotically approach baseline values when plotted over time, and tests should produce consistent results. The log-normalized drawdown should produce a straight line to reflect this exponential decay (Hvorslev, 1951; Freeze and Cherry, 1979; Butler, 1998; Landon et al., 2001).

1.5.3 Spatiotemporal Variation in Ksat

Accurately modeling patterns in stream permanence may depend on accurately predicting hyporheic exchange (Vaux, 1968; Jaeger, 2021). Indeed stream corridor Ksat in perennial systems can vary laterally by several orders of magnitude over short (<10m) distances (Leek et al., 2010; Wu et al., 2016; Abimbola et al., 2020a; Schilling et al., 2021). Furthermore, heterogeneity in Ksat values strongly correlates with areas associated with upwelling and downwelling within stream networks (Cardenas et al., 2004; Fleckenstein et al., 2006; Naganna et al., 2017; Ward et al., 2018), and different controls can affect heterogeneity in other dimensions. For example, the size and composition of valley fill sediments can vary substantially and contribute to vertical heterogeneity in Ksat values (Baxter and Hauer, 2000).

Patterns of incision and aggradation within fluvial settings can contribute to complex structures within alluvial deposits (Baxter and Hauer, 2000). Although higher Ksat values can be expected in shallow (<20cm) streambed sediments, deposition patterns and erosional properties within the stream corridor create lateral spatial patterns that are challenging to accurately predict, especially at depth (Landon et al., 2001; Leek et al., 2010; Wu et al., 2016; Naganna et al., 2017;

Libohova et al., 2018). Ksat usually decreases exponentially with depth in soil profiles (Libohova et al., 2018) and stream corridors (Wu et al., 2016). However, fluvial depositional environments often create laminations of fine-grained sediments and sedimentary structures that affect the vertical subsurface flow or create confined or perched aquifer settings within valley-fill deposits. These spatial variations may affect hyporheic exchange but are often beyond the scope of network-scale studies of hydraulic conductivity.

Temporal variation in stream corridor Ksat occurs through geomorphologic mechanisms or in conjunction with changes in stream discharge that can occur over multiple time scales (Leopold and Langbein, 1962; Naganna et al., 2017). Ksat can vary over multiple timescales due to precipitation or flow events (Naganna et al., 2017), natural or human-induced channel migration (Stewardson et al., 2016), erosion and deposition of organic matter and fine sediments (Naganna et al., 2017), and the shrinking and swelling of clays (Oosterbaan and Nijland, 1994).

1.6 Background on Spatial Analysis and Interpolation

Because Ksat varies in space and time, and because Ksat measurement techniques are so often point measurements (sections 1.4-1.5), spatial analysis and interpolation are useful to understand Ksat patterns across watersheds or stream corridors. These geostatistical methods can be used to predict values for unsampled locations and describe patterns in data, such as variation in stream corridor Ksat, that vary in both space and time (Bolstad, 2002). Because practical sampling constraints such as time, expense, and the accessibility of a study area can limit the ability to measure key parameters everywhere in the region of interest (Oosterbaan and Nijland, 1994; Butler, 1998; Landon et al., 2001), interpolation of limited observations is a critical tool. The resolution and extent of observed data across a study site can limit the scope of inference; however, interpolation is still a helpful tool for predicting values in otherwise constrained data

(Oosterbaan and Nijland, 1994; Bolstad, 2002). While there are numerous methods of interpolation, all rely on known values measured at known locations to mathematically calculate values for predicted variables at unsampled sites (Bolstad, 2002).

1.6.1 Covariance, Correlation, and Semivariance

Waldo Tobler noted that "everything in the universe is related to everything else, but closer things are more related" (Tobler 1970). The degree to which subsurface properties are related to their neighboring values is quantified by their degree of spatial autocorrelation, a measurement of how likely it is for sample sites closer together to share more similar values than those farther apart (Bolstad, 2002). Characterizing spatial autocorrelation is the focus of many geostatistical models that aim to cognize the spatial relationships between covariate and response variables (Peterson and Ver Hoef, 2010a; Ver Hoef et al., 2019). These relationships between spatial data are often quantified in terms of autocorrelation, covariance, or semivariance. Covariance is a scaled version of correlation that depends on the magnitude of the data and its deviation from average values. Expressed as Cov $(X, Y) = \Sigma((X- \bar{X})(Y-\bar{Y}))/(n-1)$, covariance is often generated as a summary statistic for scatterplots (Bolstad, 2002; Li and Heap, 2008). In spatial analysis, covariance is measured between all pairs of points, i and i+h, separated by any given lag distance of interest (h), such that X and Y in the covariance equation are more accurately represented by V_i and V_{i+h}. Semivariance is similar to covariance, and is equal to half the variance between all data that are separated by a given lag (Bolstad, 2002; Li and Heap, 2008) and is expressed as $\gamma(h_{\rightarrow})= \Theta(V_i-V_{i+h})^2/2N(h_{\rightarrow})$, where $h_{\rightarrow}$ represents the lag distance between all pairs of points V_i and V_{i+h}. The purpose of calculating semivariance is to quantify the distance and magnitude of spatial autocorrelation, or how far the autocorrelation extends and how much it varies at individual lagged intervals.

The spatial structure of variable data is best represented by plotting semivariance over lagged distance through the graphical representation known as a semivariogram (Figure 1.1). Tobler's law implies that points immediately adjacent to each other should only vary slightly, and when plotted in a semivariogram, the semivariance in a dataset should be near zero at small lags. However, plotted data will often exhibit what is known as a nugget effect, and this non-zero intercept value frequently occurs due to variation at distances smaller than sampling intervals or noise created from errors during data collection or processing. The area closest to the intercept represents the distances where autocorrelation is at the highest. At larger lags is the region where there is little to no autocorrelation and where the semivariogram levels off. The height of this plateau, known as the sill, represents the measure of background variance within the dataset, and sill height is equal to overall variance within the dataset. The range is the distance between the intercept and the point where the semivariogram plateaus and indicates the lags over which neighboring points are correlated.

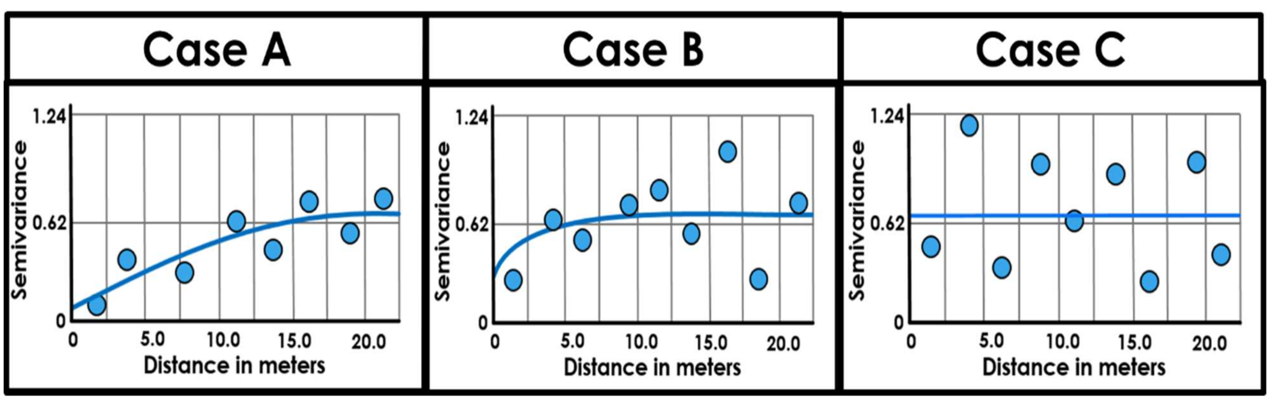

Figure 1.1. Three hypothetical results from plotting semivariance over lagged distance. Case A shows a semivariogram that indicates values are correlated on the scale of tens of meters. Case B is a semivariogram that demonstrates a single-meter scale correlation. Lastly, Case C suggests that the dataset is either correlated on a scale finer than 0.5 meters or shows no spatial autocorrelation whatsoever.

1.6.2 Components of Kriging and Uncertainty Estimates

Initially developed in 1951 to predict South African gold-ore reserves using borehole information, kriging methods have evolved to meet the needs of a vast array of geostatistical analysis (Bolstad, 2002; Li and Heap, 2008). These methods rely on interpolation based upon the following three components: spatial autocorrelation, stochastic variation, and spatial trend. Spatial autocorrelation is the tendency for proximal points to share more similar variable values than more distal ones (as described in section 1.6.1), stochastic variation reflects the random variation of an explanatory variable for points of interest, and the spatial trend is the tendency of a variable to increase or decrease in a given direction (Bolstad, 2002; Li and Heap, 2008). Kriging methods provide not only predicted values at unmeasured locations, but also estimates of the accuracy of the predicted value (Bolstad, 2002; Li and Heap, 2008).

1.6.3 Modifications to the Semivariogram and Spatial interpolations Within a Stream Network

Because we seek to characterize variations in Ksat in the stream corridor, we have to address challenges in interpolation within directional networks. That is, the configuration of flow direction, lateral conductivity, and the assemblage of channel systems within a stream network often produce patterns not well captured by Euclidean distance, which is measured in all directions instead of just along the stream network, and which underlies typical kriging-based interpolations (Dent and Grimm, 1999; Peterson and Ver Hoef, 2010a; Som et al., 2014; Zimmerman and Ver Hoef, 2017). Therefore, the spatial autocorrelation of properties within fluvial environments such as Ksat is often better described using hydrologic distance or the distance between two points within a stream network with water physically flowing downstream. (Peterson and Ver Hoef, 2010a). The Statistical Stream Network (SSN) method has evolved for modelers to express the variability in hydrologic properties within the stream corridor (Ver Hoef et al., 2019). These statistical models use hydrologic distances to determine spatial autocorrelation between flow-connected (topologically dependent) and flow-unconnected (topologically independent) distances. SSN models use graphical representations similar to the semivariogram known as torgegrams. Torgegrams share the same interpretive components as the semivariogram: the range, sill, and nugget quantify the spatially dependent variability within a dataset (Zimmerman and Ver Hoef, 2017).

SSN models rely heavily on GIS computation of network topology and are divided into two sets of moving average functions (Peterson and Ver Hoef, 2010b; Zimmerman and Ver Hoef, 2017). When water flows downstream between two sites, they are referred to as flow connected (F.C.). When sites are located in the same stream network, but do not have water flowing between them, they are considered to be flow unconnected (F.U.) (Ver Hoef et al., 2019). Autocorrelation between two points will vary depending on whether tail-up or tail-down moving average models are used. The terms "tail-up" or "tail-down" can be visualized by considering solute tracer behavior when introduced to fluvial systems (Ver Hoef et al., 2019). A "tail-up" moving average function will only consider values positioned upstream from the point of interest as impacting that site. Each subsequent upstream tributary is assigned a weight contribution to maintain stationarity in the model. In contrast, a "tail down" model will assign non-zero values only to points downstream from the point of interest. Nutrient transport (tail-up) or salmon migratory spawning patterns (tail-down) are just two examples of spatial relationships that are best represented by this directional hydrological distance (Peterson and Ver Hoef, 2010b).

The SSN model requires four pieces of location and topological information that specify both distances and network topology. These are calculated within the STARS package for ArcGIS and stored within a distance matrix: a network identifier, a binary identifier for each segment; the distance from the outlet to the uppermost point in each stream segment; and the distance from the outlet to each location (Ver Hoef et al., 2014). After generating the necessary stream network topology in STARS, the results are imported into the SSN R package for processing (Zimmerman and Ver Hoef, 2017). This package assesses the spatial structure of variables within a stream network, allowing for the development of linear models that can account for additional explanatory variables (e.g., contributing area or elevation, etc.). The package also allows for model comparison via flow-connected and flow-unconnected torgegrams, and model Akaike Information Criterion (AIC), Generalized R-Squared, and Residual Standard Error values are summarized to select the best-fit model among a suite of candidates.

One of the potential benefits of using an SSN model compared to working in Euclidean space is the assessment of flow-directional dependent variability and differences in relationships between flow-connected and flow-unconnected sites, which may be relevant in interpolating stream corridor Ksat. The SSN model can be used with large datasets and has been adopted by many stakeholder agencies and research groups (Ver Hoef et al., 2019). Because fluvial processes govern landscape evolution through the downslope and downstream mobilization and transport of sediments(Leopold and Langbein, 1962; Powell, 1998), and Ksat values are directly correlated to the size and sorting of sediments, it is possible that the spatial structure of stream bed saturated conductivity would be better represented by hydrologic than Euclidean distances.

1.7 Overview and History of the Gibson Jack Watershed

1.7.1 Geography and History of Gibson Jack

Originating in the Bannock Range of southeast Idaho, Gibson Jack Creek is one of the headwater streams that drain into the Portneuf River and eventually to the Snake and Columbia Rivers (Rodgers and Othberg, 1999; Osier, 2004; Dohman et al., 2021). Based on measured distance in ArcGIS, the Gibson Jack Creek is nearly 8 kilometers long from its confluence with the Portneuf to its most upstream headwater reach. The USFS defines Gibson Jack Creek as perennial (Osier, 2004; Capurso et al., 2010); however, I observed many tributaries to be intermittent with disconnected reaches during summer 2020. Additionally, there is an intermittent reach ~1.1 km downstream from the confluence of the perennial sections of the north and south forks that seasonally disconnects surface flows along the mainstem of Gibson Jack Creek from their upstream headwaters for ~200m (Dohman et al., 2021). Gibson Jack is located ~11.6 kilometers from Idaho State University in Pocatello, Idaho, and is part of the Pocatello Municipal Watershed, which was formalized in 1903 (Wrigley, 1943; Capurso et al., 2010). The watershed drains 25.5-km^2 to its confluence with the Portneuf River, but we have studied a smaller portion of watershed located within the Caribou-Targhee National Forest that drains ~16 km^2, bounded by a concrete weir used to measure stream discharge. The 8.94-km^2 Gibson Jack Research Natural Area created in 1982 (Capurso et al., 2010) is located within the north fork of Gibson Jack watershed.

Pocatello and surrounding areas, including Gibson Jack, were incrementally removed from the Fort Hall Indian Reservation in the late 1800s (Capurso et al., 2010). The need for early water quality protection measures arose because of overgrazing, contamination from farming, and the dumping of sanitary waste caused by the influx of white settlers that occurred during this time (Wrigley, 1943). Surface water rights for the watershed were first issued in 1902. They were allocated to help ease the pressure of securing enough water for Pocatello to continue to grow through the early 1900s. In 1903, the Pocatello Water Company began to divert surface water from Gibson Jack and neighboring Mink Creek to a reservoir above the city, and this water was then used as a primary source of municipal water until 1993 when the city switched to pumping water from the Lower Portneuf Valley Aquifer (Wrigley, 1943). Surface water from Gibson Jack is allocated for irrigation, and the combined discharge of Gibson Jack and the surrounding Bannock Range contribute up to 85% of the annual recharge for the Lower Portneuf Valley Aquifer, the sole source of drinking water for the cities of Pocatello and Chubbuck (Wrigley, 1943; Welhan et al., 1996; Capurso et al., 2010).

1.7.2 Site Setting

The climate of the Bannock range is classified as a semi-arid sagebrush steppe, with average annual precipitation increasing from 380 mm/yr at lower elevations to 760 mm/yr at higher elevations (Welhan, 2006; Capurso et al., 2010; Dohman et al., 2021). Elevations within the Gibson Jack watershed range between ~1500-2100 meters, and temperatures range from an average minimum of approximately -8°C occurring during the winter months and frequently exceed 32°C during the summer months (Dohman et al., 2021). The majority (57%) of average annual precipitation (~635 mm) is delivered in the form of snow during the winter and early spring (Capurso et al., 2010). Therefore, Gibson Jack Creek is a snowmelt-dominated stream system with typical peak flows exceeding from 0.5 m^3/s and occurring between March and May, then returning to base flow conditions of $<0.1 m^3/s$ in mid-June through July (Dohman et al., 2021). Intense monsoon-influenced rain events that can frequent the region during the summer and early fall can produce substantial spikes in stream discharge (Capurso et al., 2010).

Late Pleistocene periglacial climate conditions have shaped the topography of Gibson Jack that we see today. Lower regional temperatures allowed for more significant snowpack accumulation while concentrating melt-off to summer months, resulting in regional stream discharge that was several orders of magnitude higher than those currently observed today (Osier, 2004). In turn, greater discharges contributed to an increased incision and regional sediment transport. These processes formed hillslopes that are often steeper than 20 degrees, range between 150-300 meters in relief, and some are covered with loose talus and up to 1.5-meter boulders (Figures 1.2-1.3). Valley fill deposits are composed of transported hillslope material and typically thicken towards the south and southwest, depending upon the canyon aspect (Osier, 2004).

Pleistocene loess mantles much of the study area and is typically reworked into alluvium and hillslope colluvium (Rodgers and Othberg, 1999). Soils within the watershed comprise varying amounts of loess-influenced colluvium/alluvium draped over parent material weathered from underlying parent lithology (NRCS, 2020). Surficial stream corridor sediments were observed to consist of varying amounts of interworked pebble to boulder gravels suspended in a sandy-silt matrix (Figure 1.3).

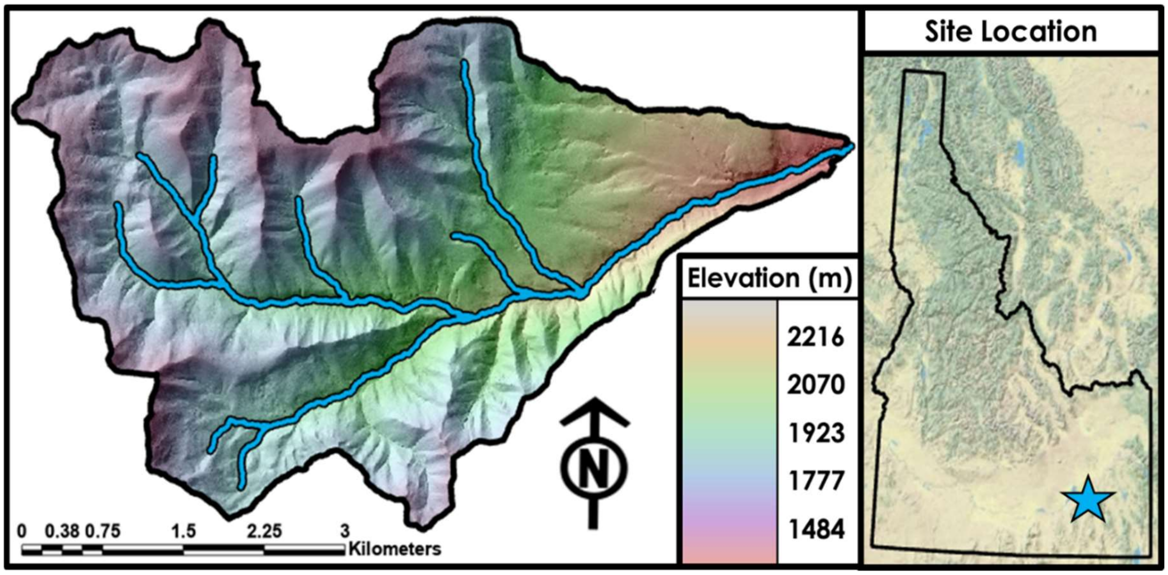

Figure 1.2. Elevations in Gibson Jack overlain on a hillshade with the channel network drawn in blue and an inset map showing the study area's location in southeastern Idaho.

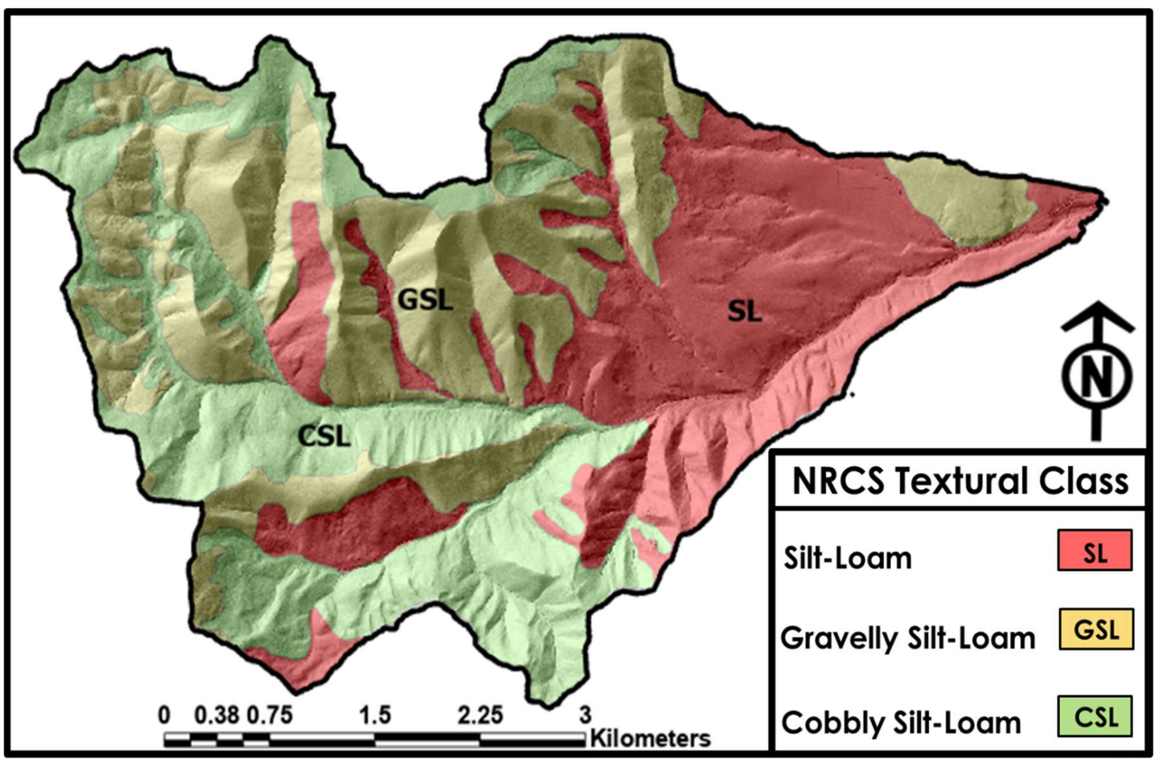

Figure 1.3. Map of soils in the Gibson Jack watershed (modified from NRCS, 2020). Soil series classifications are grouped into three textural classes based on series descriptions (see soil series details in Appendix 3).

The stream channel network exhibits a dendritic geometry and is predominantly structurally controlled by faulted bedrock (Osier, 2004). Mainstem tributaries alternate between anastomosing, braided channels located in heavily vegetated riparian areas and incised channels cutting into previously deposited alluvial sediments. Basin geomorphology has more recently evolved via fires that historically occur every 20-100 years (Ager et al., 2014) as well as intense summer storms and spring floods, insects, and floral disease (Evenden et al., 2001). Even more recently, human-related disturbances have included arson in the summer of 2020, grazing, road construction, timber harvest, water diversion, and the dynamiting of beaver dams as late as the 1970s (Capurso et al., 2010). Recreational usage has also altered this municipal watershed as numerous trails used for hiking, mountain biking, and horse riding cut through the watershed (Capurso et al., 2010; Cornell, 2013).

Bedrock geology in the watershed is dominated by Cambrian and Proterozoic sedimentary and metasedimentary units, including quartzite, limestone, sandstone, and shale (Rodgers and Othberg, 1999). The Gibson Jack Creek is predominantly bounded by the Late-Cenozoic Gibson Jack fault that strikes east to west, dipping south, cutting through the watershed (Osier, 2004). This fault is surficially manifested by the truncation of Cambrian quartzite and shale that comprises the footwall to the north and the Middle Cambrian limestone of the hanging wall to the south (Rodgers and Othberg, 1999; Osier, 2004; Trimble, 2013) (Figure 1.4). Outcrops of quartzite and shale bedrock expressed within the watershed to the north of the fault are moderately fractured or jointed at ~0.75-1 m intervals. Carbonate units south of the fault exhibit signs of karsting that include circular depressions visible in the DEM and high electrical conductivity values collected by undergraduate Alyssa DeSmit during the field season of 2020 near springs that feed the south fork along the mainstem from its south bank. I also observed tufa deposits along the south fork of Gibson Jack during the 2020 field season (see notes on wells coded as I-0.0, I-12, I-25, I-50, I-100, and IJ-1000 in Appendix 14).

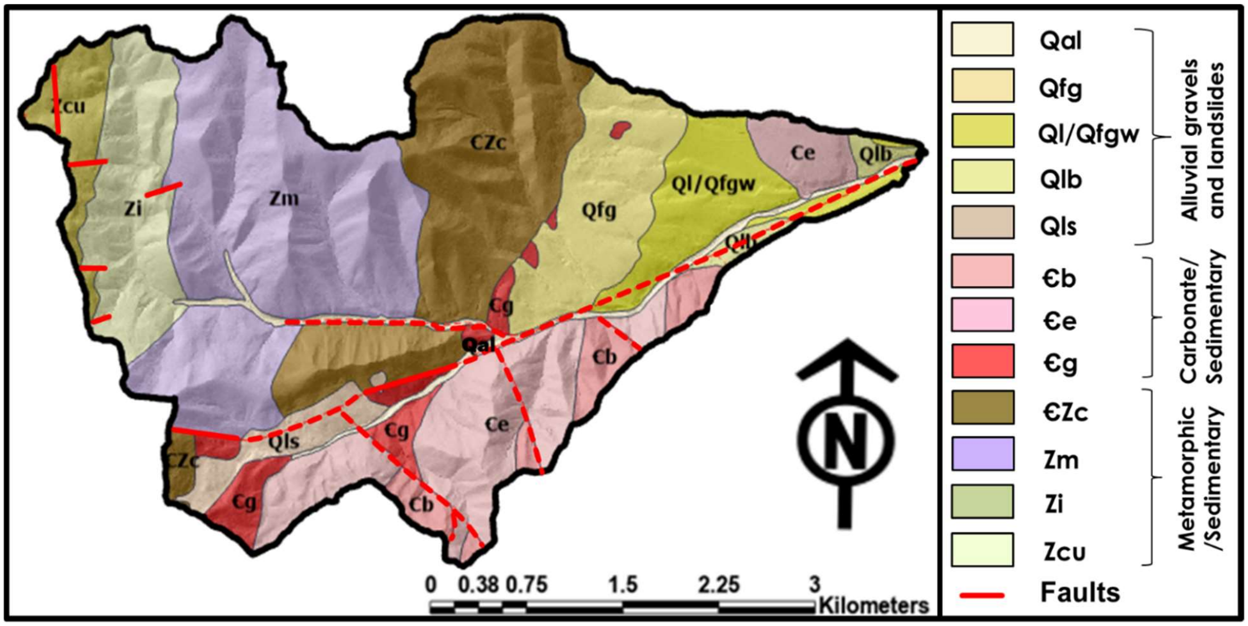

Figure 1.4. Map of the underlying lithology containing Proterozoic to Cambrian carbonates, sedimentary and metasedimentary units comprised of limestone, shale, sandstone, and quartzite (modified from Rodgers and Othberg, 1999). Known faults are represented by solid lines and inferred faults are represented by dashed lines. A table of lithologic descriptions (from Rodgers and Othberg, 1999) is included in App. 16.

Due to the combination of the semi-arid climate, geomorphology, and variation in geology, the watershed hosts a broad diversity of plant and animal species, and habitat changes can be abrupt. Habitat types within the watershed include sagebrush steppe, aspen, mixed conifer, subalpine forested, riparian, and subalpine riparian with some residential and agricultural use near the outlet (Osier, 2004; Capurso et al., 2010). The south- and west-facing hillslopes within the watershed are typically covered in talus and sparsely vegetated, with Big and black sagebrush (*Artemisia tridentata* and *Artemisia nova*), Buck brush (*Ceanothus cuneatus*), native blue/bunch grasses (including *Poa Secunda and Elymus cinerus*), as well as scattered stands of

Utah juniper (*Juniperus osteosperma*). The north-facing slopes, particularly in the south fork and along the mainstem of the Gibson Jack Creek, support densely forested tree cover and are home to thick stands of aspen (*Populus tremuloides*), Douglas fir (*Pseudotsuga menziesii*), subalpine-fir (*Abies lasiocarpa*), big-toothed maple (*Ace*r *grandidentatum*), and gamble oak (*Quercus gambelii*) (Evenden et al., 2001; Capurso et al., 2010).

A noticeable transition to impassable thickets of willows (*Salix exigua* and *Salix lucida*), serviceberry (*Amelanchier alnifolia*), dogwood (*Cornus sericea*), nettle (*Urtica dioica*), sedum (*Sedum debile*), and other lush hydrophilic vegetation occurs near the valley floor and around other riparian areas such as hillside seeps and springs. Skunks (*Mephitis mephitis*), deer (Odocoileus hemionus), elk (Cervus elaphus), black bears (*Ursus americanus)*, and moose (*Alces alces)* are more commonly observed in these riparian areas. Areas within the north fork of Gibson Jack Creek have supported active beaver *(Castor canadensis)* populations as late as 2010 (Capurso et al., 2010). Brook trout (*Salvelinus fontinalis*), brown trout (*Salmo trutta*), and rainbow trout (*Oncorhynchus mykiss*) have been introduced into the lower sections of Gibson Jack Creek. Unfortunately, they have threatened these portions of the historical range for the Yellowstone Cutthroat Trout (*Oncorhynchus clarkii bouvieri*). However, they have not been observed within the Gibson Jack Municipal Watershed boundaries, and native fish populations are still genetically intact (Capurso et al., 2010).

1.8 References Cited:

Abimbola, O.P., Mittelstet, A.R., and Gilmore, T.E., 2020a, Geostatistical features of streambed vertical hydraulic conductivities in Frenchman Creek Watershed in Western Nebraska: Hydrological Processes, v. 34, p. 3481–3491, doi:10.1002/hyp.13823.

Abimbola, O.P., Mittelstet, A.R., Gilmore, T.E., and Korus, J.T., 2020b, Influence of watershed characteristics on streambed hydraulic conductivity across multiple stream orders: Scientific Reports, v. 10, p. 1–11, doi:10.1038/s41598-020-60658-3.

Allen, D.C. et al., 2020, River ecosystem conceptual models and non-perennial rivers: A critical review: Wiley Interdisciplinary Reviews: Water, v. 7, p. 1–13, doi:10.1002/wat2.1473.

Baxter, C. V., and Hauer, F.R., 2000, Geomorphology, hyporheic exchange, and selection of spawning habitat by bull trout (*Salvelinus confluentus*): Canadian Journal of Fisheries and Aquatic Sciences, v. 57, p. 1470–1481, doi:10.1139/cjfas-57-7-1470.

Baxter, C., Hauer, F.R., and Woessner, W.W., 2003, Measuring groundwater –new techniques for installing minipiezometers and estimating hydraulic conductivity: Transactions of the American Fisheries Society, v. 132, p. 493–502, doi:10.1577/1548-8659(2003)132<0493.

Bencala, K.E., and Walters, R.A., 1983, Simulation of solute transport in a mountain pool-and-riffle stream: A transient storage model: Water Resources Research, v. 19, p. 718–724, doi:10.1029/WR019i003p00718.

Blasch, B.K.W., Constantz, J., and Stonestrom, D.A., 2007, Thermal methods for investigating ground-water recharge: USGS Professional Paper 1703, p. 353–375, https://pubs.usgs.gov/pp/pp1703/app1/.

Bolstad, P., 2002, GIS Fundamentals: St. Paul MN, Elder Press, 676 p., doi:10.1201/9781315380568.

Botter, G., and Durighetto, N., 2020, The stream length duration curve: A tool for characterizing the time variability of the flowing stream length: Water Resources Research, v. 56, doi:10.1029/2020WR027282.

Boulton, A.J., Findlay, S., Marmonier, P., Stanley, E.H., and Maurice Valett, H., 1998, The functional significance of the hyporheic zone in streams and rivers: Annual Review of Ecology and Systematics, v. 29, p. 59–81, doi:10.1146/annurev.ecolsys.29.1.59.

Brown, J.A., Robertson, B.L., and McDonald, T., 2015, Spatially Balanced Sampling: Application to environmental surveys: Procedia Environmental Sciences, v. 27, p. 6–9, doi:10.1016/j.proenv.2015.07.108.

Busch, M.H. et al., 2020, What's in a name? Patterns, trends, and suggestions for defining non-perennial rivers and streams: Water (Switzerland), v. 12, doi:10.3390/w12071980.

Butler, J.J., 1998, The Design, Performance, and Analysis of Slug Tests: Washington, D.C., Lewis Publishers, 240 p., doi:10.1201/9781482229370.

Cahn, M.A., Kamieniecki, S., and McCain-Tharnstrom, D., 2007, Bureaucracy, politics, and environmental policy in the American west, *in* Environmental Politics and Policy, Revised Edition, University Press, p. 19–47.

Capurso, J. et al., 2010, Lower Portneuf Watershed Analysis:, http://www.fs.usda.gov/Internet/FSE_DOCUMENTS/stelprdb5406258.pdf.

Cardenas, M.B., Wilson, J.L., and Zlotnik, V.A., 2004, Impact of heterogeneity, bed forms, and stream curvature on subchannel hyporheic exchange: Water Resources Research, v. 40, p. 1–14, doi:10.1029/2004WR003008.

Cooper, H.H., Bredehoeft, J.D., and Papadopulos, I.S., 1967, Response of a finite-diameter well to an instantaneous charge of water: Water Resources Research, v. 3, p. 9, doi:10.1029/WR003i001p00263.

Cornell, J.J., 2013, An investigation of the effects of recreational land use on the stream ecosystem of an urban-fringe watershed: Idaho State, 64 p., doi:ocn922975754.

Costigan, K.H., Jaeger, K.L., Goss, C.W., Fritz, K.M., and Goebel, P.C., 2016, Understanding controls on flow permanence in intermittent rivers to aid ecological research: integrating meteorology, ge: Ecohydrology, v. 9, p. 13, doi:10.1002/eco.1712.

Datry, T., Fritz, K., and Leigh, C., 2016, Challenges, developments and perspectives in intermittent river ecology: Freshwater Biology, v. 61, p. 1171–1180, doi:10.1111/fwb.12789.

Datry, T., Larned, S.T., and Tockner, K., 2014, Intermittent rivers: A challenge for freshwater ecology: BioScience, v. 64, p. 229–235, doi:10.1093/biosci/bit027.

Dent, C.L., and Grimm, N.B., 1999, Spatial heterogeneity of stream water nutrient concentrations over successional time: Ecology, v. 80, p. 2283–2298, doi:10.1890/0012-9658(1999)080[2283:SHOSWN]2.0.CO;2.

Department of Defense, 2020, The Navigable Waters Protection Rule: Definition of “Waters of t he United States”:, https://www.federalregister.gov/documents/2020/04/21/ 2020-02500/the-navigable-waters-protection-rule-definition-of-waters-of-theunited-states. Accessed 15 October 2020.

Dohman, J.M., Godsey, S.E., and Hale, R.L., 2021, Three-Dimensional Subsurface Flow Path Controls on Flow Permanence: Water Resources Research, v. 57, p. 1–18, doi:10.1029/2020wr028270.

Downing, J.A., Cole, J.J., Duarte, C.M., Middelburg, J.J., Melack, J.M., Prairie, Y.T., Kortelainen, P., Striegl, R.G., McDowell, W.H., and Tranvik, L.J., 2012, Global abundance and size distribution of streams and rivers: Inland Waters, v. 2, p. 229–236, doi:10.5268/IW-2.4.502.

Durighetto, N., Vingiani, F., Bertassello, L.E., Camporese, M., and Botter, G., 2020, Intraseasonal drainage network dynamics in a headwater catchment of the Italian Alps: Water Resources Research, v. 56, doi:10.1029/2019WR025563.

Eng, K., Carlisle, D.M., Grantham, T.E., Wolock, D.M., and Eng, R.L., 2019, Severity and extent of alterations to natural streamflow regimes based on hydrologic metrics in the conterminous United States, 1980–2014: U.S. Geological Survey Scientific Investigations Report 2019–5001, p. 25.

Eng, K., Wolock, D.M., and Dettinger, M.D., 2015, Sensitivity of Intermittent Streams to Climate Variations in the USA: River Research and Applications, v. 30, p. 132–133, doi:10.1002/rra.

Evenden, A.G., Moeur, M., Shelly, J.S., Kimball, S.F., and Wellner, C.A., 2001, Research Natural Areas in Idaho, Montana, Nevada, Utah, and Western Wyoming: A guidebook for scientists, managers, and educators: United States Department of Agriculture, 89 p., https://www.fs.fed.us/rm/pubs/rmrs_gtr069.pdf.

Fesenmyer, K.A., Wenger, S.J., Leigh, D.S., and Neville, H.M., 2021, Large portion of USA streams lose protection with new interpretation of clean water act: Freshwater Science, v. 40, p. 252–258, doi:10.1086/713084.

Fleckenstein, J.H., Niswonger, R.G., and Fogg, G.E., 2006, River-aquifer interactions, geologic heterogeneity, and low-flow management, *in* Ground Water, doi:10.1111/j.1745-6584.2006.00190.x.

Floriancic, M.G., Fischer, B.M.C., Molnar, P., Kirchner, J.W., and van Meerveld, I.H.J., 2019, Spatial variability in specific discharge and streamwater chemistry during low flows: Results from snapshot sampling campaigns in eleven Swiss catchments: Hydrological Processes, v. 33, p. 2847–2866, doi:10.1002/hyp.13532.

Freeze, R.A., and Cherry, J.A., 1979, Groundwater (Cathy Brenn, Ed.): Englewood Cliffs, New Jersey, Prentice-Hall. Inc, 671 p., http://library1.nida.ac.th/termpaper6/sd/2554/19755.pdf.

Gendaszek, A.S., Dunham, J.B., Torgersen, C.E., Hockman-Wert, D.P., Heck, M.P., Thorson, J., Mintz, J., and Allai, T., 2020, Land-cover and climatic controls on water temperature, flow permanence, and fragmentation of Great Basin stream networks: Water (Switzerland), v. 12, doi:10.3390/w12071962.

Genereux, D.P., Leahy, S., Mitasova, H., Kennedy, C.D., and Corbett, D.R., 2008, Spatial and temporal variability of streambed hydraulic conductivity in West Bear Creek, North Carolina, USA: Journal of Hydrology, v. 358, p. 332–353, doi:10.1016/j.jhydrol.2008.06.017.

Godsey, S.E., and Kirchner, J.W., 2014, Dynamic, discontinuous stream networks: Hydrologically driven variations in active drainage density, flowing channels and stream order: Hydrological Processes, v. 28, p. 5791–5803, doi:10.1002/hyp.10310.

Gomez, B., 1983, Temporal variations in bedload transport rates: The effect of progressive bed armoring: Earth Surface Processes and Landforms, v. 8, p. 41–54, doi:https://doi.org/10.1002/ESP.3290080105.

Gooseff, M.N., Anderson, J.K., Wondzell, S.M., LaNier, J., and Haggerty, R., 2005, A modelling study of hyporheic exchange pattern and the sequence, size, and spacing of stream bedforms in mountain stream networks, Oregon, USA: Hydrological Processes, v. 19, p. 2915–2929, doi:10.1002/hyp.5790.

Hafen, K.C., Blasch, K.W., Rea, A., Sando, R., and Gessler, P.E., 2020a, The influence of climate variability on the accuracy of NHD perennial and nonperennial stream classifications: Journal of the American Water Resources Association, v. 56, p. 903–916, doi:10.1111/1752-1688.12871.

Hafen, K.C., Blasch, K.W., Rea, A., Sando, R., and Gessler, P.E., 2020b, The Influence of climate variability on the accuracy of NHD perennial and nonperennial stream classifications: Journal of the American Water Resources Association, v. 56, p. 903–916, doi:10.1111/1752-1688.12871.

Hahm, W.J., Rempe, D.M., Dralle, D.N., Dawson, T.E., Lovill, S.M., Bryk, A.B., Bish, D.L., Schieber, J., and Dietrich, W.E., 2019, Lithologically Controlled Subsurface Critical Zone Thickness and Water Storage Capacity Determine Regional Plant Community Composition: Water Resources Research, v. 55, p. 3028–3055, doi:10.1029/2018WR023760.

Hale, R.L., and Godsey, S.E., 2019, Dynamic stream network intermittence explains emergent dissolved organic carbon chemostasis in headwaters: Hydrological Processes, v. 33, p. 1926–1936, doi:10.1002/hyp.13455.

Hammond, J.C. et al., 2021, Spatial patterns and drivers of nonperennial flow regimes in the contiguous United States: Geophysical Research Letters, v. 48, doi:10.1029/2020GL090794.

Harvey, J.W., and Gooseff, M.N., 2015, Consequences from bedforms to basins: Water Resources Research, v. 51, p. 6893–6922, doi:10.1002/2015WR017617.

Ver Hoef, J.M., Peterson, E.E., Clifford, D., and Shah, R., 2014, SSN: An R package for spatial statistical modeling on stream networks: Journal of Statistical Software, v. 56, ftp://sunsite2.icm.edu.pl/packages/cran/web/packages/SSN/vignettes/SSN.pdf%0Apapers3://publication/uuid/EEF33D01-D2EF-4967-99B7-C3ADF58B4183.

Ver Hoef, J.M., Peterson, E.E., and Isaak, D.J., 2019, Spatial statistical models for stream networks: Handbook of Environmental and Ecological Statistics, p. 421–444, doi:10.1201/9781315152509-20.

Hvorslev, M.J., 1951, Time lag and soil permeability in groundwater observations: No. 36. Waterways Experiment Station, Corps of Engineers, US Army, http://hdl.handle.net/2027/mdp.39015086510958 .

Jaeger, K.L., 2021, Most rivers and streams run dry every year: Nature, v. 594, p. 335–336, doi:10.1038/d41586-021-01528-4.

Jaeger, K.L., Olden, J.D., and Pelland, N.A., 2014, Climate change poised to threaten hydrologic connectivity and endemic fishes in dryland streams: Proceedings of the National

Academy of Sciences of the United States of America, v. 111, p. 13894–13899, doi:10.1073/pnas.1320890111.

Jaeger, K.L., Sando, R., McShane, R.R., Dunham, J.B., Hockman-Wert, D.P., Kaiser, K.E., Hafen, K., Risley, J.C., and Blasch, K.W., 2019, Probability of Streamflow Permanence Model (PROSPER): A spatially continuous model of annual streamflow permanence throughout the Pacific Northwest: Journal of Hydrology X, v. 2, p. 100005, doi:10.1016/j.hydroa.2018.100005.

Jasechko, S., Seybold, H., Perrone, D., Fan, Y., and Kirchner, J.W., 2021, Widespread potential loss of streamflow into underlying aquifers across the USA: Nature, v. 591, p. 391–395, doi:10.1038/s41586-021-03311-x.

Kondolf, G.M., Montgomery, D.R., Piégay, H., and Schmitt, L., 2005, Geomorphic Classification of Rivers and Streams: v. 9, 171–204 p., doi:10.1002/0470868333.ch7.

Krause, S., M., H.D., Fleckenstein, J.H., Heppell, C.M., Kaeser, D., Pickup, R., Pinay, G., Robertson, A.L., and Wood, P.J., 2010, Inter-disciplinary perspectives on processes in the hyporheic zone: Ecohydrology, v. 130, p. 126–130, doi:10.1002/eco.

Landon, M.K., Rus, D.L., and Edwin Harvey, F., 2001, Comparison of instream methods for measuring hydraulic conductivity in sandy streambeds: Ground Water, v. 39, p. 870–885, doi:10.1111/j.1745-6584.2001.tb02475.x.

Lapides, D.A., Leclerc, C.D., Moidu, H., Dralle, D.N., and Hahm, W.J., 2021, Variability of stream extents controlled by flow regime and network hydraulic scaling: Hydrological Processes, v. 35, p. 1–17, doi:10.1002/hyp.14079.

Larned, S.T., Datry, T., Arscott, D.B., and Tockner, K., 2010, Emerging concepts in temporary-river ecology: Freshwater Biology, v. 55, p. 717–738, doi:10.1111/j.1365-2427.2009.02322.x.

Leek, R., Wu, J.Q., Wang, L., Hanrahan, T.P., Barber, M.E., and Qiu, H., 2010, Heterogeneous characteristics of streambed saturated hydraulic conductivity of the Touchet River, Southeastern Washington, USA: Hydrological Processes, v. 2274, p. 2267–2274, doi:10.1002/hyp.

Leibowitz, S.G., Wigington, P.J., Rains, M.C., and Downing, D.M., 2008, Non-navigable streams and adjacent wetlands: Addressing science needs following the Supreme Court’s Rapanos decision: Frontiers in Ecology and the Environment, v. 6, p. 364–371, doi:10.1890/070068.

Leigh, C., Boulton, A.J., Courtwright, J.L., Fritz, K., May, C.L., Walker, R.H., and Datry, T., 2016, Ecological research and management of intermittent rivers: A historical review and future directions: Freshwater Biology, v. 61, p. 1181–1199, doi:10.1111/fwb.12646.

Li, J., and Heap, A.D., 2008, A review of spatial interpolation methods for environmental scientists: Journal of Public Health Management and Practice, v. 16, p. S5–S10, doi:10.1097/phh.0b013e3181e31d09.

Libohova, Z., Schoeneberger, P., Bowling, L.C., Owens, P.R., Wysocki, D., Wills, S., Williams, C.O., and Seybold, C., 2018, Soil systems for upscaling saturated hydraulic conductivity for hydrological modeling in the critical zone: Vadose Zone Journal, v. 17, p. 170051, doi:10.2136/vzj2017.03.0051.

Lovill, S.M., Hahm, W.J., and Dietrich, W.E., 2018, Drainage from the critical zone: lithologic controls on the persistence and spatial extent of wetted channels during the summer dry season: Water Resources Research, v. 54, p. 5702–5726, doi:10.1029/2017WR021903.

MacNeille, R.B., Lohse, K.A., Godsey, S.E., and Perdrial, J.N., 2020, Influence of drying and wildfire on longitudinal chemistry patterns and processes of intermittent streams: v. 2, doi:10.3389/frwa.2020.563841.

Manfredo, M.J., Teel, T.L., and Bright, A.D., 2003, Why are public values toward wildlife changing? Human Dimensions of Wildlife, v. 8, p. 287–306, doi:10.1080/716100425.

Van Meerveld, I.H.J., Kirchner, J.W., Vis, M.J.P., Assendelft, R.S., and Seibert, J., 2019, Expansion and contraction of the flowing stream network alter hillslope flow path lengths and the shape of the travel time distribution: Hydrology and Earth System Sciences, v. 23, p. 4825–4834, doi:10.5194/hess-23-4825-2019.

Messager, M.L., Lehner, B., Cockburn, C., Lamouroux, N., Pella, H., Snelder, T., Tockner, K., Trautmann, T., Watt, C., and Datry, T., 2021, Global prevalence of non-perennial rivers and streams: Nature, v. 594, p. 391–397, doi:10.1038/s41586-021-03565-5.

Nadeau, T.L., and Rains, M.C., 2007, Hydrological connectivity between headwater streams and downstream waters: How science can inform policy: Journal of the American Water Resources Association, v. 43, p. 118–133, doi:10.1111/j.1752-1688.2007.00010.x.

Naganna, S.R., Deka, P.C., Ch, S., and Hansen, W.F., 2017, Factors influencing streambed hydraulic conductivity and their implications on stream–aquifer interaction: a conceptual review: Environmental Science and Pollution Research, v. 24, p. 24765–24789, doi:10.1007/s11356-017-0393-4.

National Research Council, 2002, Riparian Areas: Functions and Strategies for Management:, doi:10.17226/10327.

Obedzinski, M., Nossaman Pierce, S., Horton, G.E., and Deitch, M.J., 2018, Effects of flow-related variables on over summer survival of juvenile Coho Salmon in intermittent streams: Transactions of the American Fisheries Society, doi:10.1002/tafs.10057.

Oosterbaan, R., and Nijland, H., 1994, Determining the saturated hydraulic conductivity: Drainage Principles and Applications, p. 37, http://www.waterlog.info/pdf/chap12.pdf.

Osier, T.A., 2004, The Neogene-Quaternary topographic development of the Portneuf Valley, Bannock County, Southeast Idaho: Idaho State.

Pate, A.A., Segura, C., and Bladon, K.D., 2020, Streamflow permanence in headwater streams across four geomorphic provinces in Northern California: Hydrological Processes, v. 34, p. 4487–4504, doi:10.1002/hyp.13889.

Patton, N.R., Lohse, K.A., Seyfried, M.S., Godsey, S.E., and Parsons, S.B., 2019, Topographic controls of soil organic carbon on soil-mantled landscapes: Scientific Reports, v. 9, p. 1–15, doi:10.1038/s41598-019-42556-5.

Payn, R.A., Gooseff, M.N., McGlynn, B.L., Bencala, K.E., and Wondzell, S.M., 2012, Exploring changes in the spatial distribution of stream baseflow generation during a seasonal recession: Water Resources Research, v. 48, doi:10.1029/2011WR011552.

Peterson, E.E., and Ver Hoef, J.M., 2010a, A mixed-model moving-average approach to geostatistical modeling in stream networks: Ecology, v. 91, p. 644–651.

Peterson, E.E., and Ver Hoef, J.M., 2010b, A mixed-model moving-average approach to geostatistical modeling in stream networks: Ecology, v. 91, p. 644–651, doi:10.1890/08-1668.1.

Pliakas, F., and Petalas, C., 2011, Determination of hydraulic conductivity of unconsolidated river alluvium from permeameter tests, empirical formulas and statistical parameters effect analysis: Water Resources Management, v. 25, p. 2877–2899, doi:10.1007/s11269-011-9844-8.

Powell, M.D., 1998, Patterns and processes of sediment sorting in gravel-bed rivers: Progress in Physical Geography, v. 22, p. 1–32, doi:10.1191/030913398666402127.

Prancevic, J.P., and Kirchner, J.W., 2019, Topographic Controls on the Extension and Retraction of Flowing Streams: Geophysical Research Letters, doi:10.1029/2018GL081799.

Rodgers, D., and Othberg, K., 1999, Geologic map of the Pocatello South Quadrangle, Bannock and Power Counties, Idaho: Idaho Geological Survey, p. 2, https://www.idahogeology.org/pub/Maps/Geologic_Maps/PDF/GM-26-m.pdf.

Rodríguez-Lozano, P., Woelfle-Erskine, C., Bogan, M.T., and Carlson, S.M., 2020, Are non-perennial rivers considered as valuable and worthy of conservation as perennial rivers? Sustainability (Switzerland), v. 12, p. 1–12, doi:10.3390/su12145782.

Sando, R. et al., 2017, Mapping and modeling the annual probability of year-round streamflow, *in* Rocky Mountain Partner Forum, p. 66, greatnorthernlcc.org/document/webinar-slides-mapping-and-modeling-annual-probability-year-round-streamflow-2004-2016-case.

Schilling, O.S., Cook, P.G., Grierson, P.F., Dogramaci, S., and Simmons, C.T., 2021, Controls on interactions between surface water, groundwater, and riverine vegetation along intermittent rivers and ephemeral streams in arid regions: Water Resources Research, v. 57, p. 1–21, doi:10.1029/2020WR028429.

Som, N.A., Monestiez, P., Ver Hoef, J.M., Zimmerman, D.L., and Peterson, E.E., 2014, Spatial sampling on streams: Principles for inference on aquatic networks: Environmetrics, v. 25, p. 306–323, doi:10.1002/env.2284.

Steward, A.L., Von Schiller, D., Tockner, K., Marshall, J.C., and Bunn, S.E., 2012, When the river runs dry: Human and ecological values of dry riverbeds: Frontiers in Ecology and the Environment, v. 10, p. 202–209, doi:10.1890/110136.

Stewardson, M.J., Datry, T., Lamouroux, N., Pella, H., Thommeret, N., Valette, L., and Grant, S.B., 2016, Variation in reach-scale hydraulic conductivity of streambeds: Geomorphology, v. 259, p. 70–80, doi:10.1016/j.geomorph.2016.02.001.

Tooth, S., 2000, Process, form and change in dryland rivers: A review of recent research: Earth Science Reviews, v. 51, p. 67–107, doi:10.1016/S0012-8252(00)00014-3.

Toth, J., 1962, A theory of groundwater motion in small drainage basins in central Alberta, Canada: Journal of Geophysical Research, v. 67, p. 4375–4388.

Trimble, D.E., 1976, Geology of the Michaud and Pocatello Quadrangles, Bannock and Power Counties, Idaho: U.S. Geological Survey, v. 1400, p.1-88, doi:10.3133/b1400.

United States Congress, 2018, Water pollution prevention and control: Title 33 — navigation and navigable waters programs: p. 326–558.

United States Environmental Protection Agency, 2015, Connectivity of streams and wetlands to downstream waters: A review and synthesis of the scientific evidence: Surveillance and Society, v. 1, p. 408, http://www.regulations.gov/#!documentDetail;D=EPA-HQ-OW-2011-0880-0004.

Vaux, W.G., 1968, Intragravel flow and interchange of water in a streambed: Fishery Bulletin, v. 66, p. 479–489.

Walsh, R., and Ward, A.S., 2019, Redefining clean water regulations reduces protections for wetlands and jurisdictional uncertainty: Frontiers in Water, v. 1, doi:10.3389/frwa.2019.00001.

Ward, A.S., Schmadel, N.M., and Wondzell, S.M., 2018, Simulation of dynamic expansion, contraction, and connectivity in a mountain stream network: Advances in Water Resources, v. 114, p. 64–82, doi:10.1016/j.advwatres.2018.01.018.

Ward, A.S., Wondzell, S.M., Schmadel, N.M., and Herzog, S.P., 2020, Climate change causes river network contraction and disconnection in the H.J. Andrews Experimental Forest, Oregon, USA: Frontiers in Water, v. 2, p. 1–10, doi:10.3389/frwa.2020.00007.

Warix, S.R., Godsey, S.E., Lohse, K.A., and Hale, R.L., 2021, Influence of groundwater and topography on stream drying in semi-arid headwater streams: Hydrological Processes, v. 35, p. 51, doi:10.1002/hyp.14185.

Welhan, J., 2006, Water balance and pumping capacity of the Lower Portneuf River Valley aquifer, Bannock County, Idaho: Idaho Geological Survey Report 06-5, p. 1–36, http://www.idwr.idaho.gov/browse/waterinfo/ESPAM/model_boundary/IGS_Welhan_06-5.pdf.

Welhan, J., Meehan, C., and Reid, T., 1996, The Lower Portneuf River Valley Aquifer: A geologic/hydrologic model and its implications for wellhead protection strategies:, https://www.idahogeology.org/pub/Staff_Reports/2006/Staff_report_06-5.pdf.

Whiting, J.A., and Godsey, S.E., 2016, Discontinuous headwater stream networks with stable flowheads, Salmon River basin, Idaho: Hydrological Processes, v. 30, p. 2305–2316, doi:10.1002/hyp.10790.

Wondzell, S.M., 2011, The role of the hyporheic zone across stream networks: Hydrological Processes, v. 25, p. 3525–3532, doi:10.1002/hyp.8119.

Wrigley, R.L., 1943, Early History of Pocatello, Idaho: Chicago, Illinois, University of Chicago Libraries, 365 p.

Wu, G., Shu, L., Lu, C., and Chen, X., 2016, The heterogeneity of 3-D vertical hydraulic conductivity in a streambed: Hydrology Research, v. 47, p. 15–26, doi:10.2166/nh.2015.224.

Zimmer, M.A., and McGlynn, B.L., 2018, Lateral, vertical, and longitudinal source area connectivity drive runoff and carbon export across watershed scales: Water Resources Research, v. 54, p. 1576–1598, doi:10.1002/2017WR021718.

Zimmerman, D.L., and Ver Hoef, J.M., 2017, The Torgegram for fluvial variography: characterizing spatial dependence on stream networks: Journal of Computational and Graphical Statistics, v. 26, p. 253–264, doi:10.1080/10618600.2016.1247006.

Zipper, S.C. et al., 2021, Pervasive changes in stream intermittency across the United States: Environmental Research Letters, v. 16, doi:10.1088/1748-9326/ac14ec.

Chapter 2: Fine-scale Spatial Structure of Saturated Hydraulic Conductivity Controls Intermittent Flow Patterns in Headwater Stream in the Northern Rocky Mountains, Idaho, USA

2. Spatial patterns of saturated hydraulic conductivity in an intermittent headwater stream network in Gibson Jack Creek

2.1 Abstract

Stream intermittency is common: over 50% of the global stream network experiences annual stream drying, affecting waterway protection status. However, predicting spatial patterns of flow intermittency remains challenging. These challenges stem from the dynamic nature of intermittent stream networks and the complex combination of climatic, land use, and geological controls that govern their variations in both space and time. Stream protection depends on flow permanence predictions, which vary in space, and flow permanence depends on variation in subsurface properties such as saturated hydraulic conductivity, also known as Ksat, but this variation is usually ignored. Therefore, this work entailed the characterization of the spatial patterns of Ksat within a ~16 km^2 mountainous headwater stream network to improve future predictions of flow permanence. We obtained 194 Ksat measurements at 50-70 cm below the channel surface using an unbalanced nested sampling design throughout a dynamic non-perennial stream network and compared interpolated network-scale Ksat estimates derived from ordinary kriging and statistical stream network (SSN) methods. We found that although Ksat was autocorrelated only over very short (<10 m) distances, it varied by three orders of magnitude within intermittent headwater stream corridors. Ksat exhibited a significant relationship with seasonal stream permanence (p-value of 3E-6) with average values that were 2.2 times higher in dry streambeds. Ksat also varied significantly with lithologic (p-value 0.001) and soil textural

classes (p-value 0.03), which may help to explain why interpolations in Euclidean space were better than those along the stream network. Our findings suggest that accurate predictions of fine-scale drying patterns via subsurface hydraulic properties will continue to require a substantial field effort.

2.2 Introduction

Despite public perceptions that non-perennial streams are less valuable than their perennial counterparts (Stewardson et al., 2016; Rodríguez-Lozano et al., 2020), they still provide many of the same human and ecological services (Steward et al., 2012; Datry et al., 2016; Leigh et al., 2016; Fesenmyer et al., 2021). For instance, humans depend on non-perennial streams for municipal and agricultural water supplies, recreation, and the evacuation of waste (Steward et al., 2012; Harvey and Gooseff, 2015). Non-perennial stream systems also provide spawning or breeding habitat for many aquatic and terrestrial organisms, migration corridors, and their heterogeneity often increases biodiversity (Larned et al., 2010; Steward et al., 2012; Allen et al., 2020).

Over half of the global stream network, regardless of climate or biome, experiences some degree of annual stream drying (Tooth, 2000; Nadeau and Rains, 2007; Costigan et al., 2016; Busch et al., 2020; Messager et al., 2021). Both magnitude and duration of drying are already expanding (Zipper et al., 2021). Drying is expected to increase further in response to predicted shifts in climate and increased human needs (Jaeger et al., 2014; Eng et al., 2015).
Concerns about dwindling water supplies and the impacts of stream drying on overall water quality have resulted in a complicated web of agencies at multiple administrative levels that regulate water quality and environmental protection (Manfredo et al., 2003; Cahn et al., 2007; Department of Defense, 2020). For example, in the United States, the definition of which waters

fall under the US Clean Water Act of 1972 (CWA) protection has long been contentious and has repeatedly gone in front of the Supreme Court, with boundaries of protected tributaries and wetlands changing over time. A revised US Clean Water Rule adopted in 2020 redefined the application of federal protection status from physiographic characteristics that indicated hydraulic communication ("Significant Nexus") to standards based on stream discharge in a typical year. Specifically, the Waters of the United States (WOTUS) are now defined as "a river, stream, or similar naturally occurring surface water channel that contributes surface water flow to a territorial sea or traditional navigable water in a typical year either directly or indirectly through other tributaries, jurisdictional lakes, ponds, or impoundments, or adjacent wetlands" (Department of Defense, 2020). Because WOTUS now excludes ephemeral streams from jurisdictional status, stream classification as perennial, intermittent, and ephemeral affects whether a tributary is protected or not (Walsh and Ward, 2019).

Within this shifting management context, there has been an accompanying shift from studies of ecological impacts of stream drying to a multi-disciplinary approach that encompasses geomorphology, biology, geochemistry, and geostatistics (Datry et al., 2016). However, the development of accurate models that can predict the dynamic behavior of stream intermittency in light of changing climatic conditions has remained difficult (Ward et al. 2018; Botter and Durighetto, 2020; Durighetto et al., 2020). Current models used to predict intermittency and, therefore, which streams are regulated under the CWA, have improved in some regions; for example, the USGS' PROSPER model developed for the Pacific Northwest performs somewhat better than models reviewed by Fritz et al. (2013) with improvements from ~50% to ~75% accuracy (Jaeger et al., 2019).

Given current model limitations and the importance of accurately defining which streams are perennial or not for regulatory purposes, scientists are striving to improve understanding of the controls on stream drying. Stream intermittency is frequently attributed to a combination of climatic, geological, and land use controls (Costigan et al., 2016). Climatic controls are most important when comparing among catchments at a regional or global scale (e.g., Messager et al. 2021; Hammond et al. 2020). At a smaller scale, such as within a catchment, surficial geomorphologic controls such as slope, aspect, contributing source area, and elevation can strongly influence the location, amount, and delivery time of precipitation to the stream (Whiting and Godsey, 2016; Zimmer and McGlynn, 2018; Prancevic and Kirchner, 2019; Ward et al., 2020; Warix et al. 2020). Land use controls, such as the presence of significant reservoirs or water bodies as well as plant water use, can further constrain streamflow and patterns of drying (e.g., Warix, 2020; Hammond et al., 2020). Finally, geologic controls such as fracturing, faulting, and karsting of bedrock can also drive flow in gaining and losing stream reaches (Vaux, 1968; Costigan et al., 2016; Pate et al., 2020). These gains and losses are governed mainly by hyporheic flow exchanges between the subsurface and surface in valley-wide stream corridors (Boulton et al., 1998; Ward et al., 2018) and vary with the saturated hydraulic conductivity (Ksat) of streambed sediments (Powell, 1998; Landon et al., 2001; Godsey and Kirchner, 2014; Stewardson et al., 2016; Wu et al., 2016).

However, unlike climate, geomorphologic metrics, and land cover, network-scale subsurface properties that may affect stream drying patterns have remained challenging to characterize. In particular, the impacts of heterogeneity in hydraulic conductivity on stream drying patterns are often overlooked or poorly constrained (Genereux et al., 2008; Abimbola et al., 2020b; Warix et al., 2021). This is because practical constraints such as time, expense, and accessibility of sample locations frequently limit the quantity and quality of subsurface hydraulic property datasets. Therefore, most models of stream intermittency have been unable to account for variations in streambed Ksat. Modelers have typically assumed uniform Ksat values or used statistical models and sediment characteristics to interpolate Ksat values between a small number of measurement locations (Ward et al., 2018; Abimbola et al., 2020; Fleckenstein et al., 2006). Accurate interpolations may be difficult because Ksat has been known to span several orders of magnitude within tens of meters in perennial and terrestrial systems (e.g., Leek et al., 2010; Wu et al., 2016; Abimbola et al., 2020a; Schilling et al., 2021). Because spatial patterns of Ksat can strongly influence surface-subsurface flow exchange by controlling the transport capacity and storativity of valley-fill and stream corridor sediments (Vaux, 1968; Fleckenstein et al., 2006; Schilling et al., 2021), accurately characterizing those spatial patterns is important to understand transport capacity within a non-perennial stream corridor.

Accurate characterization of spatial patterns within a stream corridor means quantifying the observed spatial autocorrelation – the degree and scale of similarity between measurements at neighboring locations. Because stream corridor characteristics may be more similar along hydrologically connected sites in the stream corridor than to the surrounding riparian and hillslope regions, spatial autocorrelation in near-stream environments may be captured poorly by Euclidean distances that measure separation distances as the crow flies (Ver Hoef et al. 2006; Ver Hoef et al., 2019). Instead, in-stream processes may be better described using hydrologic distance measured “as the fish swims” along a stream; autocorrelation along hydrologic distances can be modeled using a Statistical Stream Network approach to generate a torgegram (Zimmerman and Ver Hoef, 2017). A torgegram is a graphical representation analogous to the semivariogram, and is used to describe the spatial extent and magnitude of spatial autocorrelation within a dataset separated by different hydrologic (rather than Euclidean) distances (Peterson and Ver Hoef, 2010a; Zimmerman and Ver Hoef, 2017; Ver Hoef et al., 2019). Because non-perennial systems exhibit both terrestrial and aquatic characteristics at different times, it remains unclear which of these spatial analysis approaches is best suited to characterize the spatial structure of Ksat in non-perennial stream corridors.

Here we focus on characterizing hydrogeological processes within a non-perennial mountain headwater stream network. We aim to accurately quantify the *in situ* network-scale spatial structure of streambed Ksat and test the following hypotheses:

H1: Stream corridor saturated hydraulic conductivity is spatially correlated at the scale of tens of meters;

H2: Geomorphological controls drive the spatial scale of saturated hydraulic conductivity in the stream corridor; and

H3: Spatial patterns of Ksat covary with the spatial patterns of seasonal stream drying.

These hypotheses were tested based on field measurements in the northern Rocky Mountains in the Gibson Jack watershed in southeastern Idaho (described in the Methods and Site Description section below) and through soil profile and spatial analysis techniques (outlined in the Methods section below).

2.2 Methods and Site Description:

2.2.1 Site Description

Draining ~16 km^2, the Gibson Jack watershed is nested in the Caribou-Targhee National Forest and encompasses the 8.94 km^2 Gibson Jack Research Natural Area. Gibson Jack was designated part of the Pocatello Municipal Watershed in 1903 and is located ~11.6 km from Idaho State University in the city of Pocatello, Idaho (Capurso et al., 2010). Originating in the

Bannock Range of southeastern Idaho, Gibson Jack Creek is one of the headwater streams draining to the Portneuf River (Rodgers and Othberg, 1999; Osier, 2004; Dohman et al., 2021) and eventually to the Snake and Columbia Rivers. Elevations in Gibson Jack range between ~1500-2200m (Figure 2.1), and the watershed receives the majority (57%) of its average annual precipitation (~635 mm) in the form of snow between April and June (Welhan et al., 1996; Capurso et al., 2010; Dohman et al., 2021). The regional climate is formally classified as a semi-arid steppe. Due to strong aspect gradients, south- and west-facing hillslopes are typically sparsely vegetated and dominated by big and black sage (*Artemisia tridentata* and *Artemisia nova*), Buck brush (*Ceanothus cuneatus*), native blue/bunch grasses (including *Poa Secunda and Elymus cinerus*), and patches of pine and (*Juniperus osteosperma*). By contrast, north- and east-facing hillslopes are typically home to dense stands of (*Populus tremuloides*), Douglas fir (*Pseudotsuga menziesii*), subalpine-fir (*Abies lasiocarpa*), big-toothed maple (*Acer grandidentatum*), and gamble oak (*Quercus gambelii*) (Evenden et al., 2001; Capurso et al., 2010). The stream corridors support relatively lush riparian vegetation comprised of thickets of (*Salix exigua* and *Salix lucida*), dogwood (*Cornus sericea*), nettle (*Urtica dioica*), and sedum (*Sedum debile).*

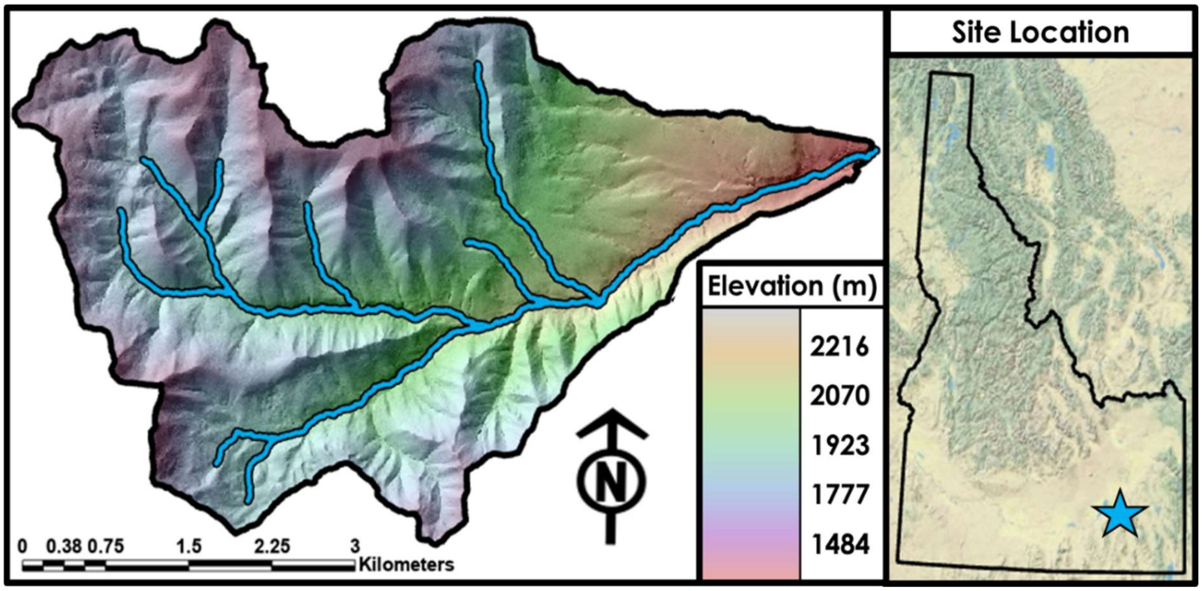

Figure 2.1. Elevations in Gibson Jack overlain on a hillshade with the channel network drawn in blue and an inset map showing the study area's location in southeastern Idaho.

Bedrock geology in the region is dominated by Cambrian and Proterozoic sedimentary and metasedimentary units, including quartzite, limestone, sandstone, and shale (Rodgers and Othberg, 1999) (Figure 2.2). The Late-Cenozoic, east- to west-dipping Gibson Jack fault cuts through the study area and is surficially manifested by the truncation of Cambrian quartzite that comprises the footwall to the north and the Middle Cambrian limestone of the hanging wall to the south (Osier, 2004; Trimble, 2013). Headwater channels are predominantly structurally controlled by fractured/faulted bedrock or incised into thick valley-fill deposits composed of reworked loess and colluvial bedrock material (Rodgers and Othberg, 1999). The mainstem tributaries are predominantly incised into thick packages >4m of reworked alluvial sediments/hillslope colluvium and loess; however, some segments are locally aggrading and contain braided channels that cut through heavily vegetated riparian areas.

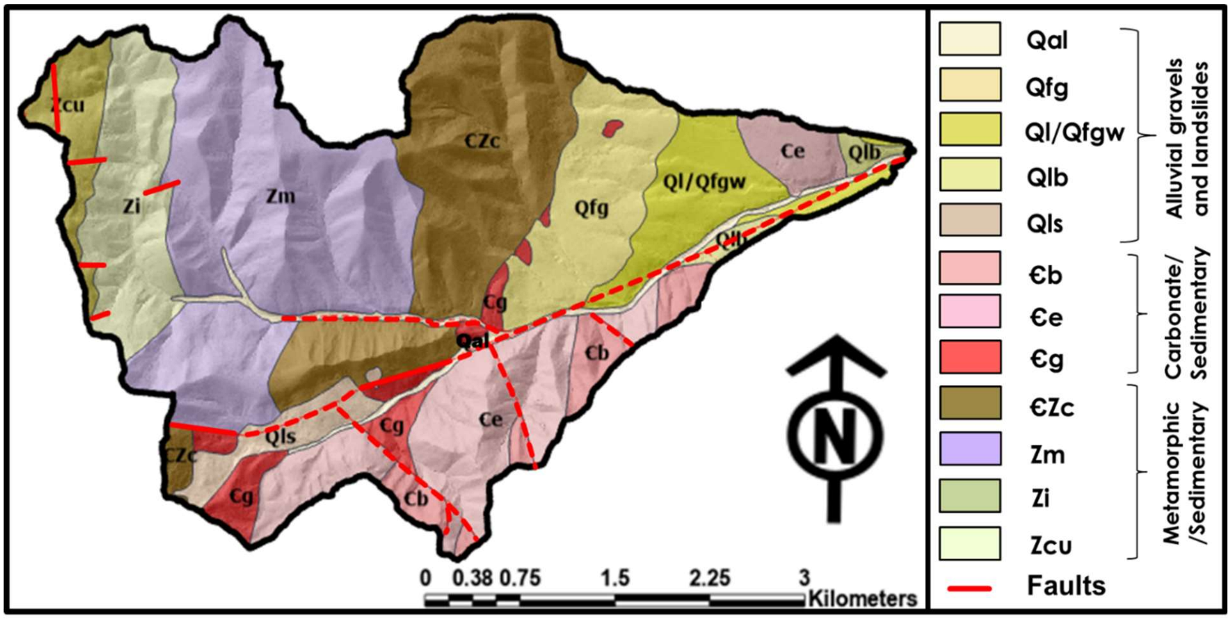

Figure 2.2. Map of the underlying lithology containing Proterozoic to Cambrian carbonates, sedimentary and metasedimentary units comprised of limestone, shale, sandstone, and quartzite (modified from Rodgers and Othberg, 1999). Known faults are represented by solid lines and inferred faults are represented by dashed lines. A table of lithologic descriptions (from Rodgers and Othberg, 1999) is included in App. 16.

In addition to these geological controls, the watershed has been influenced by geomorphic, climatic, and biological controls. Regional uplift and faulting have resulted in hillslopes that exceed 20 degrees and are often soil-mantled or occasionally covered with loose talus (Osier, 2004; Dohman et al., 2021). These hillslope sediments have windblown sediments described by the NRCS as being “predominantly composed of varying percentages of loess-influenced colluvium and reworked alluvium over residuum weathered from parent lithologic units” (NRCS, 2020). They have accumulated along the north-facing slopes and valley bottoms, particularly in the south fork and along the mainstem of Gibson Jack Creek (Figure 2.3). The subsequent landforms have also been shaped by fires that historically occur every 20-100 years

(Ager et al., 2014) and by intense summer storms and spring floods, insects, and floral disease (Evenden et al., 2001). More recently, human-related disturbances include recreation, grazing, road construction, timber harvest, water diversion, and the dynamiting of beaver dams as late as the 1970s (Capurso et al., 2010).

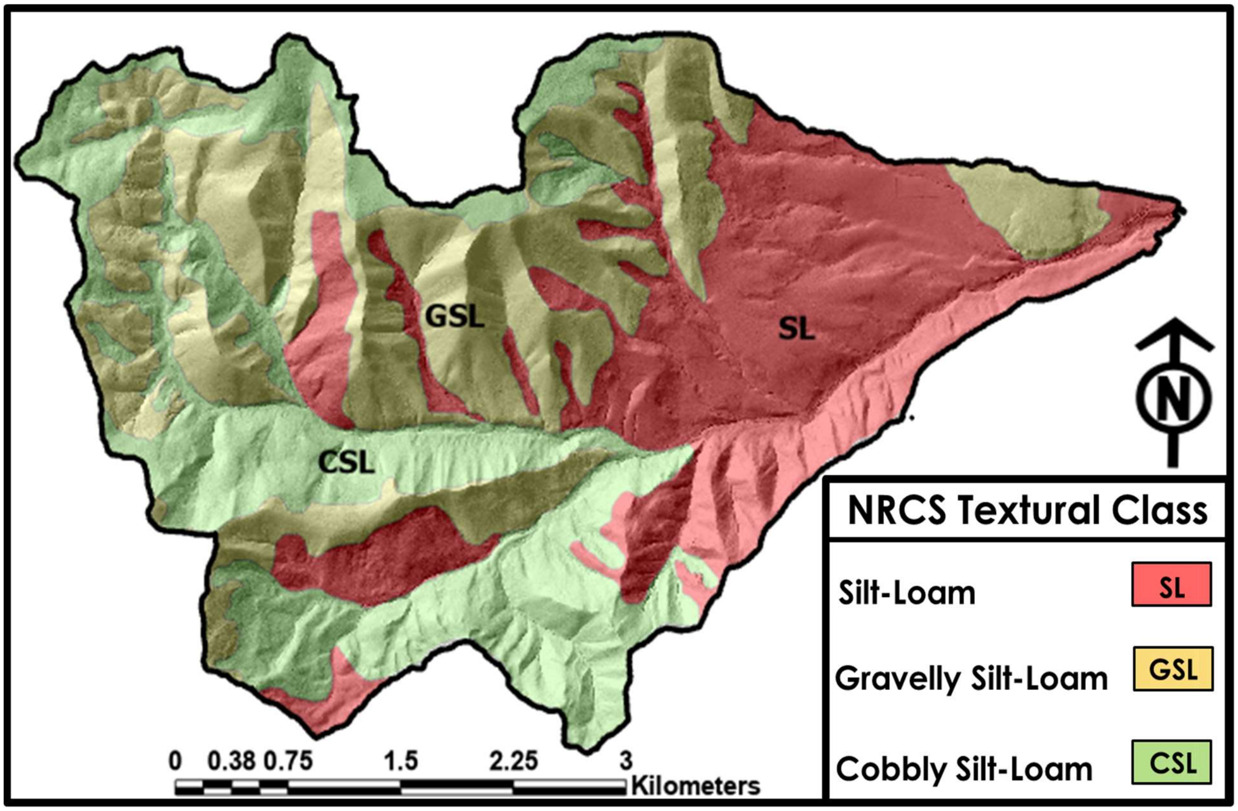

Figure 2.3. Map of soils in the Gibson Jack watershed (modified from NRCS, 2020). Soil series classifications are grouped into three textural classes based on series descriptions (see soil series details in Appendix 3).

2.2.2 Sample Design

Because existing measurements of hydraulic conductivity of streambed sediments have been shown to vary over short distances (Vaux, 1968; Dohman et al., 2021). We sought to characterize the fine-scale variability in Ksat within the stream network at Gibson Jack, then predict values for the entire stream corridor. We used a spatially unbalanced sampling design which has proven helpful in environmental and geostatistical studies, especially when regions of interest are too large, terrain too complicated, or when time/expense becomes a limiting factor for spatially continuous sampling (e.g., Brown et al., 2015). These methods help increase sample efficiency by allowing for uneven sample distances within a series of nests while ensuring ample coverage of the area of interest with representative samples without requiring an extraordinary number of measurements. Following this approach, piezometers were installed near channel heads in each of the tributaries, and then at distances of 0.5, 1, 2, 3, 6, 9, 12, 25, 50, 100, 1000, and 2000 meters below those channel head locations. (Channel head identification is described in section 2.2.3.) Groups of piezometers were also installed every ~2000 meters below these headwater tributaries to the watershed outlet. An additional five wells were installed in areas of interest, such as near springs or seeps that were identified in the field for a total of 194 piezometers (Figure 2.4).

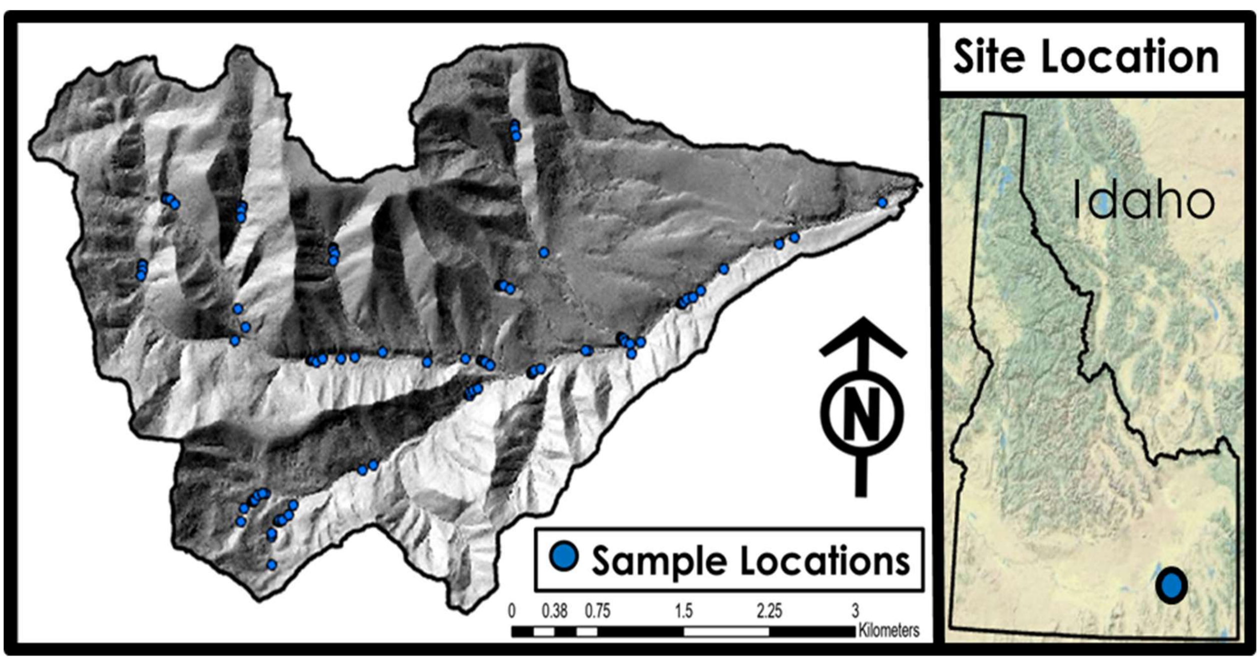

Figure 2.4. Hillshade of the study area with sample locations marked by blue circles.

2.2.3 Well-Drive System Construction, Installation and Development

To accommodate high-frequency sensors that can accurately measure recovery from slug tests, we modified the design of a hand-powered well-drive system (Baxter et al., 2003). This modification was an effective and cost-efficient means of installing removable ~5-cm (I.D.) piezometers in unconsolidated sediments at depths of up to 2 meters. Furthermore, this system can be deployed by a single person via haul pack into remote settings. Well construction consisted of 1.5” schedule 40 PVC cut to 1.5-m lengths and capped using a PVC test cap. Well screens were hand drilled using a 2” ID jig with holes pre-drilled throughout the screened interval at a 1-cm grid spacing, staggered into a repeating diamond pattern. The screened intervals extended from 2 to 22 cm from the bottom of the PVC, with the bottommost 2 cm left unscreened to serve as a tailpipe that allows for sediment accumulation inside the well during development without hindering the performance of the screen during subsequent slug tests.

Using this system, I installed and developed 194 wells at target depths of 0.75 meters throughout the channel network from channel heads to the watershed outlet. Channel head locations were identified in the field by changes in armoring of the streambed, riparian vegetation, and other indicators of surface flow such as flow-deposited debris, in-stream algal mats, and flow-parallel compacted vegetation within the stream channel. Typically, the upstream-most well was installed in the thalweg (Figure 2.5) within 3 m of the identified channel head location; additional wells were then installed at distances up to 2 km downstream from this “channel head well” (as described in section 2.2.2). In the south fork, streambed sediments in the channel head were too shallow to maintain a consistent target depth of 0.75m, so channel head wells for both the south fork tributaries were moved downstream by 100-150 meters to locations where target depths could be consistently achieved. Because piezometers were not immediately tested, streamflow filled any gaps around the piezometers caused through the well installation process by shifting local sediments; however, if there was no streamflow at a particular piezometer, it was developed by pumping at least a 1.5L slug and then validating the seal for consistent slug test performance. This process was repeated at least three times to ensure proper development before later running the slug tests. These methods permitted the installation of 10-15 piezometers/day.

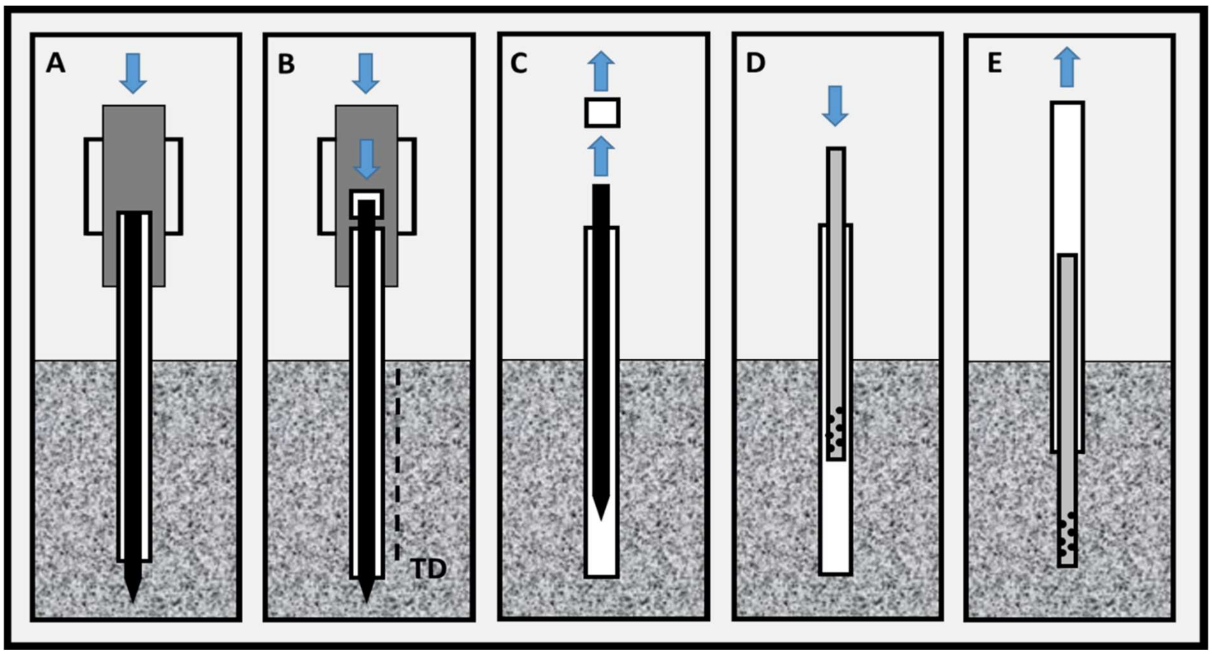

Figure 2.5. Step-by-step instructions for well installation using the well-drive system manufactured for this project: (A) Sleeve driveshaft into drive collar and drive to target depth with a well driver. (B) Put retraction collar on top of drive collar and pound the drive collar down until the top of the drive shaft is exposed. (C) Use a crescent wrench to twist/loosen the driveshaft and pull it out. (D) Put PVC piezometer into drive collar. (E) Use a pipe wrench to spin and lift the drive collar. Use the driveshaft to tamp down the upper surface around the piezometer to close the annular gap and begin well development. These methods were modified from Baxter et al. (2003) to accommodate a 2" ID steel drive collar and hollow driveshaft with

welded solid point and drive cap to depths of 0.75 m. This method was efficient and successfully installed 1.5" ID PVC piezometers in beds with a range of alluvial sediment grain sizes (up to 0.5m boulders). These modifications were necessary to use HOBO pressure transducers to measure the decline in head over time during slug tests. Further details of well-drive system designs appear in Appendix 2.

2.2.3 Slug Tests

After the piezometers had been installed for at least 24 hours, a pressure transducer and paired pressure logger on the adjacent stream bank were deployed to measure water level in each well, corrected for barometric pressure. We performed at least eight repeated falling head tests at each location by adding a 1.25 L slug of water to raise the local water level and measuring the rate at which the water flowed out of the piezometer and returned to the background water level. After performing eight slug tests, pressure data were downloaded and visually assessed to ensure full development and consistent well recovery behavior. If well recovery was inconsistent among the slug tests, we checked well development, returned to the site later if necessary, and repeated the falling head test with at least seven additional slug tests. After completing all tests, the piezometers were extracted and used at the following location. This work was completed in multiple 2-3-day campaigns during the 2020 field season (June-Oct, installation details and test timing for each well are summarized in Appendices 3 and 15).

Initial falling head data was downloaded via Hoboware and then exported into Excel. Log-normalized drawdown was then plotted over time, and the return to static level was visually assessed. Any irregular tests were excluded from the series; these may have occurred due to well development issues, a poor slug addition, or failure to return to near static conditions. Five high-quality falling head tests were typically retained for each location though for a few sites, final calculations were occasionally restricted to 2-4 tests (see Appendix 15); based on these tests, Ksat values were then calculated using the Hvorslev method (Freeze and Cherry, 1979). Mean Ksat and its standard deviation were calculated for all high-quality tests at each sample site. Mean Ksat values were then compared with geomorphic, soil, and lithologic metrics determined within ArcGIS (as described in section 2.2.6).

2.2.5 Stream Drying Data and Analysis

Stream Temperature, Intermittency, and Conductivity (STIC) sensors were deployed at 92 of the piezometer locations throughout the stream network, and water presence/absence data were collected every 15 minutes during the dry season of 2020 (August 19 to October 17) using methods described by Chapin et al. (2014). Seasonal flow permanence was then calculated as a fraction of the timesteps during the field deployment that reflected "flowing" conditions (following Warix et al., 2020). Because there were not enough STIC sensors to measure intermittency at each well location, the most closely spaced wells (wells 0-12.5m) were assumed to have similar wetting and drying behavior. This assumption was validated by spatial analysis of the STIC data (Kindred et al., *personal communication*). Because the distribution of seasonal flow permanence at these STIC locations was bimodal with mostly dry or wet sites during the 2020 season, we categorized each site as "dry" or "wet" based on a threshold of seasonal flow permanence below or above 50% during the study period, and the Ksat values for these categories were then compared.

2.2.6 Digital Mapping and Data Analysis

The watershed boundary and stream network was delineated from a 1m DEM of the study area (NOAA, 2020) using the ArcGIS watershed tool. A 10m buffer around the stream network was then created to represent the stream corridor. Each Ksat measurement location was snapped to the stream network, and its corresponding contributing watershed area, channel slope, elevation, and curvature were determined. A digitized version of the Pocatello South Quadrangle (Link and Stanford, 1999) and digital soils map (NRCS Web Soil Survey, 2021) were used to identify the underlying lithology and soil type at every sample location. We grouped lithologic types into three categories: carbonate-sedimentary, metamorphic-sedimentary, and mixed lithologies. We also grouped NRCS soil classifications into three categories based on textural data. Soil profile descriptions from the target interval of 0.5-0.7cm were grouped by NRCS textural descriptions into silt loam, gravelly silt loam, and cobbly silt loam.

We assessed spatial autocorrelation of the mean Ksat at each location in two ways that accounted for both Euclidean and hydrologic distances. First, for Euclidean distances, we generated an empirical semivariogram that was then used to interpolate Ksat throughout the stream corridor. The semivariogram was generated using ArcPro's Ordinary Kriging tool with first-order detrending; interpolation was performed assuming a standard neighbor type using between two and five neighbors in four sectors oriented at 45 degrees. We then compared the modeled range, nugget, and sill of each model along with the average standard errors and residuals associated with best-fit modeled semivariograms that assumed the following model shapes: Circular, Spherical, Exponential, and Gaussian. We clipped the interpolated Ksat values from the best-fit model to the 10-m stream buffer around the geomorphic channel network.

To assess the effect of Euclidean vs. hydrologic distances on the spatial structure of stream corridor Ksat values, we also used the Stream Statistical Network and STARS packages to create a digital stream network and develop a series of interpolated "tail-up" Ksat models in R (Epanechnikov, Spherical, Exponential, and Gaussian) to assess the spatial structure of the stream corridor Ksat along with the hydrological distance. This package produces a torgegram, which is analogous to a semivariogram except that it measures relationships between points using both hydrological connected and disconnected sites along with the stream corridor. The interpolated results of stream corridor Ksat were then mapped using ArcGIS. The residual standard error values at each sample location were then assessed to select the best model variant.

2.3. Results

Contrary to our expectations for our first hypothesis (H1), we found that Ksat was only autocorrelated at the sub-10m scale instead of at the scale of tens of meters (Figure 2.6a) when interpolated over the entire watershed using Euclidean distances. Because Ksat varied over the study area, our best-fit model included a detrending term from southwest to northeast to ensure first-order stationarity. The resulting semivariogram models showed minor differences among the best-fit models for different model shapes with ranges from 1.8-5.2 m and nuggets of 0.5-1.8 x 10^{-4} cm/s (Table 2.1; full model details in Appendix 5). The root mean square error and the distribution of residuals reveal that the spherical model using Euclidean distances performed best. Interpolated Ksat values based on this model show that saturated hydraulic conductivity varies by three orders of magnitude within the Gibson Jack stream network corridor (Figure 2.6b).

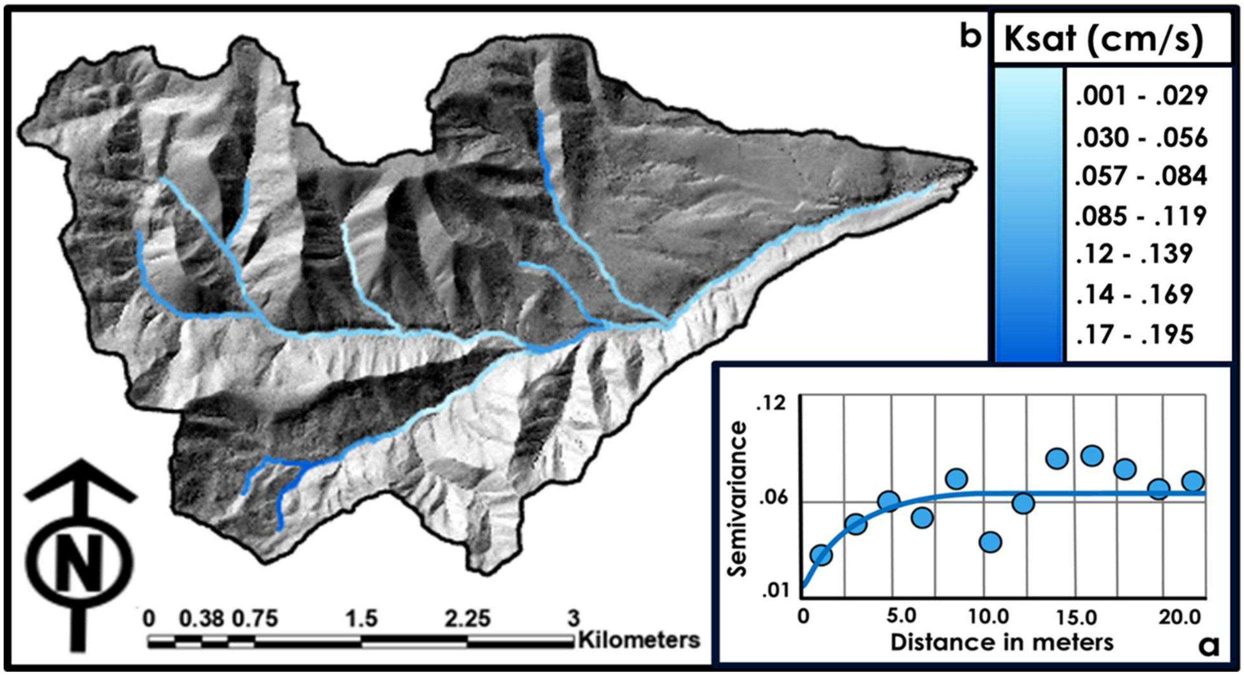

Figure 2.6. (a) Autocorrelation in Ksat in the intermittent stream corridor in Gibson Jack occurs at a single-meter scale within the study area, as evidenced by the separation distance at which the best-fit spherical semivariance reaches its sill. (b) Interpolated stream corridor Ksat values from the best-fit spherical model varied by three orders of magnitude. Because autocorrelation was limited to the single-meter scale, Ksat values vary substantially among reaches within the stream corridor.

Spatial stream network torgegrams using along-network distances instead of Euclidean distances revealed no measurable autocorrelation for all models. All torgegrams showed a large nugget effect regardless of whether flow-connected or flow-unconnected pairs were included (Appendix 10); estimated ranges were on the order of kilometers instead of meters, which was reflected in the interpolated Ksat maps from this approach (Appendix 9). The associated interpolation standard error and cross-validation for each model variation suggested that all models performed poorly (full model details in Appendices 6 and 8). We compared the average standard errors from the cross-validation of ordinary kriging and SSN models and found the errors for the Euclidean best-fit models were smaller than those using along-network distance (0.0250-0.0252 vs. 0.0475-0.0514 cm/s); we note that these errors are all large relative to the average measured Ksat of 0.042 cm/s.

Ordinary Kriging n=194	Circular	Spherical	Gaussian	Exponential
Root-Mean-Square Error (cm/s)	2.51E-02	2.51E-02	2.52E-02	2.50E-02
Range (m)	4.42	1.83	3.56	5.01
SSN n=194	Epanechnikov	Spherical	Mariah	
Residual Standard Error (cm/s)	4.75E-02	5.14E-02	4.96E-02	
Range (m)	2.40E+03	2.81E+02	1.60E+02	

Table 2.1. Summary of results produced using ordinary kriging interpolation performed for circular, spherical, Gaussian and exponential models in ArcGIS as well as the SSN R package using the Epanechnikov, spherical, and Mariah models. Detrending was completed for both analyses using first-order trend removal for the ordinary kriging approach or based on the area draining to each point along the network for SSN. Interpolation and cross-validation were completed using a standard neighborhood with two to five neighbors. These results suggest that the exponential model using the ordinary kriging approach outperformed all other options. The large differences in estimated range between the SSN and ordinary kriging models are surprising.

Contrary to our expectations that geomorphological controls would drive variations in saturated hydraulic conductivity within the stream corridor, our results showed that Ksat varied significantly with lithological and soil, but not geomorphological controls (Figures 2.7-2.10). We found that sites influenced primarily by a carbonate-sedimentary parent lithology had significantly lower Ksat values (p=0.001) than sites influenced by slightly metamorphosed sedimentary parent lithology or mixed lithologies (Figure 2.7). Average metamorphic-sedimentary Ksat was a factor of 2.1x larger than Ksat of wells influenced by carbonate-sedimentary and 2.4x larger than Ksat in wells influenced by mixed lithologies. Pairwise analysis also indicated that there was a significant difference in Ksat among soil textural groupings (p = 0.0272 for SL v. CSL and 0.0314 for GSL v. CSL) (Figure 2.10).

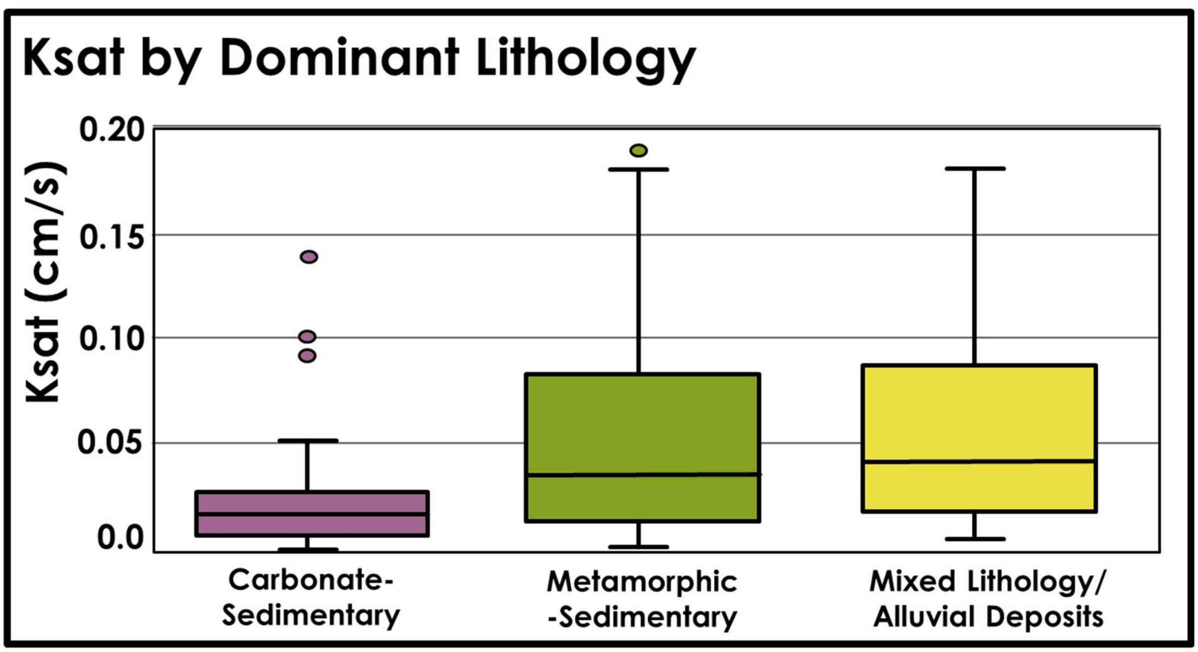

Figure 2.7. Areas with carbonate parent lithology were significantly lower Ksat values than Ksat in areas dominated by metasedimentary and mixed lithology (p-values for carbonates vs. metasedimentary and mixed lithology = 0.0011 and 0.0014, respectively). Ksat values collected in areas where carbonate lithology dominated had a mean value of 0.018 cm/s. In contrast, Ksat

values collected in areas dominated by metamorphic-sedimentary or mixed lithology had mean values of 0.037 and 0.044 cm/s, respectively.

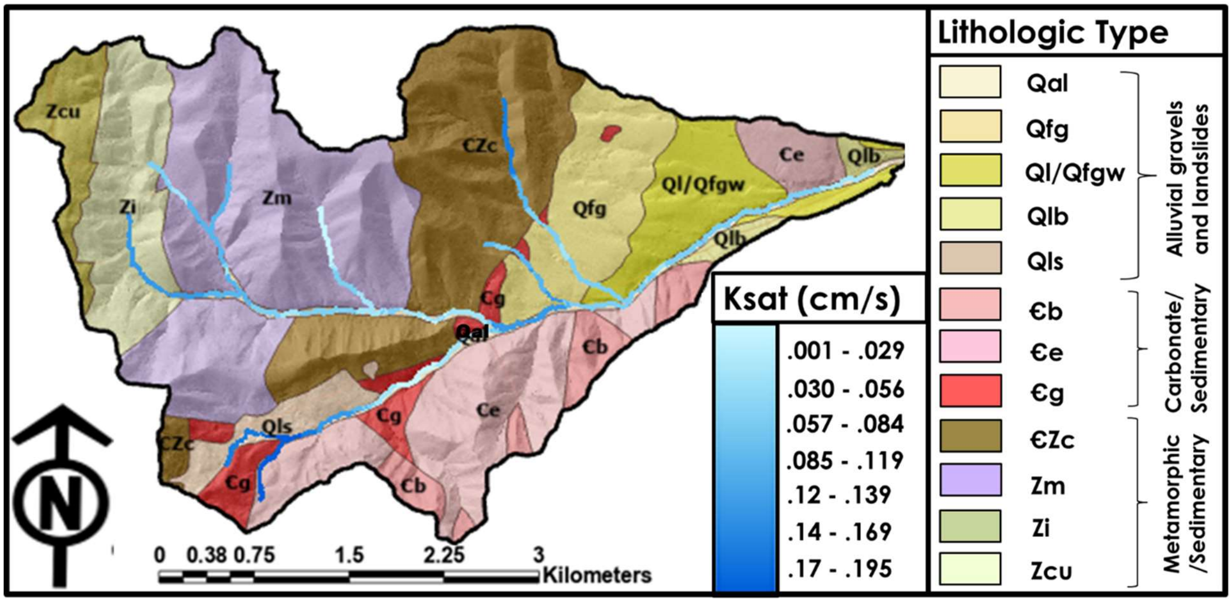

Figure 2.8. Interpolated stream corridor Ksat values overlain on the map of the underlying lithology containing Proterozoic to Cambrian carbonates, as well as sedimentary and metasedimentary units comprised of limestone, shale, sandstone, and quartzite (modified from Rodgers and Othberg, 1999).

Contrary to our expectations (H2), we found no significant relationship between Ksat and any morphometrics such as slope, contributing area, or curvature as indicated by the low R^2 values in Figure 2.9.

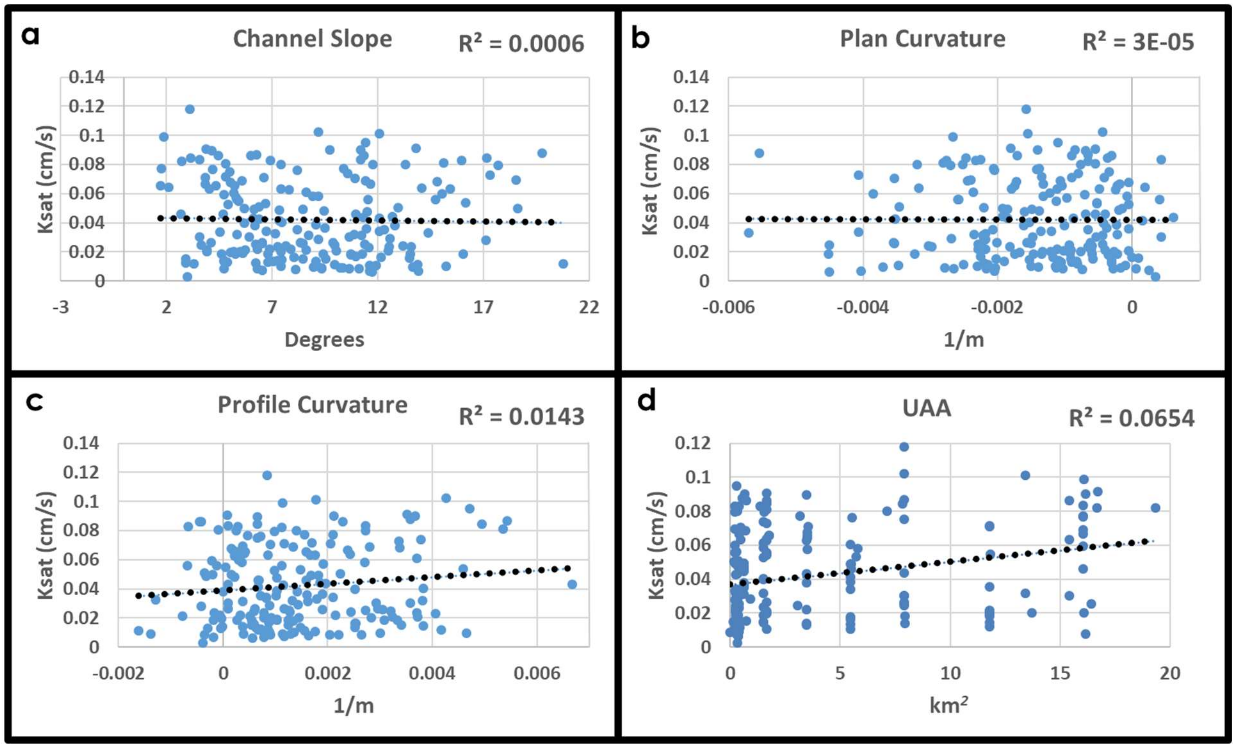

Figure 2.9. The low R^2 values of the (a) slope (b) plan curvature, (c) profile curvature, and (d) upstream accumulation area (UAA) with Ksat indicate a statistically insignificant correlation with geomorphological parameters. A zero value indicates a flat surface in both plan and profile curvature; however, a negative value in profile curvature indicates upward convexity, and a negative value in plan curvature indicates lateral convexity (Patton et al., 2019).

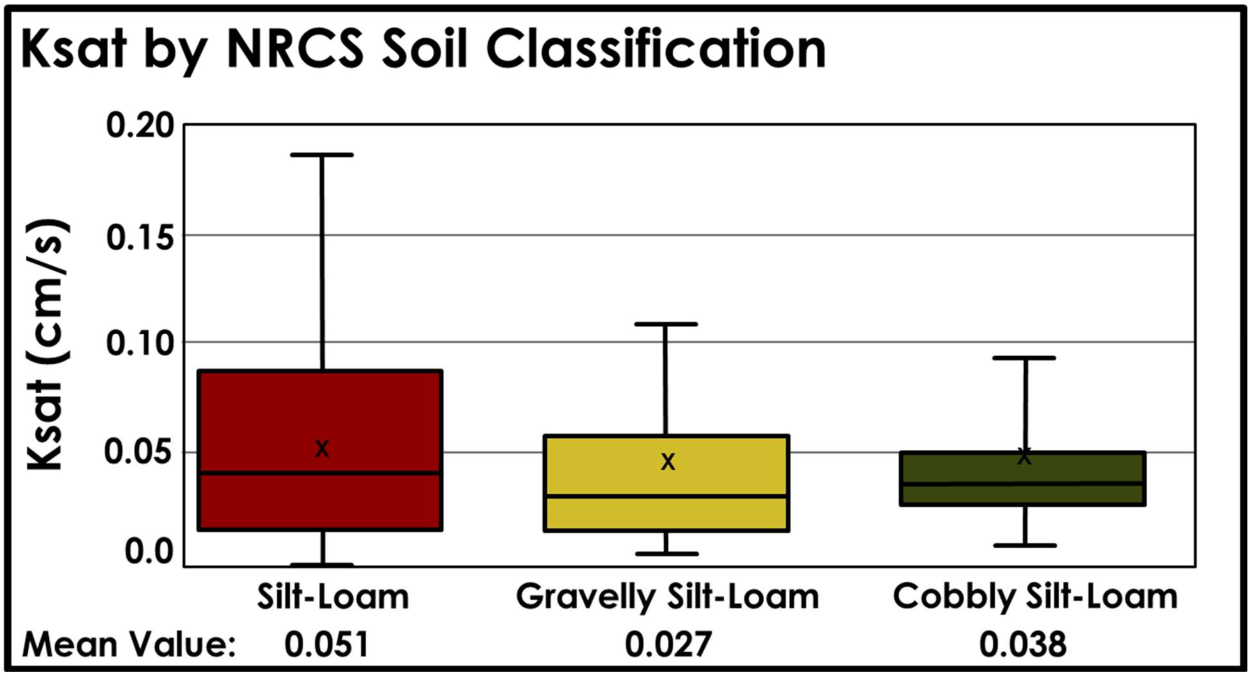

Figure 2.10. Boxplots of Ksat by NRCS soil textural category. Ksat was significantly lower in gravelly silt-loam areas at ~50-70 cm depth compared to silt-loam and cobbly silt-loam (p values of 0.0272 for SL v. CSL and 0.0314 for GSL v. CSL). Gravelly silt-loams had a slightly lower mean Ksat of 0.027 cm/s compared to ~0.038 to 0.051 cm/s in cobbly silt-loam and silt-loam categories, respectively. Detailed soil descriptions can be found in Appendix 4.

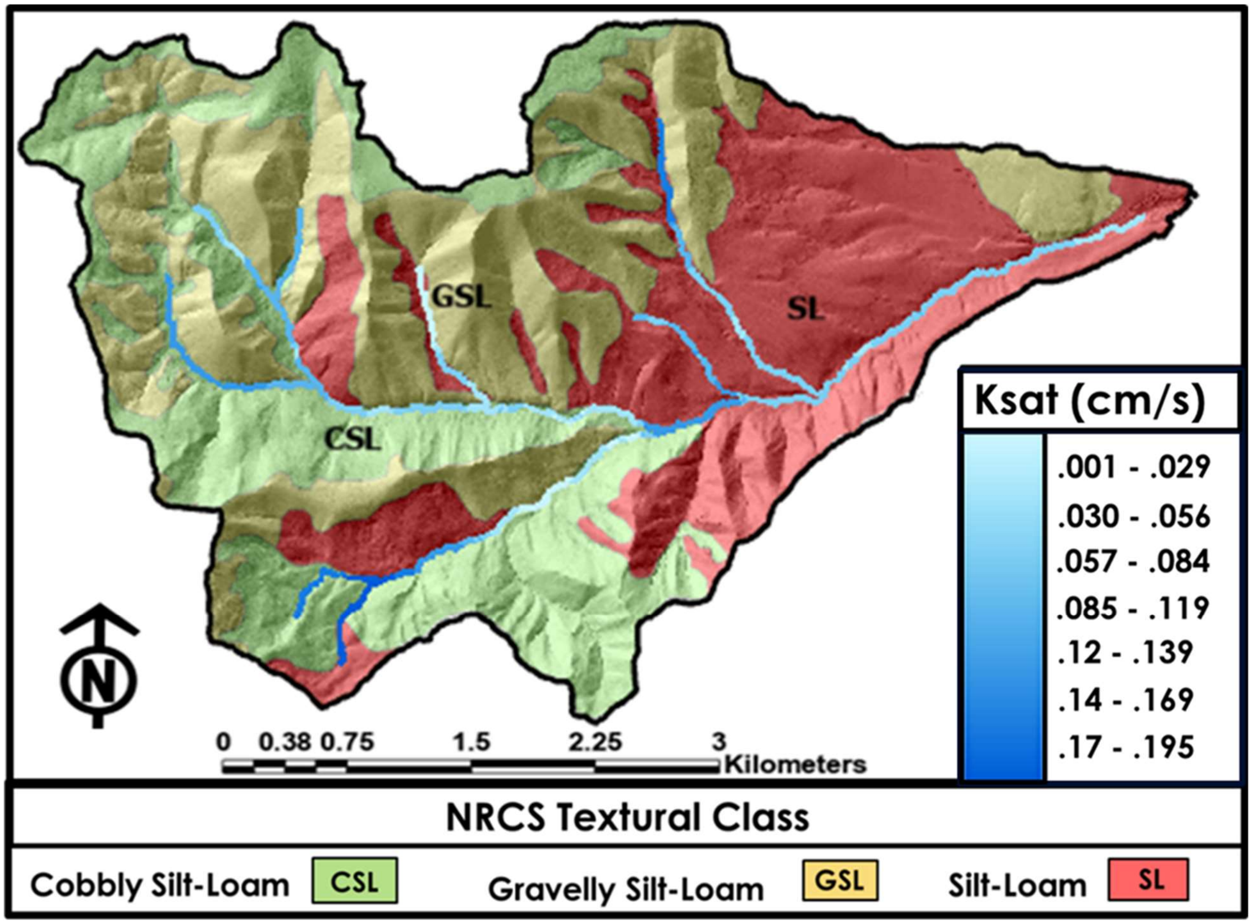

Figure 2.11. Interpolated stream corridor Ksat values overlain on the map of soils in the Gibson Jack watershed (modified from NRCS, 2020). Soil series classifications are grouped into three textural classes based on series descriptions (details in Appendix 4).

We also found that Ksat was significantly lower in perennial than non-perennial reaches in Gibson Jack when testing whether spatial patterns of Ksat covaried with the spatial patterns of seasonal stream drying(*H3)*. Ksat in drier sites exceeded that in wetter sites by a factor of ~2.2 (Figure 2.12).

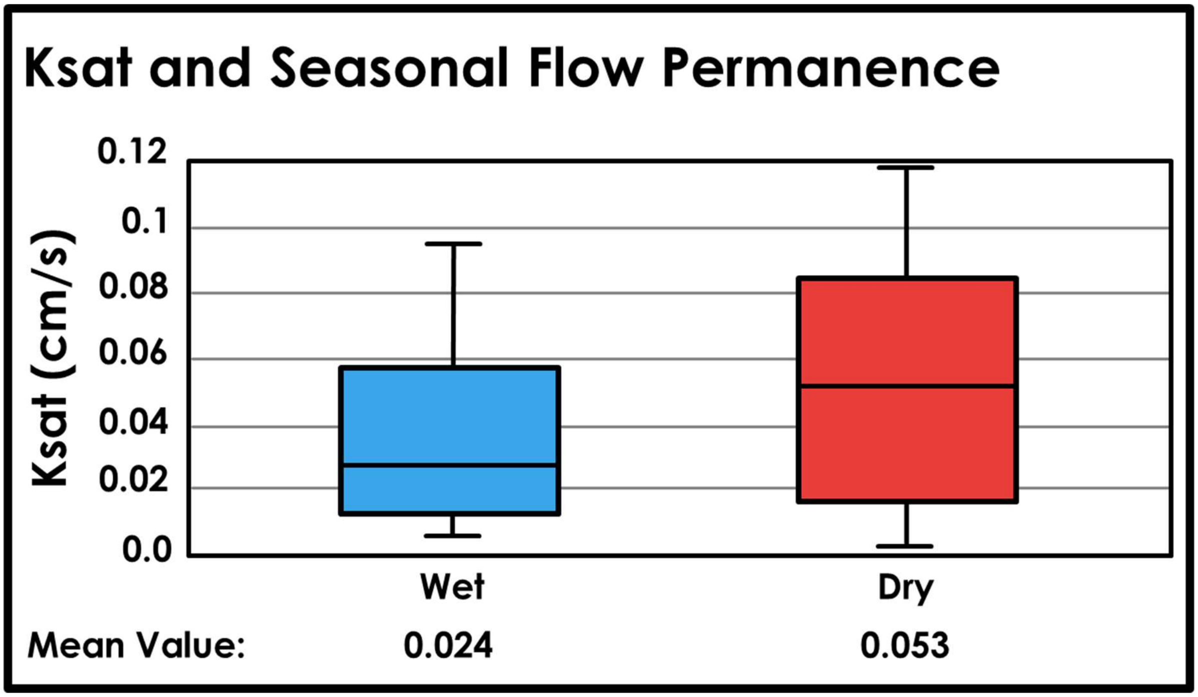

Figure 2.12. Box plots of Ksat by seasonal flow permanence. Ksat was significantly higher ($p=1e^{-6}$) at locations that were dry from August through October 2020.

2.4 Discussion

2.4.1 Coarse- and Fine-scale Patterns and Drivers of Ksat and Drying

We found that Ksat varied at multiple spatial scales, including by >3 orders of magnitude across single meter scales (Figure 2.6a) with lower Ksat in areas dominated by carbonates (Figure 2.7) or gravelly silt loams (Figure 2.10) and in locations that remained flowing most of the period between Aug and Oct 2020 (Figure 2.12). Thus, it is plausible that there are multiple drivers of the different observed scales of variations in Ksat. Geologic controls on surface flow permanence in streams have typically been inferred from existing mapped units that are often available only at relatively coarse resolutions. Those mapped units rarely reflect variations at the fine scales over which Ksat and subsurface hydraulics vary along the stream corridor (Dohman et al., 2021). Our work suggests that that accurately characterizing fine-scale variation may be especially helpful when predicting surface flow disconnections. Thus, models that have assumed a constant Ksat throughout the stream corridor (e.g., Ward et al. 2018) may be missing significant heterogeneity in drying patterns.

The impact of fine-scale variations in Ksat in headwater systems is consistent with modeling results in larger river corridors (Fleckenstein et al., 2006), which assumed Ksat for the hydro-facies of the Laguna-Riverbank complex within the lower Consumes River corridor were autocorrelated at scales of 1.94 to 4.24 meters. Importantly, Fleckenstein et al. (2006) showed that different transition probabilities among hydrofacies could drive significant changes in drying durations and frequencies. This suggests that the observed changes in Ksat throughout headwater systems could correlate with hydrologically distinct spatial patterns of drying.

Our results are consistent with limited Ksat measurements in Dohman et al.'s (2021) work, which found higher Ksat values in two intermittent reaches than in a pair of nearby perennial reaches in the same Gibson Jack watershed. All four study reaches in Dohman et al. (2021) exhibited downward vertical hydraulic gradients, implying that all were losing reaches, with more considerable losses in the sections that dried. By contrast, this more extensive study (n=194) occurred throughout the network and included both gaining and losing reaches. Because most stream networks contain losing reaches (Jasechko et al., 2021), our finding that dry (and likely, losing) reaches tended to have higher Ksat may help explain which locations are likely to dry.

Channel geomorphic features associated with sediment size sorting due to fluvial erosion and deposition in the stream corridor are correlated with Ksat patterns, with higher fluxes through eroded or incised areas (Vaux, 1968; Powell, 1998; Naganna et al., 2017; Abimbola et al., 2020a). Because Ksat values decrease in reaches with valley-fill deposits, especially those with extensive fine sediments, valley-fill deposits may indirectly affect stream intermittency by storing water during wetter periods and then releasing it during dry periods (Floriancic et al., 2019; Warix et al., 2021).

Warix et al. (2021) suggest that characterizing Ksat might improve local seasonal flow permanence models after demonstrating that geomorphic metrics explained about 40% of the variance in seasonal flow permanence. Although we found that Ksat was higher in wetter sites, we could not quantify the effect of changes in Ksat on seasonal flow permanence due to observed bimodal seasonal flow permanence values. However, we did not observe any correlations between geomorphological characteristics and Ksat, so further Ksat measurements in reaches that encompassed the full distribution of stream permanence values might still provide independent information to improve stream permanence predictions.

2.4.2 Spatial Patterns of Ksat in Euclidean vs. Along-Stream Hydrologic Space

It was expected that the spatial stream network (SSN) model would be more appropriate than Euclidean methods for representing the spatial structure in this dataset because the SSN would account for network characteristics, like the potential upstream-downstream influence of sediment transport. Furthermore, alluvial processes that might occur in two tributaries of the same mainstem may not influence Ksat despite being located relatively close together in Euclidean space. However, we found that the SSN models tended to underperform relative to the models in Euclidean space (Table 2.1). It is possible that because underlying lithology was such a strong driver of Ksat (Figure 2.7) and because points in neighboring tributaries were often more lithologically similar than those found along hydrologically connected sites (Figure 2.8), ordinary kriging techniques in Euclidean space were more accurate than SSN models. These findings are consistent with Durighetto et al. (2020), which identified that the heterogeneity of bedrock properties and parent material impacted the structure of the active drainage network. Furthermore, Euclidean distances may better represent patterns in stream corridor Ksat as parent lithologic unit weathering, fracturing, soil development, and erosion patterns may affect subsurface transport capacity throughout the watershed rather than only in the stream corridor, allowing subterranean flow along fractures, macropores, or in bedrock-confined regions.

2.4.3 Potential Ksat Variations with Time

Within heterogeneous streambed deposits, fine sediments exert more control on Ksat values than coarse fractions (Stewardson et al., 2016), and their deposition and transport are more sensitive to changes in flow. In addition to the variations in space that have been explored here, Ksat values have been shown to vary in time due to the expansion and contraction of clays (Oosterbaan and Nijland, 1994; Powell, 1998) or the erosion and deposition of sediments. Channel migration, erosion, and deposition have been shown to change substrate properties such as Ksat, and stream corridor Ksat values tend to decrease with time since disturbance (Stewardson et al., 2016; Abimbola et al., 2020b). Future work would benefit from exploring changes in Ksat over drydown and rewetting of different portions of the stream network.

Such changes with flow could be large; for example, Blasch et al. (2007) observed that streambed Ksat varied by four orders of magnitude due to sediment redistribution during and after storm events. High suspended loads are correlated with low streambed Ksat values due to colmation or the entrapment of fine-grained sediments or precipitation of solutes such as calcium carbonate within the armored layer (Gomez, 1983; Powell, 1998; Blasch et al., 2007; Stewardson et al., 2016). These trapped fine sediments can potentially be scoured during peaks in discharge. Though we only measured Ksat at one moment in time, streambed changes due to flow are unlikely to have affected the spatial patterns presented here because of limited storm activity during the field season. Still, repeated Ksat measurements from longer term piezometer installations might help explain local trends in drying patterns.

2.5 Conclusions

Channel migration, layered sedimentary deposition, and additions of organic soil material within fluvial environments contribute to spatial heterogeneity within fluvial sedimentary structures (Oosterbaan and Nijland, 1994; Landon et al., 2001; Wu et al., 2016). Because of the growing recognition that processes in the stream corridor extend well below and adjacent to stream channels and beds (National Research Council, 2002), the importance of accurate characterization of lateral and horizontal variations in subsurface properties has received growing attention (Baxter et al., 2003; Wondzell, 2011; Godsey and Kirchner, 2014; Wu et al., 2016; Dohman et al., 2021; Warix et al., 2021). Horizontal variation can be characterized both laterally across the channel corridor from bank to bank and longitudinally along the stream network. I focused my efforts in this thesis on characterizing longitudinal variations.

Unlike surficially observed properties such as slope, curvature, and surficial geology, subsurface properties such as hydraulic conductivity remain challenging to accurately characterize. More efficient methods for obtaining subsurface field measurements and interpolating those datasets throughout the stream corridor are still needed. To begin to meet that need, the results of this thesis were acquired using a scaled-up and modified version of a dual-tube well-drive system as described by Baxter et al. (2003). This inexpensive equipment is easily manufactured and has effectively installed ~300 piezometers; the approach has been adopted into the standard operating procedures for the National Science Foundation's Aquatic Intermittency effects on Microbiomes in Streams (AIMS) project. This equipment has achieved target depths of up to two meters in unconsolidated sediments that range from silts to boulders and can feasibly be transported via haul pack into remote, roadless settings.

Falling head tests throughout one non-perennial headwater stream network in the northern Rocky Mountains, Idaho, USA, revealed that the hydraulic conductivity of stream corridor sediments at a consistent depth interval of 50-75 cm varied by approximately three orders of magnitude throughout the network. Stream corridor Ksat values are correlated at the single-meter range or spatial scales finer than most geologic mapping. Ksat was higher in reaches that remained drier than average throughout the field season. Together, this suggests that spatially dense Ksat measurements may be necessary to predict fine-scale seasonal streamflow permanence. Conversely, streamflow permanence may be easier to observe than Ksat; indeed, observations of seasonal flow permanence may be helpful to constrain spatial patterns of Ksat, especially if remotely sensed flow permanence observations become available (Warix, 2020).

2.6 References Cited:

Abimbola, O.P., Mittelstet, A.R., and Gilmore, T.E., 2020a, Geostatistical features of streambed vertical hydraulic conductivities in Frenchman Creek Watershed in Western Nebraska: Hydrological Processes, v. 34, p. 3481–3491, doi:10.1002/hyp.13823.

Abimbola, O.P., Mittelstet, A.R., Gilmore, T.E., and Korus, J.T., 2020b, Influence of watershed characteristics on streambed hydraulic conductivity across multiple stream orders: Scientific Reports, v. 10, p. 1–11, doi:10.1038/s41598-020-60658-3.

Allen, D.C. et al., 2020, River ecosystem conceptual models and non-perennial rivers: A critical review: Wiley Interdisciplinary Reviews: Water, v. 7, p. 1–13, doi:10.1002/wat2.1473.

Baxter, C. V., and Hauer, F.R., 2000, Geomorphology, hyporheic exchange, and selection of spawning habitat by bull trout (*Salvelinus confluentus*): Canadian Journal of Fisheries and Aquatic Sciences, v. 57, p. 1470–1481, doi:10.1139/cjfas-57-7-1470.

Baxter, C., Hauer, F.R., and Woessner, W.W., 2003, Measuring groundwater –new techniques for installing minipiezometers and estimating hydraulic conductivity: Transactions of the American Fisheries Society, v. 132, p. 493–502, doi:10.1577/1548-8659(2003)132<0493.

Bencala, K.E., and Walters, R.A., 1983, Simulation of solute transport in a mountain pool-and-riffle stream: A transient storage model: Water Resources Research, v. 19, p. 718–724, doi:10.1029/WR019i003p00718.

Blasch, B.K.W., Constantz, J., and Stonestrom, D.A., 2007, Thermal methods for investigating ground-water recharge: USGS Professional Paper 1703, p. 353–375, https://pubs.usgs.gov/pp/pp1703/app1/.

Bolstad, P., 2002, GIS Fundamentals: St. Paul MN, Elder Press, 676 p., doi:10.1201/9781315380568.

Botter, G., and Durighetto, N., 2020, The stream length duration curve: A tool for characterizing the time variability of the flowing stream length: Water Resources Research, v. 56, doi:10.1029/2020WR027282.

Boulton, A.J., Findlay, S., Marmonier, P., Stanley, E.H., and Maurice Valett, H., 1998, The functional significance of the hyporheic zone in streams and rivers: Annual Review of Ecology and Systematics, v. 29, p. 59–81, doi:10.1146/annurev.ecolsys.29.1.59.

Brown, J.A., Robertson, B.L., and McDonald, T., 2015, Spatially Balanced Sampling: Application to environmental surveys: Procedia Environmental Sciences, v. 27, p. 6–9, doi:10.1016/j.proenv.2015.07.108.

Busch, M.H. et al., 2020, What's in a name? Patterns, trends, and suggestions for defining non-perennial rivers and streams: Water (Switzerland), v. 12, doi:10.3390/w12071980.

Butler, J.J., 1998, The Design, Performance, and Analysis of Slug Tests: Washington, D.C., Lewis Publishers, 240 p., doi:10.1201/9781482229370.

Cahn, M.A., Kamieniecki, S., and McCain-Tharnstrom, D., 2007, Bureaucracy, politics, and environmental policy in the American west, *in* Environmental Politics and Policy, Revised Edition, University Press, p. 19–47.

Capurso, J. et al., 2010, Lower Portneuf Watershed Analysis:, http://www.fs.usda.gov/Internet/FSE_DOCUMENTS/stelprdb5406258.pdf.

Cardenas, M.B., Wilson, J.L., and Zlotnik, V.A., 2004, Impact of heterogeneity, bed forms, and stream curvature on subchannel hyporheic exchange: Water Resources Research, v. 40, p. 1–14, doi:10.1029/2004WR003008.

Cooper, H.H., Bredehoeft, J.D., and Papadopulos, I.S., 1967, Response of a finite-diameter well to an instantaneous charge of water: Water Resources Research, v. 3, p. 9, doi:10.1029/WR003i001p00263.

Cornell, J.J., 2013, An investigation of the effects of recreational land use on the stream ecosystem of an urban-fringe watershed: Idaho State, 64 p., doi:ocn922975754.

Costigan, K.H., Jaeger, K.L., Goss, C.W., Fritz, K.M., and Goebel, P.C., 2016, Understanding controls on flow permanence in intermittent rivers to aid ecological research: integrating meteorology, ge: Ecohydrology, v. 9, p. 13, doi:10.1002/eco.1712.

Datry, T., Fritz, K., and Leigh, C., 2016, Challenges, developments and perspectives in intermittent river ecology: Freshwater Biology, v. 61, p. 1171–1180, doi:10.1111/fwb.12789.

Datry, T., Larned, S.T., and Tockner, K., 2014, Intermittent rivers: A challenge for freshwater ecology: BioScience, v. 64, p. 229–235, doi:10.1093/biosci/bit027.

Dent, C.L., and Grimm, N.B., 1999, Spatial heterogeneity of stream water nutrient concentrations over successional time: Ecology, v. 80, p. 2283–2298, doi:10.1890/0012-9658(1999)080[2283:SHOSWN]2.0.CO;2.

Department of Defense, 2020, The Navigable Waters Protection Rule: Definition of "Waters of the United States":, https://www.federalregister.gov/documents/2020/04/21/ 2020-02500/the-navigable-waters-protection-rule-definition-of-waters-of-theunited-states. Accessed 15 October 2020.

Dohman, J.M., Godsey, S.E., and Hale, R.L., 2021, Three-Dimensional Subsurface Flow Path Controls on Flow Permanence: Water Resources Research, v. 57, p. 1–18, doi:10.1029/2020wr028270.

Downing, J.A., Cole, J.J., Duarte, C.M., Middelburg, J.J., Melack, J.M., Prairie, Y.T., Kortelainen, P., Striegl, R.G., McDowell, W.H., and Tranvik, L.J., 2012, Global abundance and size distribution of streams and rivers: Inland Waters, v. 2, p. 229–236, doi:10.5268/IW-2.4.502.

Durighetto, N., Vingiani, F., Bertassello, L.E., Camporese, M., and Botter, G., 2020, Intraseasonal drainage network dynamics in a headwater catchment of the Italian Alps: Water Resources Research, v. 56, doi:10.1029/2019WR025563.

Eng, K., Carlisle, D.M., Grantham, T.E., Wolock, D.M., and Eng, R.L., 2019, Severity and extent of alterations to natural streamflow regimes based on hydrologic metrics in the conterminous United States, 1980–2014: U.S. Geological Survey Scientific Investigations Report 2019–5001, p. 25.

Eng, K., Wolock, D.M., and Dettinger, M.D., 2015, Sensitivity of Intermittent Streams to Climate Variations in the USA: River Research and Applications, v. 30, p. 132–133, doi:10.1002/rra.

Evenden, A.G., Moeur, M., Shelly, J.S., Kimball, S.F., and Wellner, C.A., 2001, Research Natural Areas in Idaho, Montana, Nevada, Utah, and Western Wyoming: A guidebook for scientists, managers, and educators: United States Department of Agriculture, 89 p., https://www.fs.fed.us/rm/pubs/rmrs_gtr069.pdf.

Fesenmyer, K.A., Wenger, S.J., Leigh, D.S., and Neville, H.M., 2021, Large portion of USA streams lose protection with new interpretation of clean water act: Freshwater Science, v. 40, p. 252–258, doi:10.1086/713084.

Fleckenstein, J.H., Niswonger, R.G., and Fogg, G.E., 2006, River-aquifer interactions, geologic heterogeneity, and low-flow management, *in* Ground Water, doi:10.1111/j.1745-6584.2006.00190.x.

Floriancic, M.G., Fischer, B.M.C., Molnar, P., Kirchner, J.W., and van Meerveld, I.H.J., 2019, Spatial variability in specific discharge and streamwater chemistry during low flows: Results from snapshot sampling campaigns in eleven Swiss catchments: Hydrological Processes, v. 33, p. 2847–2866, doi:10.1002/hyp.13532.

Freeze, R.A., and Cherry, J.A., 1979, Groundwater (Cathy Brenn, Ed.): Englewood Cliffs, New Jersey, Prentice-Hall. Inc, 671 p., http://library1.nida.ac.th/termpaper6/sd/2554/19755.pdf.

Gendaszek, A.S., Dunham, J.B., Torgersen, C.E., Hockman-Wert, D.P., Heck, M.P., Thorson, J., Mintz, J., and Allai, T., 2020, Land-cover and climatic controls on water temperature, flow permanence, and fragmentation of Great Basin stream networks: Water (Switzerland), v. 12, doi:10.3390/w12071962.

Genereux, D.P., Leahy, S., Mitasova, H., Kennedy, C.D., and Corbett, D.R., 2008, Spatial and temporal variability of streambed hydraulic conductivity in West Bear Creek, North Carolina, USA: Journal of Hydrology, v. 358, p. 332–353, doi:10.1016/j.jhydrol.2008.06.017.

Godsey, S.E., and Kirchner, J.W., 2014, Dynamic, discontinuous stream networks: Hydrologically driven variations in active drainage density, flowing channels and stream order: Hydrological Processes, v. 28, p. 5791–5803, doi:10.1002/hyp.10310.

Gomez, B., 1983, Temporal variations in bedload transport rates: The effect of progressive bed armoring: Earth Surface Processes and Landforms, v. 8, p. 41–54, doi:https://doi.org/10.1002/ESP.3290080105.

Gooseff, M.N., Anderson, J.K., Wondzell, S.M., LaNier, J., and Haggerty, R., 2005, A modelling study of hyporheic exchange pattern and the sequence, size, and spacing of stream bedforms in mountain stream networks, Oregon, USA: Hydrological Processes, v. 19, p. 2915–2929, doi:10.1002/hyp.5790.

Hafen, K.C., Blasch, K.W., Rea, A., Sando, R., and Gessler, P.E., 2020a, The influence of climate variability on the accuracy of NHD perennial and nonperennial stream classifications: Journal of the American Water Resources Association, v. 56, p. 903–916, doi:10.1111/1752-1688.12871.

Hafen, K.C., Blasch, K.W., Rea, A., Sando, R., and Gessler, P.E., 2020b, The Influence of climate variability on the accuracy of NHD perennial and nonperennial stream classifications: Journal of the American Water Resources Association, v. 56, p. 903–916, doi:10.1111/1752-1688.12871.

Hahm, W.J., Rempe, D.M., Dralle, D.N., Dawson, T.E., Lovill, S.M., Bryk, A.B., Bish, D.L., Schieber, J., and Dietrich, W.E., 2019, Lithologically Controlled Subsurface Critical Zone Thickness and Water Storage Capacity Determine Regional Plant Community Composition: Water Resources Research, v. 55, p. 3028–3055, doi:10.1029/2018WR023760.

Hale, R.L., and Godsey, S.E., 2019, Dynamic stream network intermittence explains emergent dissolved organic carbon chemostasis in headwaters: Hydrological Processes, v. 33, p. 1926–1936, doi:10.1002/hyp.13455.

Hammond, J.C. et al., 2021, Spatial patterns and drivers of nonperennial flow regimes in the contiguous United States: Geophysical Research Letters, v. 48, doi:10.1029/2020GL090794.

Harvey, J.W., and Gooseff, M.N., 2015, Consequences from bedforms to basins: Water Resources Research, v. 51, p. 6893–6922, doi:10.1002/2015WR017617.

Ver Hoef, J.M., Peterson, E.E., Clifford, D., and Shah, R., 2014, SSN: An R package for spatial statistical modeling on stream networks: Journal of Statistical Software, v. 56, ftp://sunsite2.icm.edu.pl/packages/cran/web/packages/SSN/vignettes/SSN.pdf%0Apapers3://publication/uuid/EEF33D01-D2EF-4967-99B7-C3ADF58B4183.

Hvorslev, M.J., 1951, Time lag and soil permeability in groundwater observations: No. 36. Waterways Experiment Station, Corps of Engineers, US Army, http://hdl.handle.net/2027/mdp.39015086510958 .

Jaeger, K.L., 2021, Most rivers and streams run dry every year: Nature, v. 594, p. 335–336, doi:10.1038/d41586-021-01528-4.
111, p. 13894–13899, doi:10.1073/pnas.1320890111.

Jaeger, K.L., Sando, R., McShane, R.R., Dunham, J.B., Hockman-Wert, D.P., Kaiser, K.E., Hafen, K., Risley, J.C., and Blasch, K.W., 2019, Probability of Streamflow Permanence Model (PROSPER): A spatially continuous model of annual streamflow permanence throughout the Pacific Northwest: Journal of Hydrology X, v. 2, p. 100005, doi:10.1016/j.hydroa.2018.100005.

Jasechko, S., Seybold, H., Perrone, D., Fan, Y., and Kirchner, J.W., 2021, Widespread potential loss of streamflow into underlying aquifers across the USA: Nature, v. 591, p. 391–395, doi:10.1038/s41586-021-03311-x.

Kondolf, G.M., Montgomery, D.R., Piégay, H., and Schmitt, L., 2005, Geomorphic Classification of Rivers and Streams: v. 9, 171–204 p., doi:10.1002/0470868333.ch7.

Krause, S., M., H.D., Fleckenstein, J.H., Heppell, C.M., Kaeser, D., Pickup, R., Pinay, G., Robertson, A.L., and Wood, P.J., 2010, Inter-disciplinary perspectives on processes in the hyporheic zone: Ecohydrology, v. 130, p. 126–130, doi:10.1002/eco.

Landon, M.K., Rus, D.L., and Edwin Harvey, F., 2001, Comparison of instream methods for measuring hydraulic conductivity in sandy streambeds: Ground Water, v. 39, p. 870–885, doi:10.1111/j.1745-6584.2001.tb02475.x.

Lapides, D.A., Leclerc, C.D., Moidu, H., Dralle, D.N., and Hahm, W.J., 2021, Variability of stream extents controlled by flow regime and network hydraulic scaling: Hydrological Processes, v. 35, p. 1–17, doi:10.1002/hyp.14079.

Larned, S.T., Datry, T., Arscott, D.B., and Tockner, K., 2010, Emerging concepts in temporary-river ecology: Freshwater Biology, v. 55, p. 717–738, doi:10.1111/j.1365-2427.2009.02322.x.

Leek, R., Wu, J.Q., Wang, L., Hanrahan, T.P., Barber, M.E., and Qiu, H., 2010, Heterogeneous characteristics of streambed saturated hydraulic conductivity of the Touchet River, Southeastern Washington, USA: Hydrological Processes, v. 2274, p. 2267–2274, doi:10.1002/hyp.

Leibowitz, S.G., Wigington, P.J., Rains, M.C., and Downing, D.M., 2008, Non-navigable streams and adjacent wetlands: Addressing science needs following the Supreme Court's Rapanos decision: Frontiers in Ecology and the Environment, v. 6, p. 364–371, doi:10.1890/070068.

Leigh, C., Boulton, A.J., Courtwright, J.L., Fritz, K., May, C.L., Walker, R.H., and Datry, T., 2016, Ecological research and management of intermittent rivers: A historical review and future directions: Freshwater Biology, v. 61, p. 1181–1199, doi:10.1111/fwb.12646.

Li, J., and Heap, A.D., 2008, A review of spatial interpolation methods for environmental scientists: Journal of Public Health Management and Practice, v. 16, p. S5–S10, doi:10.1097/phh.0b013e3181e31d09.

Libohova, Z., Schoeneberger, P., Bowling, L.C., Owens, P.R., Wysocki, D., Wills, S., Williams, C.O., and Seybold, C., 2018, Soil systems for upscaling saturated hydraulic conductivity for hydrological modeling in the critical zone: Vadose Zone Journal, v. 17, p. 170051, doi:10.2136/vzj2017.03.0051.

Lovill, S.M., Hahm, W.J., and Dietrich, W.E., 2018, Drainage from the critical zone: lithologic controls on the persistence and spatial extent of wetted channels during the summer dry season: Water Resources Research, v. 54, p. 5702–5726, doi:10.1029/2017WR021903.

MacNeille, R.B., Lohse, K.A., Godsey, S.E., and Perdrial, J.N., 2020, Influence of drying and wildfire on longitudinal chemistry patterns and processes of intermittent streams: v. 2, doi:10.3389/frwa.2020.563841.

Manfredo, M.J., Teel, T.L., and Bright, A.D., 2003, Why are public values toward wildlife changing? Human Dimensions of Wildlife, v. 8, p. 287–306, doi:10.1080/716100425.

Van Meerveld, I.H.J., Kirchner, J.W., Vis, M.J.P., Assendelft, R.S., and Seibert, J., 2019, Expansion and contraction of the flowing stream network alter hillslope flow path lengths and the shape of the travel time distribution: Hydrology and Earth System Sciences, v. 23, p. 4825–4834, doi:10.5194/hess-23-4825-2019.

Ver Hoef, J.M., Peterson, E.E., and Isaak, D.J., 2019, Spatial statistical models for stream networks: Handbook of Environmental and Ecological Statistics, p. 421–444, doi:10.1201/9781315152509-20.

Messager, M.L., Lehner, B., Cockburn, C., Lamouroux, N., Pella, H., Snelder, T., Tockner, K., Trautmann, T., Watt, C., and Datry, T., 2021, Global prevalence of non-perennial rivers and streams: Nature, v. 594, p. 391–397, doi:10.1038/s41586-021-03565-5.

Nadeau, T.L., and Rains, M.C., 2007, Hydrological connectivity between headwater streams and downstream waters: How science can inform policy: Journal of the American Water Resources Association, v. 43, p. 118–133, doi:10.1111/j.1752-1688.2007.00010.x.

Naganna, S.R., Deka, P.C., Ch, S., and Hansen, W.F., 2017, Factors influencing streambed hydraulic conductivity and their implications on stream–aquifer interaction: a conceptual review: Environmental Science and Pollution Research, v. 24, p. 24765–24789, doi:10.1007/s11356-017-0393-4.

National Research Council, 2002, Riparian Areas: Functions and Strategies for Management:, doi:10.17226/10327.

Obedzinski, M., Nossaman Pierce, S., Horton, G.E., and Deitch, M.J., 2018, Effects of flow-related variables on over summer survival of juvenile Coho Salmon in intermittent streams: Transactions of the American Fisheries Society, doi:10.1002/tafs.10057.

Oosterbaan, R., and Nijland, H., 1994, Determining the saturated hydraulic conductivity: Drainage Principles and Applications, p. 37, http://www.waterlog.info/pdf/chap12.pdf.

Osier, T.A., 2004, The Neogene-Quaternary topographic development of the Portneuf Valley, Bannock County, Southeast Idaho: Idaho State.

Pate, A.A., Segura, C., and Bladon, K.D., 2020, Streamflow permanence in headwater streams across four geomorphic provinces in Northern California: Hydrological Processes, v. 34, p. 4487–4504, doi:10.1002/hyp.13889.

Patton, N.R., Lohse, K.A., Seyfried, M.S., Godsey, S.E., and Parsons, S.B., 2019, Topographic controls of soil organic carbon on soil-mantled landscapes: Scientific Reports, v. 9, p. 1–15, doi:10.1038/s41598-019-42556-5.

Payn, R.A., Gooseff, M.N., McGlynn, B.L., Bencala, K.E., and Wondzell, S.M., 2012, Exploring changes in the spatial distribution of stream baseflow generation during a seasonal recession: Water Resources Research, v. 48, doi:10.1029/2011WR011552.

Peterson, E.E., and Ver Hoef, J.M., 2010b, A mixed-model moving-average approach to geostatistical modeling in stream networks: Ecology, v. 91, p. 644–651, doi:10.1890/08-1668.1.

Pliakas, F., and Petalas, C., 2011, Determination of hydraulic conductivity of unconsolidated river alluvium from permeameter tests, empirical formulas and statistical parameters effect analysis: Water Resources Management, v. 25, p. 2877–2899, doi:10.1007/s11269-011-9844-8.

Powell, M.D., 1998, Patterns and processes of sediment sorting in gravel-bed rivers: Progress in Physical Geography, v. 22, p. 1–32, doi:10.1191/030913398666402127.

Prancevic, J.P., and Kirchner, J.W., 2019, Topographic Controls on the Extension and Retraction of Flowing Streams: Geophysical Research Letters, doi:10.1029/2018GL081799.

Rodgers, D., and Othberg, K., 1999, Geologic map of the Pocatello South Quadrangle, Bannock and Power Counties, Idaho: Idaho Geological Survey, p. 2, https://www.idahogeology.org/pub/Maps/Geologic_Maps/PDF/GM-26-m.pdf.

Rodríguez-Lozano, P., Woelfle-Erskine, C., Bogan, M.T., and Carlson, S.M., 2020, Are non-perennial rivers considered as valuable and worthy of conservation as perennial rivers? Sustainability (Switzerland), v. 12, p. 1–12, doi:10.3390/su12145782.

Sando, R. et al., 2017, Mapping and modeling the annual probability of year-round streamflow, *in* Rocky Mountain Partner Forum, p. 66, greatnorthernlcc.org/document/webinar-slides-mapping-and-modeling-annual-probability-year-round-streamflow-2004-2016-case.

Schilling, O.S., Cook, P.G., Grierson, P.F., Dogramaci, S., and Simmons, C.T., 2021, Controls on interactions between surface water, groundwater, and riverine vegetation along intermittent rivers and ephemeral streams in arid regions: Water Resources Research, v. 57, p. 1–21, doi:10.1029/2020WR028429.

Som, N.A., Monestiez, P., Ver Hoef, J.M., Zimmerman, D.L., and Peterson, E.E., 2014, Spatial sampling on streams: Principles for inference on aquatic networks: Environmetrics, v. 25, p. 306–323, doi:10.1002/env.2284.

Steward, A.L., Von Schiller, D., Tockner, K., Marshall, J.C., and Bunn, S.E., 2012, When the river runs dry: Human and ecological values of dry riverbeds: Frontiers in Ecology and the Environment, v. 10, p. 202–209, doi:10.1890/110136.

Stewardson, M.J., Datry, T., Lamouroux, N., Pella, H., Thommeret, N., Valette, L., and Grant, S.B., 2016, Variation in reach-scale hydraulic conductivity of streambeds: Geomorphology, v. 259, p. 70–80, doi:10.1016/j.geomorph.2016.02.001.

Tooth, S., 2000, Process, form and change in dryland rivers: A review of recent research: Earth Science Reviews, v. 51, p. 67–107, doi:10.1016/S0012-8252(00)00014-3.

Toth, J., 1962, A theory of groundwater motion in small drainage basins in central Alberta, Canada: Journal of Geophysical Research, v. 67, p. 4375–4388.

Trimble, D.E., 1976, Geology of the Michaud and Pocatello Quadrangles, Bannock and Power Counties, Idaho: U.S. Geological Survey, v. 1400, p.1-88, doi:10.3133/b1400.

United States Environmental Protection Agency, 2015, Connectivity of streams and wetlands to downstream waters: A review and synthesis of the scientific evidence: Surveillance and Society, v. 1, p. 408, http://www.regulations.gov/#!documentDetail;D=EPA-HQ-OW-2011-0880-0004.

Vaux, W.G., 1968, Intragravel flow and interchange of water in a streambed: Fishery Bulletin, v. 66, p. 479–489.

Walsh, R., and Ward, A.S., 2019, Redefining clean water regulations reduces protections for wetlands and jurisdictional uncertainty: Frontiers in Water, v. 1, doi:10.3389/frwa.2019.00001.

Ward, A.S., Schmadel, N.M., and Wondzell, S.M., 2018, Simulation of dynamic expansion, contraction, and connectivity in a mountain stream network: Advances in Water Resources, v. 114, p. 64–82, doi:10.1016/j.advwatres.2018.01.018.

Ward, A.S., Wondzell, S.M., Schmadel, N.M., and Herzog, S.P., 2020, Climate change causes river network contraction and disconnection in the H.J. Andrews Experimental Forest, Oregon, USA: Frontiers in Water, v. 2, p. 1–10, doi:10.3389/frwa.2020.00007.

Warix, S.R., Godsey, S.E., Lohse, K.A., and Hale, R.L., 2021, Influence of groundwater and topography on stream drying in semi-arid headwater streams: Hydrological Processes, v. 35, p. 51, doi:10.1002/hyp.14185.

Welhan, J., 2006, Water balance and pumping capacity of the Lower Portneuf River Valley aquifer, Bannock County, Idaho: Idaho Geological Survey Report 06-5, p. 1–36, http://www.idwr.idaho.gov/browse/waterinfo/ESPAM/model_boundary/IGS_Welhan_06-5.pdf.

Welhan, J., Meehan, C., and Reid, T., 1996, The Lower Portneuf River Valley Aquifer: A geologic/hydrologic model and its implications for wellhead protection strategies:, https://www.idahogeology.org/pub/Staff_Reports/2006/Staff_report_06-5.pdf.

Whiting, J.A., and Godsey, S.E., 2016, Discontinuous headwater stream networks with stable flowheads, Salmon River basin, Idaho: Hydrological Processes, v. 30, p. 2305–2316, doi:10.1002/hyp.10790.

Wondzell, S.M., 2011, The role of the hyporheic zone across stream networks: Hydrological Processes, v. 25, p. 3525–3532, doi:10.1002/hyp.8119.

Wrigley, R.L., 1943, Early History of Pocatello, Idaho: Chicago, Illinois, University of Chicago Libraries, 365 p.

Wu, G., Shu, L., Lu, C., and Chen, X., 2016, The heterogeneity of 3-D vertical hydraulic conductivity in a streambed: Hydrology Research, v. 47, p. 15–26, doi:10.2166/nh.2015.224.

Zimmer, M.A., and McGlynn, B.L., 2018, Lateral, vertical, and longitudinal source area connectivity drive runoff and carbon export across watershed scales: Water Resources Research, v. 54, p. 1576–1598, doi:10.1002/2017WR021718.

Zimmerman, D.L., and Ver Hoef, J.M., 2017, The Torgegram for fluvial variography: characterizing spatial dependence on stream networks: Journal of Computational and Graphical Statistics, v. 26, p. 253–264, doi:10.1080/10618600.2016.1247006.

Zipper, S.C. et al., 2021, Pervasive changes in stream intermittency across the United States: Environmental Research Letters, v. 16, doi:10.1088/1748-9326/ac14ec.

Chapter 3: Conclusions and Recommendations

3.1 Improving Subsurface Hydraulic Datasets

3.1.1 Modifications and Value of Assessing Temporal Variations in Hydraulic Conductivity

Soil and streambed Ksat values vary over time due to channel migration or disturbances (Stewardson et al., 2016), patterns of sediment transport and deposition (Powell, 1998), and the colmation, or clogging of stream corridor sediments through the deposition of fine-grained material that reduce porosity and alter hyporheic exchange (Krause et al., 2010; Stewardson et al., 2016). Furthermore, seasonal variation in the hydraulic head directly affects hyporheic exchange (Gooseff et al., 2005) and preferential hyporheic flow paths within stream corridor sediments (Dohman et al., 2021). Therefore, installing permanent stream corridor wells would allow for the measure of quarterly changes during baseflow, wetting, peak, and dry-down conditions. If repeated over multiple years, these measurements could improve our understanding of spatiotemporal variability in hyporheic flow. Additional continuous measurements of the hydraulic head could be coupled with these repeated Ksat values to assess potential changes in in-stream gain/loss dynamics and other groundwater-surface water interactions.

Accompanying these changes in Ksat are likely changes in sediment transport. Assessing sediment fluxes within the stream corridor may thus also prove useful. Therefore, I recommend carefully surveying long-term wells to capture each well's casing elevation on a quarterly basis while measuring Ksat. This survey should include the depth from the top of the casing to the water level inside the well, stream water level above the bed, and streambed elevation. In the absence of wells, rebar stakes driven into the channel thalweg could potentially be used as reference points to measure sedimentation flux within the stream channel. With these regular surveys, changes in sedimentation or erosion that might affect hyporheic exchange and subsurface flow paths could be quantified. In conjunction with these efforts, it would be beneficial to develop a stage-discharge relationship for each station to assess how varying flow and geomorphology affect subsurface flow parameters over time.

3.1.2 Linkages to Spatial Stream Drying Patterns

In chapter 2, I demonstrated a significant relationship between stream drying and spatial patterns of stream corridor Ksat: drier sites typically had higher Ksat values. Combining my observations of the spatial structure of Ksat with measurements of stream corridor geometry, perhaps through independent geophysical techniques, should help predict surface flow permanence to identify intermittent and ephemeral reaches. Measuring changes in channel position, geometry, streambed sediment size/sorting, and variations in Ksat across a range of reaches with varying seasonal flow permanence could improve models of stream intermittency.

3.1.3 References Cited:

Dohman, J.M., Godsey, S.E., and Hale, R.L., 2021, Three-Dimensional Subsurface Flow Path Controls on Flow Permanence: Water Resources Research, v. 57, p. 1–18, doi:10.1029/2020wr028270.

Gooseff, M.N., Anderson, J.K., Wondzell, S.M., LaNier, J., and Haggerty, R., 2005, A modelling study of hyporheic exchange pattern and the sequence, size, and spacing of stream bedforms in mountain stream networks, Oregon, USA: Hydrological Processes, v. 19, p. 2915–2929, doi:10.1002/hyp.5790.

Krause, S., M., H.D., Fleckenstein, J.H., Heppell, C.M., Kaeser, D., Pickup, R., Pinay, G., Robertson, A.L., and Wood, P.J., 2010, Inter-disciplinary perspectives on processes in the hyporheic zone: Ecohydrology, v. 130, p. 126–130, doi:10.1002/eco.

Powell, M.D., 1998, Patterns and processes of sediment sorting in gravel-bed rivers: Progress in Physical Geography, v. 22, p. 1–32, http://dx.doi.org/10.1016/j.geomorph.2016.02.001.

Stewardson, M.J., Datry, T., Lamouroux, N., Pella, H., Thommeret, N., Valette, L., and Grant, S.B., 2016, Variation in reach-scale hydraulic conductivity of streambeds: Geomorphology, v. 259, p. 70–80, doi:10.1016/j.geomorph.2016.02.001.

Trimble, D.E., 1976, Geology of the Michaud and Pocatello Quadrangles, Bannock and Power Counties, Idaho:, doi:10.3133/b1400.

Appendix 1: Additional Methods

Initial falling head data was download via Hoboware and exported as a CSV file. This file was then uploaded into Excel, and timestamps for each set of falling head tests were extracted based on the field-recorded times of each experiment. Each test was separated based on the return to static conditions punctuated by the addition of a slug. The water levels were log-transformed and normalized to vary between each test's slug peak and background value. This log-normalized drawdown was then plotted as a function of time and visually assessed to ensure adequate development of wells, instantaneous additions of slugs, and return to static conditions between each falling head test. Irregular tests were excluded from further analysis, typically leaving five (and always at least two) falling head tests for each location used in the Hvorslev calculation. A summary of which tests were used for each well is included in Appendix 15, along with the start and end times of each set of falling head tests.

Appendix 2: Observed Ksat values and geomorphic parameters within site locations grouped by underlying lithologic category. Each panel includes a regression line fit to each lithological group and R^2 values listed separately for each group under their respective legend.

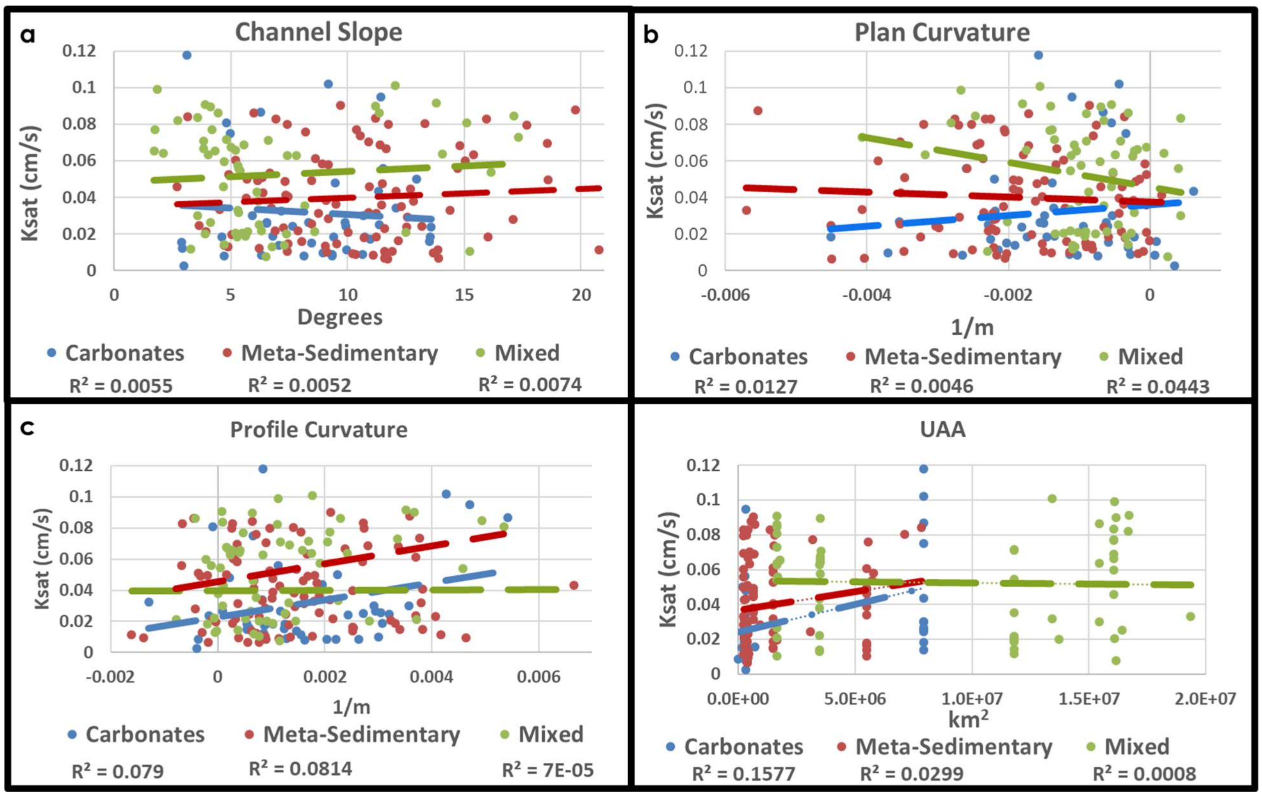

Appendix 3: Well-Drive Schematics

Figure A3.1: Schematic and photographs of the driveshaft designed and built for this project.

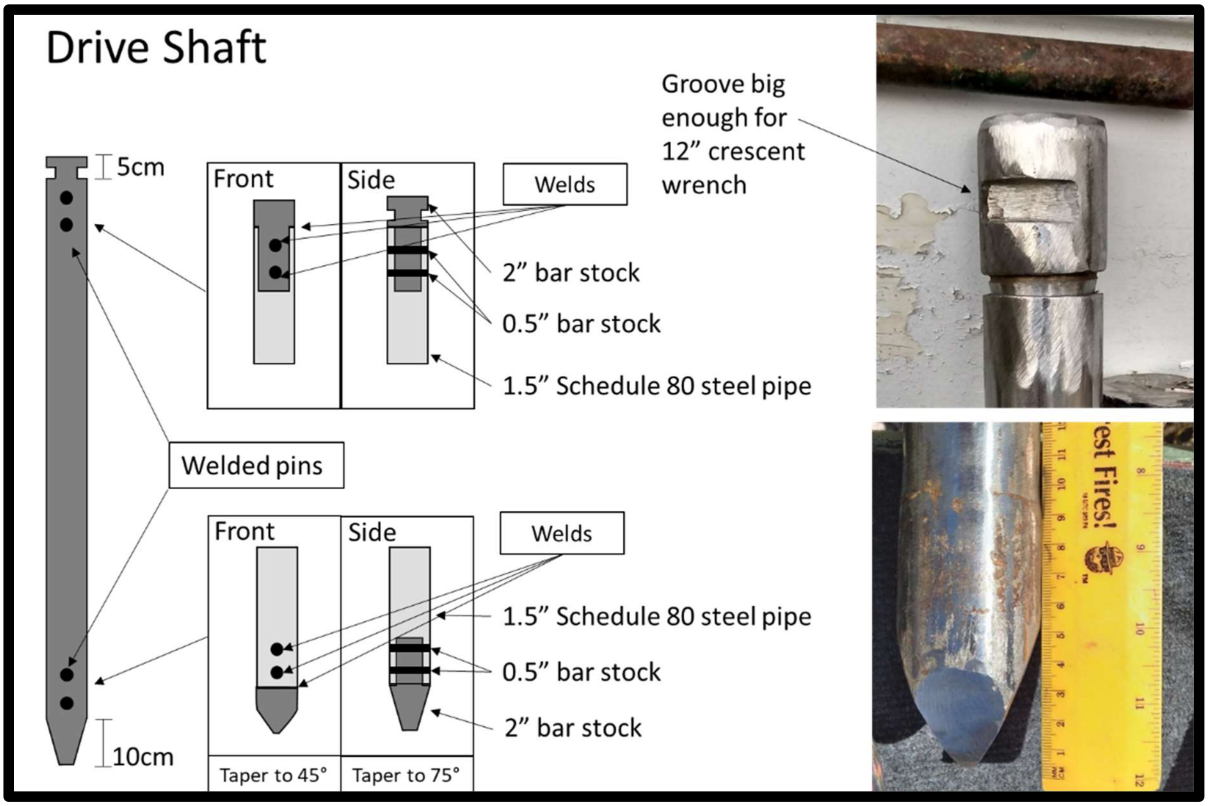

Figure A3.2: Schematic and photograph of drive collar and picture of driveshaft sleeved into the drive collar.

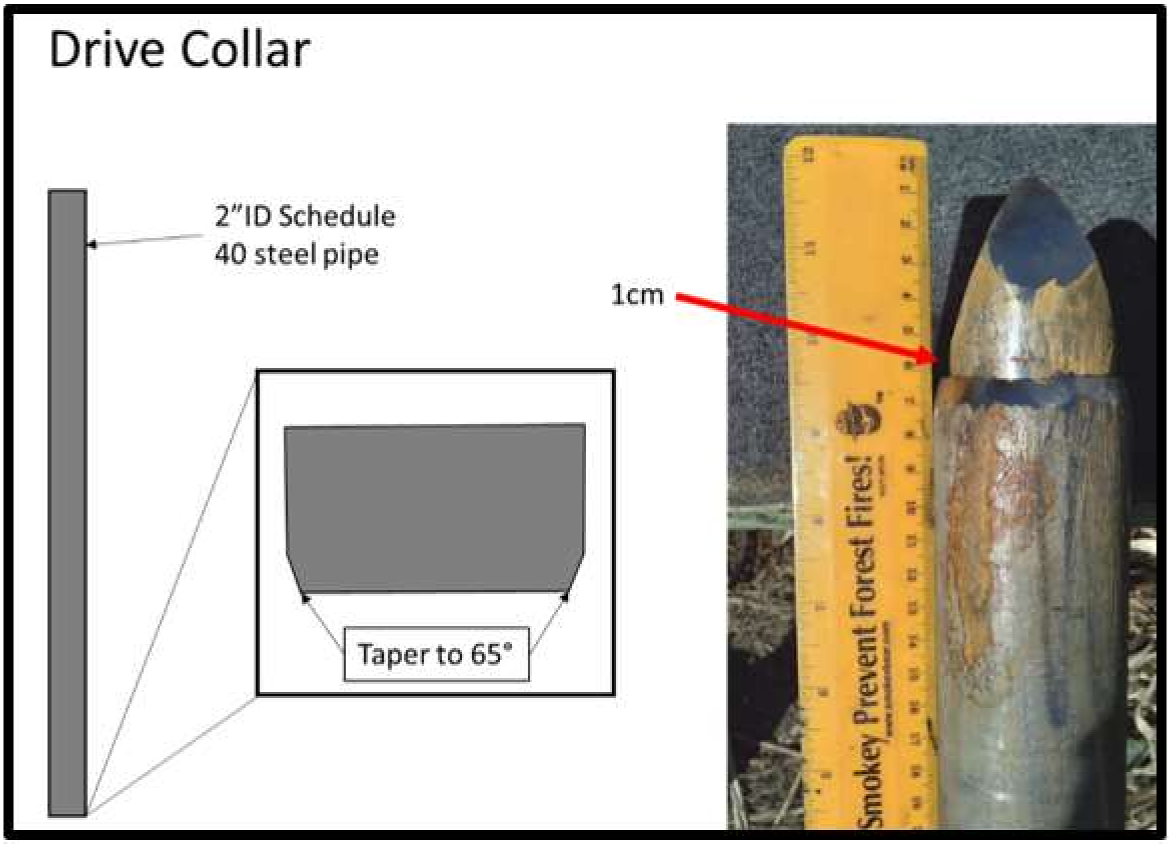

Figure A3.2: Schematic and photograph of drive collar and picture of driveshaft sleeved into the drive collar. Note The 1cm of space between the drive shaft's tapered tip and the drive collar's end is critical to avoid difficult extractions caused by sediment entrapment between the driveshaft and collar.*

Figure A3.3: Well-driver schematics.

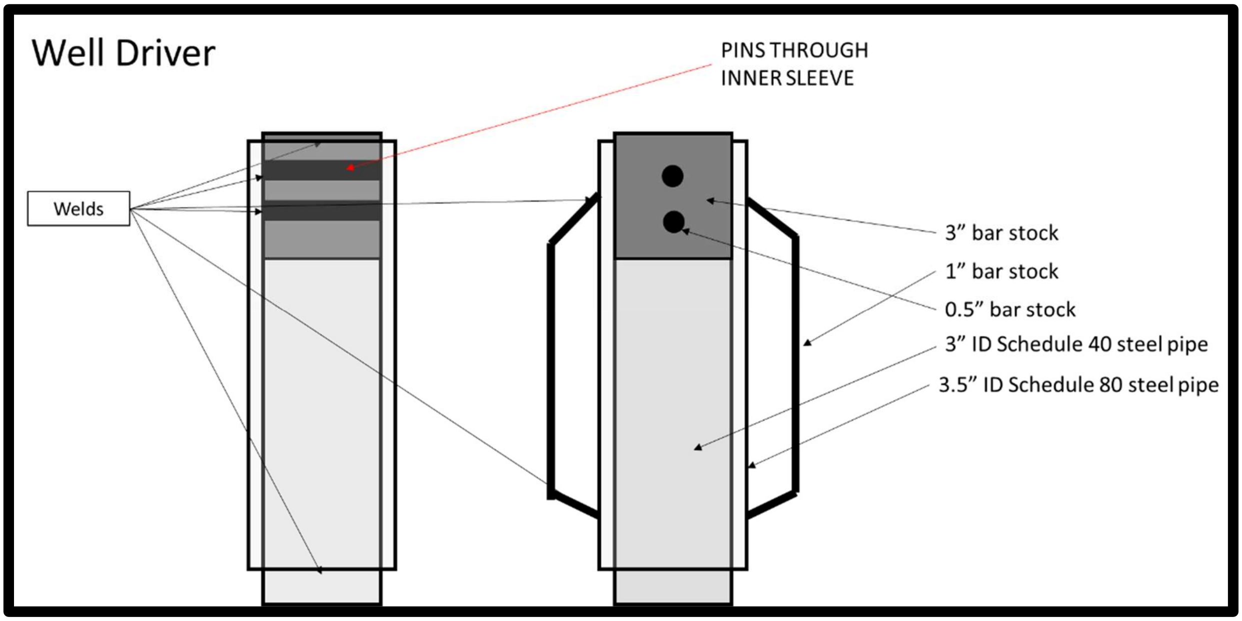

Appendix 4: Soil type and landform for each NRCS soil classification within the Gibson Jack Municipal Watershed (NRCS Web Soil Survey, accessed October 2021).

Table A4.1 includes the following abbreviations: extremely (x), very (V), loam (L), silt (Sl), clay (C), sand (Sn), gravel (G), stony (St), bedrock (Br), slightly decomposed plant material (Sd), and moderately decomposed plant material (Md).

Class	Map Unit Name	Landform	Profiles	Depth (cm)	NRCS Class
30	Cedarhill, high precipitation-Hades-Ricrest complex	Mountain Slope	A, Bk, C	<22, 22-71, 71-150	VCSL, VCSL, VCL
67	Wiskisprings-Sawtelpeak families	Drainageways on Flood Plains	A, Ag, Bg1, Bg2, 2Bg1, 2Bg2	<13, 13-55, 55-76, 76-100, 100 to 106, 106 to 150	SlCL, SlCL, SlCl, CL, SnCL, GSnCL
72	Lanoak-Hades complex	Fan Remnants	A, Bt, Bk	<55, 55-112, 112-150	SlL, SlL, SlL
79	Moonlight-Camelback association	Mountain Slopes	Oi, Oe, A, Bw	<1, 1-2, 2-26, 26-150	Sd, Md, SlL, SlL
94	Rexburg silt loam	Fan Remnants, Hillslopes	A, Bw, Bk	<25, 25-62, 62-150	SlL, SlL, SlL

Class	Map Unit Name	Landform	Profiles	Depth (cm)	NRCS Class
116	Valmar-Camelback-Hades complex	Mountain Slopes, Ridges	A, Bt, R	<36, 36-60, 60-200	VCSlL, XStSll
208	Jedediah-Middlehill families	Swales on Mountain Slopes	Oi,A1,A2,Bt1,Bt2,BCk	0, 0-12,12-43, 43-59, 59-137, 137-150	Sd, SL, SL, SL, Sl, SlCL, SLL
211	Chokecherry-Povey complex	Mountaintop	A, Bw, Cr, R	<5, 5-31, 31-45, 45-150	VGL, VGL, Br, Br
307	Lanoak family-Robin complex	Mountain Slopes	A1, A2, Bt1, Bt2, Bk	<20, 20-40, 40-63, 63-109, 109-150	SlL, SlL, SlL, SlL, SlL
563	Robin-Davtone family	Mountain Slopes	Oi, A1, A2, BA, Bt	0, 0-5, 5-58, 58-152	Sd, SlL, SlL, SlL, SlCL
749	Sparky-Jedediah family	Mountain Slopes	OI, A, AB, Bw	<5, 5-17, 17-51, 51-150	Sd, L, SlL, VGL
3002	Valmar-Warshod family	Mountain Slopes	A, Bw, Bt, R	<23,23-36, 36-61, 61-200	SlL, SlL, SlL

Appendix 5a: Summary of semivariogram and torgegram modeling equations fit to empirical values for both ordinary kriging and SSN approaches.

Table A5.1: Kriging equations used to characterize the spatial pattern of Ksat via the semivariance (g(h)) within the active channel network of Gibson Jack Creek.

Ordinary Kriging equations (ESRI, 2016)	
Spherical	$g(h) = \frac{3h}{2a} - \frac{1}{2}\left(\frac{h}{a}\right)^3$ $if\ \ 0 < h \leq a$
Exponential	$g(h)\ =\ 1\ -\ exp\left(\frac{-3h}{a}\right)$
Gaussian	$g(h)\ =\ 1\ -\ exp\,(-3h^2/a^2)$
Circular	$g(h) = 1 - \frac{2}{\pi}\cos^{-1}\left(\frac{h}{a}\right) + \sqrt{1 - \frac{h^2}{a^2}}\ \ if\ \ 0 <$ $h \leq a$

The variables above include: the separation distance, h; and the range, a.

Table A5.2: SSN shapes and equations used to characterize the spatial pattern of Ksat via the covariance (Ct(h)) within the active channel network of Gibson Jack Creek (Ver Hoef et al., 2014).

SSN equations (Ver Hoef et al. 2014)	
Tail-up spherical	$C(h\|\theta_u) = \sigma_u^2\left(1 - \frac{3h}{2\theta_u} + \frac{1h^3}{2\theta_u^3}\right)$ if $\left(\frac{h}{\alpha_u} \leq 1\right)$
Tail-up Mariah	$C(h\|\theta_u) = \sigma_u^2 \frac{\log\left(\frac{90h}{\theta_{u+1}}\right)}{\frac{90h}{\theta_u}}$ if $h > 0$ or, $C(h\|\theta_u) = \sigma_u^2$ if $h = 0$
Tail up Epanechnikov model	$C(h\|\theta_u) = \frac{f_{eu}\sigma_u^2(h-\theta_u)^2}{16\theta_u^5}$ if $\left(\frac{h}{\theta_u} \leq 1\right)$

The variables above include: the separation distance, h; the partial sill, σ_u^2 the range, α_u; feu= 16α_u^2+17α_u^2 h-2α_u^2 h^2-h^3; and θ_u = (σ_u^2, α_u)T.

Appendix 5b: References Cited

ESRI, 2016, How Kriging works:, https://desktop.arcgis.com/en/arcmap/10.3/tools/3d-analyst-toolbox/how-kriging-works.htm#ESRI_SECTION1_7797FD7C7E384913963B8F0DC1FE69F2.

Ver Hoef, J.M., Peterson, E.E., Clifford, D., and Shah, R., 2014, SSN: An R package for spatial statistical modeling on stream networks: Journal of Statistical Software, v. 56, ftp://sunsite2.icm.edu.pl/packages/cran/web/packages/SSN/vignettes/SSN.pdf%0Apapers3://publication/uuid/EEF33D01-D2EF-4967-99B7-C3ADF58B4183.

Appendix 6: Ordinary kriging cross-validation results and summary statistics

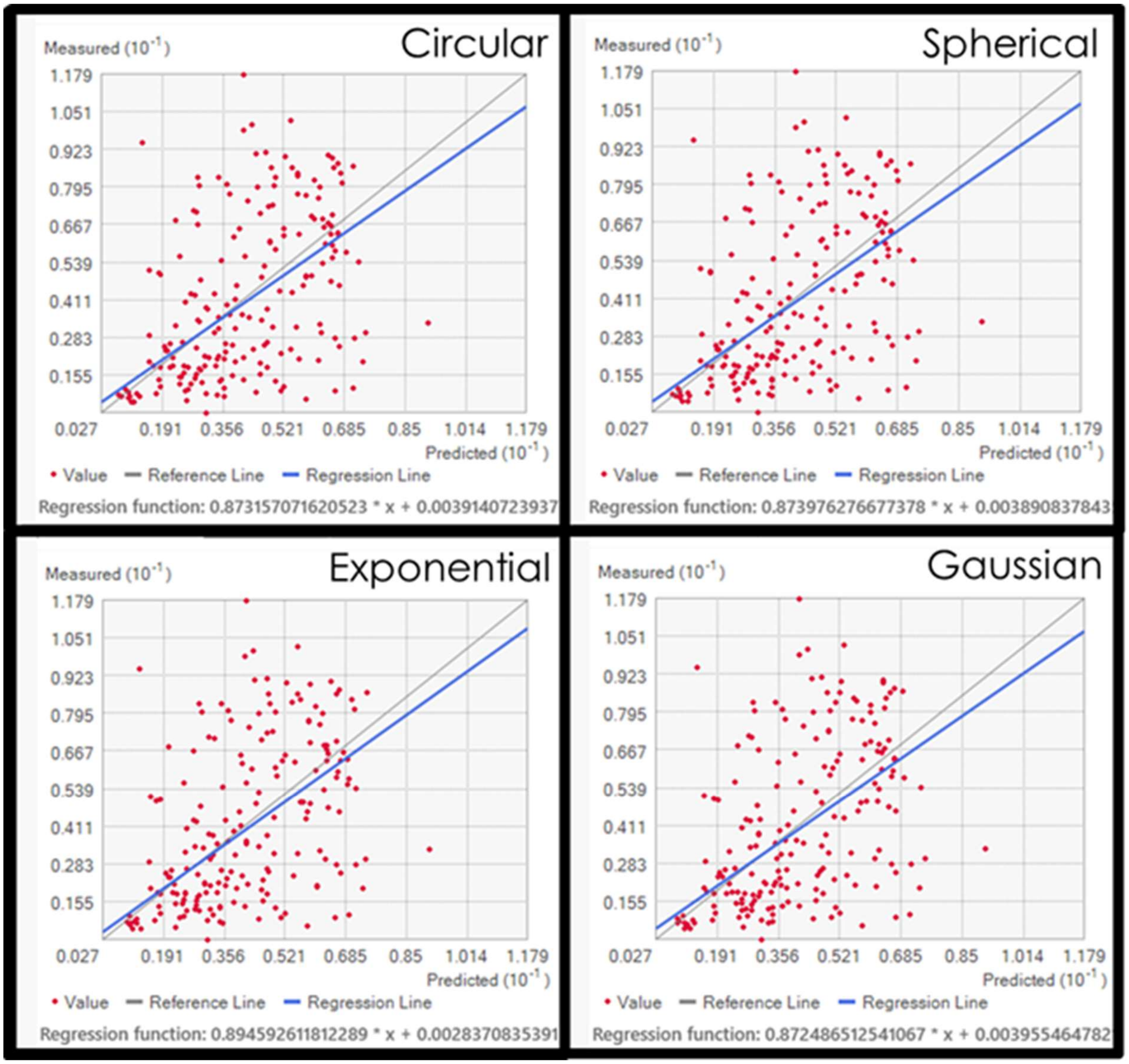

Figure A6.1 Cross-validation for Circular, Spherical, Exponential, and Gaussian ordinary kriging models. Both axes show Ksat in cm/s with the gray 1:1 diagonal line showing that predicted (x axis) values perfectly match the measured (y axis) values.

Ordinary Kriging n=194	Circular	Spherical	Gaussian	Exponential
Mean Error (cm/s)	-5.61E-04	-5.70E-04	-5.75E-04	-6.32E-04
Root-Mean-Square Error (cm/s)	2.51E-02	2.51E-02	2.52E-02	2.50E-02
Mean Standardized Error	-8.86E-03	-8.85E-03	-9.00E-03	-1.16E-02
Root-Mean-Square Standardized Error	1.06	1.06	1.06	1.05
Average Standard Error (cm/s)	2.31E-02	2.31E-01	2.32E-02	2.33E-02
Nugget (cm/s)	1.43E-04	1.34E-04	1.86E-04	5.29E-05
Sill (cm/s)	4.76E-04	4.81E-04	4.11E-04	5.61E-04
Range (m)	4.42	1.83	3.56	5.01

Table A6.1. Summary of results produced in ArcGIS for the Circular, Spherical, Gaussian, and Exponential model shapes using the Ordinary Prediction Kriging tool with first-order trend removal. Interpolation and cross-validation were completed using a standard neighborhood with two to five neighbors.

Appendix 7: Semivariograms and prediction error maps for all ordinary kriging models.

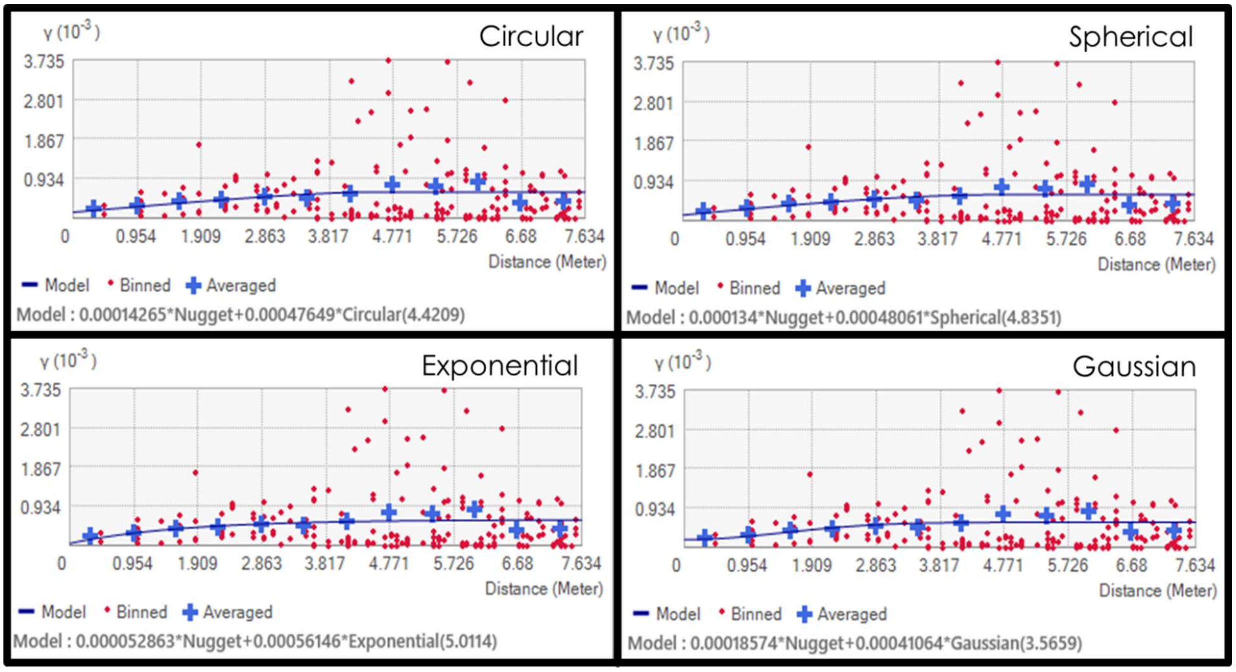

Figure A7.1. Semivariogram results from the ordinary kriging analysis performed in ArcGIS. The y axis in all panels is semivariance of Ksat in (cm/s)2 as a function of separation distance (m) on the x axis.

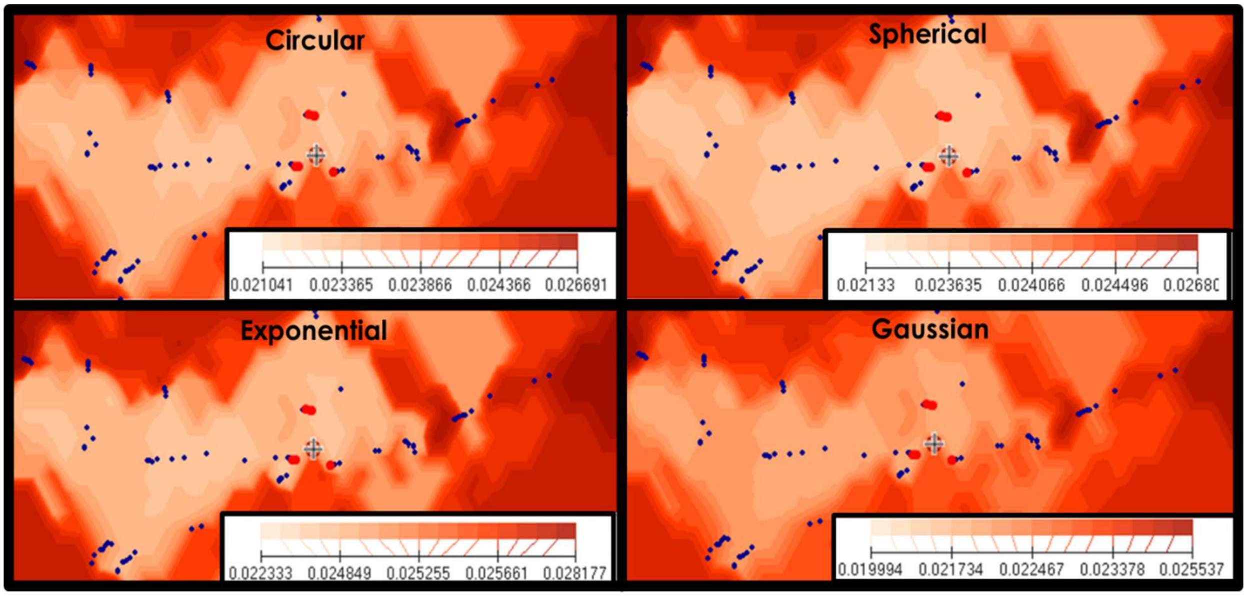

Figure A7.2: Prediction standard error from the ordinary kriging analysis performed in ArcGIS for Ksat throughout Gibson Jack watershed. All values are reported in the original Ksat units of cm/s.

Appendix 8: Cross-validation results from the SSN spatial analysis for Ksat in Gibson Jack watershed.

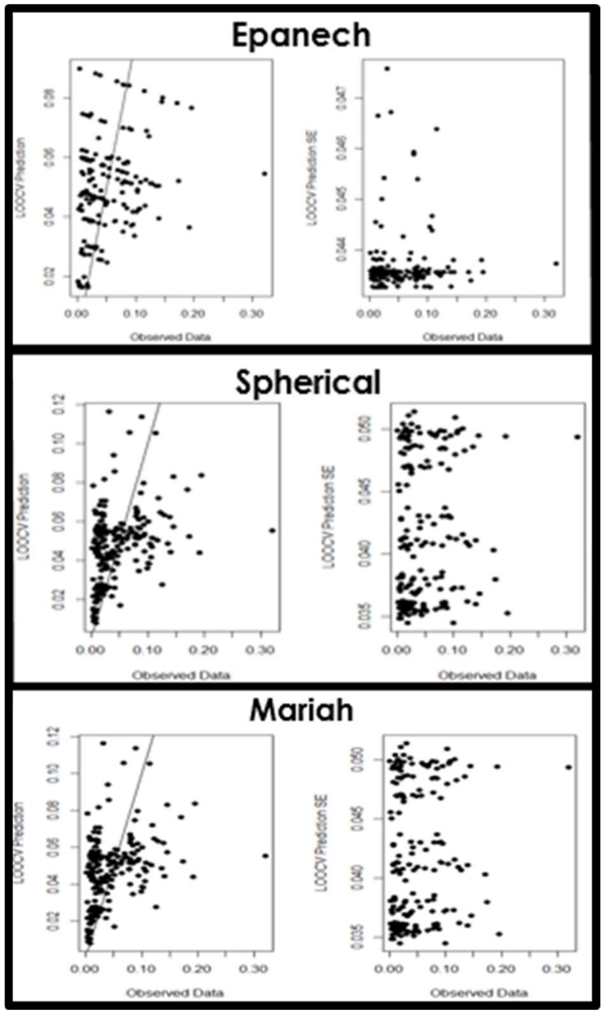

Figure A8.1. Cross-validation of the following tail-up variants: Epanechnikov ("Epanech" below), Mariah, and Spherical. The left plot in each panel shows Ksat on both axes in units of cm/s. The right plot in each panel shows Ksat against its associated prediction error, both in units of cm/s.

.

SSN n=194	Epanechnikov	Spherical	Mariah
Residual Standard Error (cm/s)	4.75E-01	5.14E-02	4.96E-02
Generalized R-Squared	3.23E-04	9.82E-06	1.54E-05
Nugget (cm/s)	4.83E-04	9.42E-03	1.35E-03
Range (m)	2.40E+03	2.81E+02	1.60E+02
Residuals (cm/s)	Epanechnikov	Spherical	Mariah
Min	-4.52E-02	-5.22E-02	-5.12E-02
1Q	-3.37E-02	-3.81E-02	-3.81E-02
Median	-1.99E-02	-2.55E-02	-2.47E-02
3Q	2.97E-02	2.42E-02	2.49E-02
Max	2.73E-01	2.67E-01	2.68E-01

Table A8.1. Summary of results produced by the along-network spatial structure assessment performed by the SSN package for R using the Epanechnikov, Spherical, and Mariah model shapes after detrending with area draining to each point along the network

Appendix 9: Interpolated Ksat values from the SSN spatial analysis

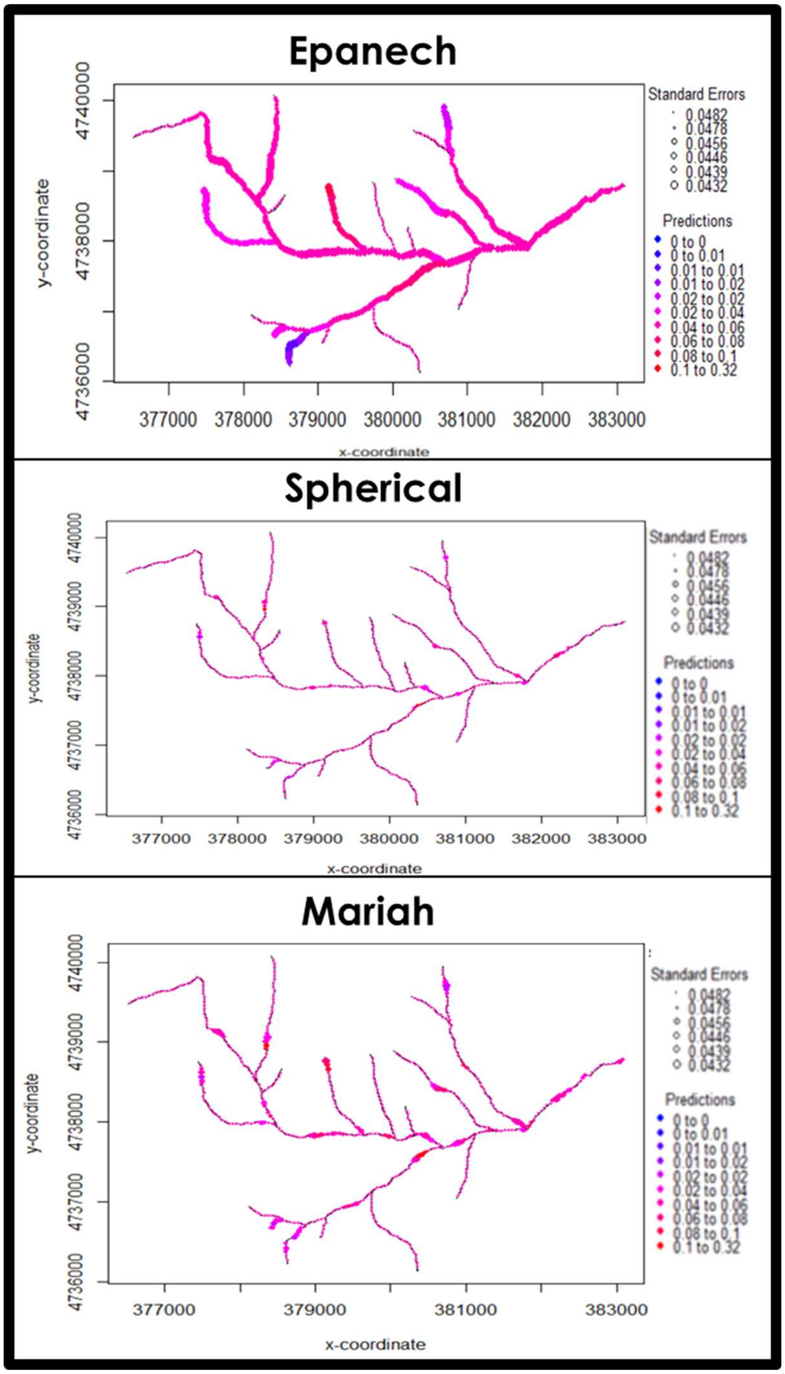

Figure A9.1 Predicted Ksat with associated standard errors shown in cm/s from the SSN spatial analysis with the following tail-up variants: Epanechnikov (below "Epanech"), Mariah, and Spherical.

Appendix 10: Torgegram results from the SSN spatial analysis of Ksat at Gibson Jack watershed.

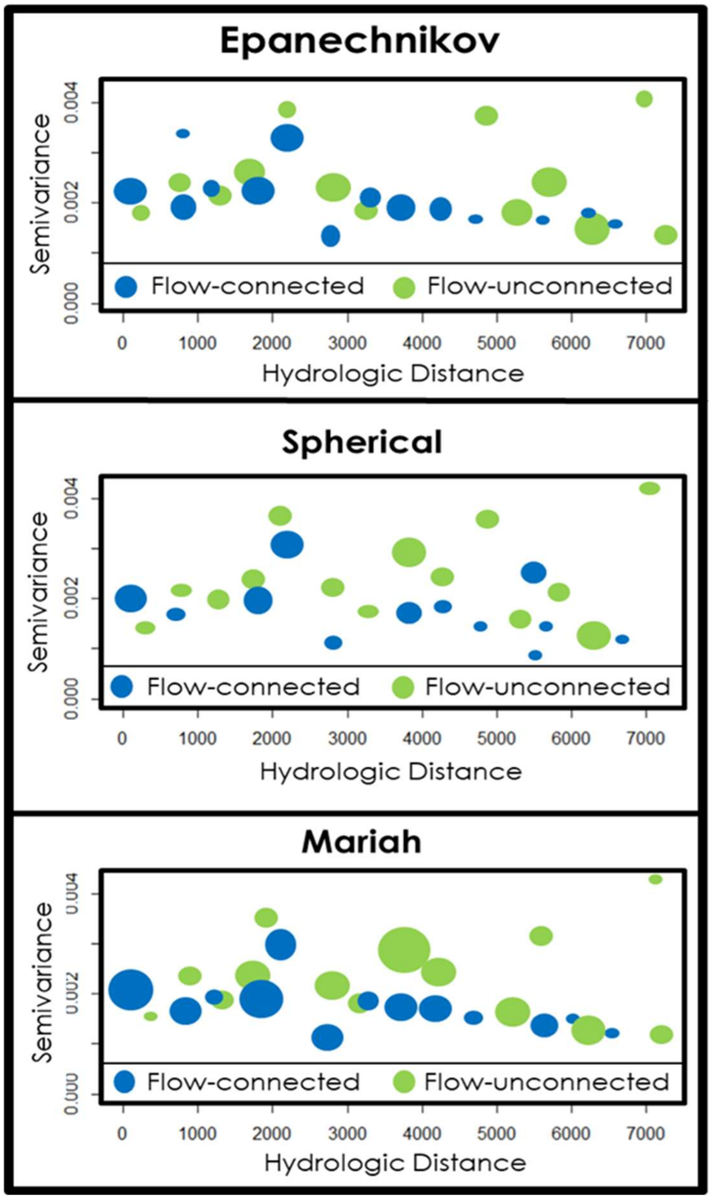

Figure A10.1 Torgegrams with the following tail-up variants: Epanechnikov, Mariah, and Spherical. The y axes in each panel show the semivariance of Ksat in units of (cm/s)2 as a function of the hydrological separation distance (in units of meters) along the stream network for both flow-connected and flow-unconnected pairs of points (see section 1.6.3 for details).

Appendix 11: Data Summary: location information and average Ksat for all Gibson Jack sites:

Table A11.1. Longitude, latitude, elevation in meters, average Ksat (determined using the Hvorslev method in cm/s), and slope (in degrees) for each site.

OID	Name	Lat	Long	Ksat (cm/s)	Elev. (m)	Slope (deg)
1	A_250	42.768	-112.484	0.019	1951.65	6.8
2	A_100	42.771	-112.484	0.019	1929.95	4.6
3	A_0.0	42.772	-112.483	0.008	1921.05	6.3
4	A_0.5	42.772	-112.483	0.008	1921.05	8.1
5	A_1.0	42.772	-112.483	0.009	1919.92	9.3
6	A_1.5	42.772	-112.483	0.008	1919.92	9.3
7	A_2.0	42.772	-112.483	0.010	1919.92	8.9
8	A_3.0	42.772	-112.483	0.011	1919.92	10.0
9	A_6.0	42.772	-112.483	0.095	1919.92	11.4
10	A_9.0	42.772	-112.483	0.008	1919.92	4.7
11	A_12	42.772	-112.483	0.012	1918.50	2.9
12	A_25	42.772	-112.483	0.003	1927.37	3.0
13	A_50	42.772	-112.482	0.048	1915.84	9.5
14	A_100	42.772	-112.482	0.081	1912.31	4.8
15	A_1000	42.776	-112.473	0.066	1830.10	1.7
16	A_20	42.773	-112.481	0.016	1902.22	13.5
17	B_250	42.772	-112.487	0.015	1985.51	8.5

OID	Name	Lat	Long	Ksat (cm/s)	Elev. (m)	Slope (deg)
18	B_100	42.773	-112.487	0.050	1962.88	13.0
19	B_0.0	42.773	-112.486	0.033	1952.99	7.2
20	B_0.5	42.773	-112.486	0.027	1952.95	8.3
21	B_1.0	42.773	-112.486	0.018	1952.95	9.4
22	B_1.5	42.773	-112.486	0.017	1952.95	11.0
23	B_2.0	42.773	-112.486	0.034	1952.95	12.1
24	B_3.0	42.773	-112.486	0.056	1952.95	11.5
25	B_6.0	42.773	-112.486	0.018	1953.11	13.5
26	B_9.0	42.773	-112.486	0.024	1953.11	13.6
27	B_12	42.773	-112.486	0.024	1953.11	7.7
28	B_25	42.773	-112.485	0.025	1950.49	11.4
29	B_50	42.774	-112.485	0.026	1941.29	9.9
30	B_100	42.774	-112.484	0.015	1934.93	2.9
31	B_1000	42.776	-112.474	0.066	1838.77	4.3
32	Spring	42.774	-112.485	0.009	1937.17	10.6
33	C_0.0	42.790	-112.498	0.032	1988.25	8.7
34	C_0.5	42.790	-112.498	0.023	1988.25	7.3
35	C_1.0	42.790	-112.498	0.043	1988.25	6.4
36	C_1.5	42.790	-112.498	0.034	1988.25	4.5
37	C_2.0	42.790	-112.498	0.025	1988.25	3.6
38	C_3.0	42.790	-112.498	0.016	1988.25	8.0
39	C_6.0	42.790	-112.498	0.021	1987.41	3.9

OID	Name	Lat	Long	Ksat (cm/s)	Elev. (m)	Slope (deg)
40	C_9.0	42.790	-112.498	0.021	1987.41	10.0
41	C_12	42.790	-112.498	0.022	1987.41	7.9
42	C_25	42.790	-112.498	0.022	1986.79	6.9
43	C_50	42.790	-112.498	0.043	1986.33	12.1
44	C_100	42.789	-112.498	0.080	1985.61	11.8
45	C_1000	42.785	-112.488	0.020	1900.63	5.0
46	C_2000	42.784	-112.475	0.058	1814.55	9.2
47	D_0.0	42.795	-112.496	0.024	1987.68	12.5
48	D_0.5	42.795	-112.496	0.019	1987.68	11.2
49	D_1.0	42.795	-112.496	0.015	1987.68	9.5
50	D_1.5	42.795	-112.496	0.015	1987.68	7.5
51	D_2.0	42.795	-112.496	0.041	1987.68	7.5
52	D_3.0	42.795	-112.496	0.040	1987.18	5.7
53	D_6.0	42.795	-112.496	0.053	1986.66	4.9
54	D_9.0	42.795	-112.496	0.061	1986.66	8.6
55	D_12	42.795	-112.495	0.058	1986.66	8.9
56	D_25	42.795	-112.495	0.032	1986.54	10.9
57	D_50	42.795	-112.495	0.074	1986.16	10.6
58	D_100	42.794	-112.495	0.080	1984.03	7.4
59	D_1000	42.787	-112.488	0.024	1903.71	13.2
60	D_2000	42.783	-112.480	0.016	1849.89	12.2
61	D.2_0.5	42.783	-112.480	0.011	1849.89	11.9

OID	Name	Lat	Long	Ksat (cm/s)	Elev. (m)	Slope (deg)
62	D.2_1.0	42.783	-112.480	0.018	1849.89	10.7
63	D.2_1.5	42.783	-112.480	0.039	1849.89	9.1
64	D.2_2.0	42.783	-112.480	0.041	1849.89	7.4
65	D.2_3.0	42.783	-112.480	0.061	1849.89	5.2
66	D.2_6.0	42.783	-112.480	0.034	1848.99	6.7
67	D.2_9.0	42.783	-112.480	0.014	1848.99	4.7
68	D.2_12	42.783	-112.480	0.049	1848.99	6.1
69	D.2_25	42.783	-112.480	0.046	1845.63	2.7
70	D.2_50	42.783	-112.479	0.049	1846.27	7.3
71	D.2_100	42.783	-112.479	0.076	1837.61	8.2
72	D.2_1000	42.783	-112.467	0.080	1767.14	13.3
73	D.2_2000	42.783	-112.456	0.019	1707.26	5.6
74	D.3_0.5	42.783	-112.456	0.020	1707.26	3.9
75	D.3_1.0	42.783	-112.456	0.012	1707.26	3.3
76	D.3_1.5	42.783	-112.456	0.014	1707.26	4.7
77	D.3_2.0	42.783	-112.456	0.018	1707.26	5.3
78	D.3_3.0	42.783	-112.456	0.022	1705.13	5.7
79	D.3_6.0	42.783	-112.456	0.020	1705.13	5.5
80	D.3_9.0	42.783	-112.456	0.072	1704.79	4.8
81	D.3_12	42.783	-112.456	0.071	1704.79	6.6
82	D.3_25	42.783	-112.456	0.021	1704.98	8.6
83	D.3_50	42.783	-112.456	0.035	1704.36	8.2

OID	Name	Lat	Long	Ksat (cm/s)	Elev. (m)	Slope (deg)
84	D.3_100	42.783	-112.455	0.055	1702.90	5.4
85	D.3_1000	42.784	-112.446	0.020	1659.62	7.4
86	D.3_2000	42.791	-112.436	0.025	1596.36	6.2
87	E_0.0	42.795	-112.487	0.035	1998.33	12.3
88	E_0.5	42.795	-112.487	0.031	1998.33	11.2
89	E_1.0	42.795	-112.487	0.036	1998.33	9.5
90	E_1.5	42.795	-112.487	0.036	1998.33	11.5
91	E_2.0	42.795	-112.487	0.046	1998.33	11.0
92	E_3.0	42.795	-112.487	0.038	1998.33	12.8
93	E_6.0	42.795	-112.487	0.044	1997.73	12.7
94	E_9.0	42.795	-112.487	0.049	1998.33	8.4
95	E_12	42.794	-112.487	0.048	1998.33	11.5
96	E_25	42.794	-112.487	0.090	1996.79	9.7
97	E_50	42.794	-112.487	0.069	1995.57	11.4
98	E_100	42.794	-112.487	0.086	1986.28	6.0
99	E_1000	42.786	-112.487	0.077	1891.75	10.4
100	E_2000	42.784	-112.477	0.053	1822.44	6.7
101	F_0.0	42.792	-112.478	0.056	1970.04	14.7
102	F_0.5	42.792	-112.478	0.083	1970.04	15.9
103	F_1.0	42.792	-112.478	0.028	1970.04	17.1
104	F_1.5	42.792	-112.478	0.050	1970.04	18.6
105	F_2.0	42.792	-112.478	0.069	1970.04	18.6

OID	Name	Lat	Long	Ksat (cm/s)	Elev. (m)	Slope (deg)
106	F_3.0	42.792	-112.478	0.080	1970.04	17.7
107	F_6.0	42.792	-112.478	0.060	1967.57	15.0
108	F_9.0	42.792	-112.478	0.033	1967.57	14.4
109	F_12	42.792	-112.478	0.011	1964.47	13.9
110	F_25	42.791	-112.478	0.063	1962.27	15.4
111	F_50	42.791	-112.477	0.070	1958.75	10.9
112	F_100	42.791	-112.477	0.088	1947.80	19.8
113	F_1000	42.784	-112.472	0.028	1814.27	9.2
114	F_2000	42.784	-112.463	0.084	1752.69	3.1
115	G_0.0	42.789	-112.460	0.009	1830.54	10.2
116	G_0.5	42.789	-112.460	0.009	1830.54	10.3
117	G_1.0	42.789	-112.460	0.009	1830.54	11.1
118	G_1.5	42.789	-112.460	0.007	1830.54	11.6
119	G_2.0	42.789	-112.460	0.011	1830.54	11.6
120	G_3.0	42.789	-112.460	0.006	1830.54	11.7
121	G_6.0	42.789	-112.460	0.007	1830.54	13.9
122	G_9.0	42.789	-112.460	0.029	1830.74	12.6
123	G_12	42.789	-112.460	0.010	1830.74	7.4
124	G_25	42.789	-112.460	0.051	1828.12	6.4
125	G_50	42.789	-112.459	0.019	1829.74	16.0
126	G_100	42.789	-112.459	0.009	1816.77	11.6
127	G_1000	42.784	-112.450	0.101	1680.67	12.1

OID	Name	Lat	Long	Ksat (cm/s)	Elev. (m)	Slope (deg)
128	G_2000	42.788	-112.439	0.099	1619.26	1.9
129	H_0.0	42.801	-112.458	0.068	1925.28	14.8
130	H_0.5	42.801	-112.458	0.010	1925.28	13.7
131	H_1.0	42.801	-112.458	0.014	1925.28	9.1
132	H_1.5	42.801	-112.458	0.050	1924.76	5.7
133	H_2.0	42.801	-112.458	0.013	1924.76	4.9
134	H_3.0	42.801	-112.458	0.012	1924.76	6.2
135	H_6.0	42.801	-112.458	0.023	1924.76	11.6
136	H_9.0	42.801	-112.458	0.067	1924.76	11.7
137	H_12	42.801	-112.458	0.010	1924.76	9.1
138	H_25	42.801	-112.458	0.083	1925.30	6.9
139	H_50	42.800	-112.458	0.026	1919.11	8.5
140	H_100	42.800	-112.458	0.012	1913.16	20.8
141	H_1000	42.792	-112.455	0.083	1790.80	11.2
142	H_2000	42.785	-112.447	0.010	1677.11	15.2
143	H.2_0.5	42.785	-112.447	0.085	1677.11	17.1
144	H.2_1.0	42.785	-112.447	0.073	1677.11	17.3
145	H.2_1.5	42.785	-112.447	0.081	1677.11	15.1
146	H.2_2.0	42.785	-112.447	0.054	1677.11	16.2
147	H.2_3.0	42.785	-112.447	0.064	1675.93	14.1
148	H.2_6.0	42.785	-112.447	0.021	1674.33	12.5
149	H.2_9.0	42.785	-112.447	0.086	1674.33	11.4

OID	Name	Lat	Long	Ksat (cm/s)	Elev. (m)	Slope (deg)
150	H.2_12	42.785	-112.447	0.063	1674.33	7.4
151	H.2_25	42.785	-112.447	0.027	1671.25	4.1
152	H.2_50	42.785	-112.446	0.091	1668.96	3.9
153	H.2_100	42.785	-112.446	0.056	1659.37	5.3
154	H.2_1000	42.789	-112.438	0.090	1610.43	11.2
155	H.2_2000	42.793	-112.428	0.091	1558.98	13.8
156	I_0.0	42.781	-112.463	0.043	1752.80	6.1
157	I_0.5	42.781	-112.463	0.038	1752.80	6.2
158	I_1.0	42.781	-112.463	0.022	1752.80	6.3
159	I_1.5	42.781	-112.463	0.013	1752.80	6.8
160	I_2.0	42.781	-112.463	0.014	1752.80	7.3
161	I_3.0	42.781	-112.463	0.063	1752.80	7.8
162	I_6.0	42.781	-112.463	0.090	1753.18	4.1
163	I_9.0	42.781	-112.463	0.064	1753.18	2.1
164	I_12	42.781	-112.463	0.066	1752.64	5.2
165	I_25	42.781	-112.463	0.057	1752.40	5.3
166	I_50	42.781	-112.462	0.068	1750.95	5.0
167	I_100	42.782	-112.462	0.071	1742.21	3.8
168	J_0.0	42.784	-112.462	0.087	1743.63	6.3
169	J_0.5	42.784	-112.462	0.102	1743.63	9.2
170	J_1.0	42.784	-112.462	0.030	1743.63	10.7
171	J_1.5	42.784	-112.462	0.024	1743.63	9.9

OID	Name	Lat	Long	Ksat (cm/s)	Elev. (m)	Slope (deg)
172	J_2.0	42.784	-112.462	0.026	1743.63	6.5
173	J_3.0	42.784	-112.462	0.026	1743.63	6.6
174	J_6.0	42.784	-112.462	0.030	1743.63	5.9
175	J_9.0	42.784	-112.462	0.044	1743.99	11.3
176	J_12	42.784	-112.462	0.118	1743.99	3.1
177	J_25	42.784	-112.461	0.075	1743.33	5.0
178	J_50	42.783	-112.461	0.018	1742.87	10.7
179	J_100	42.783	-112.461	0.014	1740.61	7.1
180	IJ_1000	42.784	-112.451	0.032	1680.71	5.4
181	IJ_2000	42.785	-112.445	0.086	1646.75	4.5
182	IJ.2_0.5	42.788	-112.440	0.064	1620.78	4.0
183	IJ.2_1.0	42.788	-112.440	0.030	1620.78	3.6
184	IJ.2_1.5	42.788	-112.440	0.084	1620.78	3.6
185	IJ.2_2.0	42.788	-112.440	0.066	1620.78	3.9
186	IJ.2_3.0	42.788	-112.440	0.060	1620.78	4.7
187	IJ.2_6.0	42.788	-112.440	0.077	1620.44	1.7
188	IJ.2_9.0	42.788	-112.440	0.069	1620.82	5.6
189	IJ.2_12	42.788	-112.440	0.077	1620.82	4.2
190	IJ.2_25	42.788	-112.440	0.046	1620.22	4.7
191	IJ.2_50	42.788	-112.440	0.020	1620.04	5.2
192	IJ.2_100	42.789	-112.439	0.008	1619.00	6.5
193	IJ.2_1000	42.792	-112.430	0.082	1561.50	2.7

OID	Name	Lat	Long	Ksat (cm/s)	Elev. (m)	Slope (deg)
194	IJ.2_2000	42.796	-112.419	0.033	1512.09	5.3

Appendix 12: Continued Data Summary: geomorphic and stream permanence characteristics for all Gibson Jack sites

Table A12.1. Name, curvature (1/m), profile curvature (1/m), plan curvature (1/m), and stream permanence (i.e., the fraction of the season with surface water as discussed in chapter 2).

OID	Name	Curvature	Profile Curve	Plan Curve	Stream Permanence
1	A_250	-22.631289	9.1730175	-13.45827	0.38
2	A_100.0	-45.41048	30.783205	-14.62727	0.07
3	A_0.0	-32.388752	22.0908623	-10.29789	0.04
4	A_0.5	-23.733664	16.3291473	-7.404516	
5	A_1.0	-24.228222	12.8939781	-11.33424	
6	A_1.5	-46.974396	20.4610748	-26.51332	
7	A_2.0	-67.067123	30.029274	-37.03785	
8	A_3.0	-36.972519	15.5476465	-21.42488	
9	A_6.0	-58.109959	47.0880203	-11.02194	
10	A_9.0	-25.784666	26.4079552	0.6232901	
11	A_12	-11.674932	8.58762074	-3.08731	0.41
12	A_25	7.41969967	-3.9189568	3.5007429	0.58
13	A_50.0	-16.063713	2.21132231	-13.85239	1
14	A_100.0	-4.4530792	-0.9864614	-5.43954	1
15	A_1000	-5.0005307	2.8081224	-2.192408	1
16	A_200.0	-4.9714646	5.90849447	0.9370299	1
17	B_250	-25.740662	5.48962164	-20.25104	0

OID	Name	Curvature	Profile Curve	Plan Curve	Stream Permanence
18	B_100	-44.413956	22.3822289	-22.03173	0
19	B_0.0	-8.9554348	-12.883331	-21.83877	0
20	B_0.5	-36.392269	0.96582896	-35.42644	
21	B_1.0	-57.641327	12.5292292	-45.1121	
22	B_1.5	-31.287741	8.74584198	-22.5419	
23	B_2.0	-21.843086	8.24797153	-13.59511	
24	B_3.0	-37.269718	11.2937489	-25.97597	
25	B_6.0	-22.926657	5.52865744	-17.398	
26	B_9.0	-16.514278	-1.6409281	-18.15521	
27	B_12	-30.321859	24.3753471	-5.946514	0
28	B_25	-50.009418	27.1692924	-22.84013	0
29	B_50	-17.921106	11.6931067	-6.228	0
30	B_100	-18.336807	12.447134	-5.889673	0
31	B_1000	-14.616639	4.19507408	-10.42157	1
32	Spring	0.78895485	-3.5611007	-2.772146	1
33	C_0.0	-26.005251	3.78272796	-22.22252	0
34	C_0.5	-37.565353	7.7639637	-29.80139	
35	C_1.0	-46.816368	11.5763779	-35.23999	
36	C_1.5	-48.939362	8.26995468	-40.66941	
37	C_2.0	-51.011024	5.96700525	-45.04402	
38	C_3.0	-37.106079	25.3528671	-11.75321	
39	C_6.0	-3.0154548	-1.0522674	-4.067722	

OID	Name	Curvature	Profile Curve	Plan Curve	Stream Permanence
40	C_9.0	-32.798634	32.3244629	-0.474174	
41	C_12	-25.098827	3.33447456	-21.76435	0
42	C_25	-44.411003	21.5492401	-22.86176	0.06
43	C_50	-85.209496	66.671257	-18.53823	0.04
44	C_100	-59.326706	27.3035622	-32.02314	0.08
45	C_1000	-16.380392	-0.3328703	-16.71326	1
46	C_2000	-16.879507	3.60164452	-13.27786	1
47	D_0.0	-43.544773	36.9757767	-6.568999	0
48	D_0.5	-39.167942	33.2391167	-5.928826	
49	D_1.0	-43.113873	34.0129204	-9.100952	
50	D_1.5	-53.52763	38.3031044	-15.22452	
51	D_2.0	-53.52763	38.3031044	-15.22452	
52	D_3.0	-29.58264	25.2567635	-4.325876	
53	D_6.0	-10.279352	9.75400734	-0.525344	
54	D_9.0	-60.732643	37.0999985	-23.63265	
55	D_12	-27.81938	27.1164303	-0.702948	0
56	D_25	-61.533714	38.0618935	-23.47182	0.05
57	D_50	-45.774174	37.7491684	-8.025006	0.16
58	D_100	-10.223177	2.58134317	-7.641834	0.02
59	D _ 1000	-42.932434	12.7020292	-30.23041	1
60	D_2000	-25.266903	25.227705	-0.039199	1
61	D.2_0.5	-18.635153	17.6700592	-0.965094	

OID	Name	Curvature	Profile Curve	Plan Curve	Stream Permanence
62	D.2_1.0	-16.84581	13.3564138	-3.489395	
63	D.2_1.5	-12.601963	10.2909098	-2.311053	
64	D.2_2.0	-5.1792364	6.7695179	1.5902815	
65	D.2_3.0	-15.296384	3.03480029	-12.26158	
66	D.2_6.0	-32.980419	20.9632206	-12.0172	
67	D.2_9.0	-15.000996	6.29468155	-8.706314	
68	D.2_12	-35.397537	16.8239727	-18.57356	1
69	D.2_25	-13.740796	6.7924757	-6.948321	1
70	D.2_50	1.2628684	-3.2338684	-1.971	1
71	D.2_100	-27.649876	7.16807175	-20.4818	1
72	D.2_1000	-39.264137	14.0876236	-25.17651	1
73	D.2_2000	-19.489651	10.254838	-9.234813	1
74	D.3_0.5	-21.100094	7.71996307	-13.38013	
75	D.3_1.0	-17.667803	6.75594139	-10.91186	
76	D.3_1.5	-6.8483939	3.79709888	-3.051295	
77	D.3_2.0	-1.5391127	-1.8646868	-3.4038	
78	D.3_3.0	-14.336241	5.22744799	-9.108792	
79	D.3_6.0	-21.347099	9.1792326	-12.16787	
80	D.3_9.0	-30.422112	16.9328518	-13.48926	
81	D.3_12	-29.468397	20.5100346	-8.958364	1
82	D.3_25	1.67372584	-7.7647395	-6.091014	1
83	D.3_50	-13.738711	7.22060728	-6.518104	1

OID	Name	Curvature	Profile Curve	Plan Curve	Stream Permanence
84	D.3_100	-11.785669	0.55867743	-11.22699	1
85	D.3_1000	-35.951866	28.290617	-7.661247	1
86	D.3_2000	-16.993656	12.5445633	-4.449092	1
87	E_0.0	-30.807514	10.1034718	-20.70404	0
88	E_0.5	-20.530672	16.1709652	-4.359708	
89	E_1.0	-22.756247	19.0043488	-3.751898	
90	E_1.5	-16.616545	16.0692215	-0.547324	
91	E_2.0	-19.904961	15.9386349	-3.966324	
92	E_3.0	-30.396919	14.2367611	-16.16016	
93	E_6.0	-37.918659	18.5951481	-19.32351	
94	E_9.0	-33.021332	18.1416569	-14.87967	
95	E_12	-26.254236	10.2671728	-15.98706	0
96	E_25	-29.730577	21.1690102	-8.561566	0
97	E_50	-52.528355	28.0425816	-24.48577	0
98	E_100	-12.649201	-4.4587579	-17.10796	0.08
99	E_1000	-36.084499	15.4972019	-20.5873	1
100	E_2000	-20.010851	14.7775154	-5.233335	1
101	F_0.0	-19.059683	-6.7607737	-25.82046	1
102	F_0.5	-16.709482	-6.5936713	-23.30315	
103	F_1.0	-17.845003	-4.179863	-22.02487	
104	F_1.5	-17.332617	-1.9887047	-19.32132	
105	F_2.0	-27.658731	3.67376828	-23.98496	

OID	Name	Curvature	Profile Curve	Plan Curve	Stream Permanence
106	F_3.0	-36.810604	9.75392246	-27.05668	
107	F_6.0	-41.403961	2.93148565	-38.47248	
108	F_9.0	-74.944443	17.9307213	-57.01372	
109	F_12	-8.9675083	-16.098013	-25.06552	1
110	F_25	-34.577469	16.6633835	-17.91409	1
111	F_50	-44.32098	8.99149895	-35.32948	1
112	F_100	-91.245529	35.8257294	-55.4198	1
113	F_1000	-30.624557	8.8727808	-21.75178	1
114	F_2000	-10.101088	6.49702787	-3.60406	1
115	G_0.0	-24.262707	3.95383906	-20.30887	0.19
116	G_0.5	-39.206532	11.3797169	-27.82681	
117	G_1.0	-30.628387	8.99280357	-21.63558	
118	G_1.5	-28.282383	7.77272177	-20.50966	
119	G_2.0	-43.290051	8.51102543	-34.77902	
120	G_3.0	-50.556713	5.55332518	-45.00339	
121	G_6.0	-38.469147	-1.8503428	-40.31949	
122	G_9.0	-41.297657	14.3640699	-26.93358	
123	G_12	-23.85882	8.87632275	-14.9825	0.01
124	G_25	-31.063227	-3.6080222	-34.67125	0.32
125	G_50	-35.087521	2.73099923	-32.35652	0.45
126	G_100	12.1875048	-13.892987	-1.705483	0.09
127	G_1000	-33.225342	17.6785831	-15.54676	1

OID	Name	Curvature	Profile Curve	Plan Curve	Stream Permanence
128	G_2000	-38.020771	11.3346949	-26.68608	1
129	H_0.0	-50.961044	33.7812653	-17.17978	0.05
130	H_0.5	-60.425522	46.4768562	-13.94867	
131	H_1.0	-33.544956	25.280138	-8.264819	
132	H_1.5	-3.0404708	1.59904659	-1.441424	
133	H_2.0	-6.1277456	-2.886013	-9.013759	
134	H_3.0	-29.319172	7.21809959	-22.10107	
135	H_6.0	-62.966217	40.6852608	-22.28096	
136	H_9.0	-37.01701	23.8196182	-13.19739	
137	H_12	-24.976545	13.626852	-11.34969	0.03
138	H_25	-30.384737	2.8131218	-27.57162	0
139	H_50	-54.22887	18.9208641	-35.308	0.2
140	H_100	-49.81152	41.7049446	-8.106573	0.08
141	H_1000	-49.726368	27.1780682	-22.5483	
142	H_2000	-30.677801	7.71737337	-22.96043	1
143	H.2_0.5	-74.0989	49.4297791	-24.66912	
144	H.2_1.0	-74.251358	33.6153488	-40.63601	
145	H.2_1.5	-81.646843	53.5155144	-28.13132	
146	H.2_2.0	-51.100189	45.832901	-5.267286	
147	H.2_3.0	-55.984936	24.2610168	-31.72392	
148	H.2_6.0	-47.295986	37.1190643	-10.17692	
149	H.2_9.0	-40.887985	22.9205208	-8.95853	

OID	Name	Curvature	Profile Curve	Plan Curve	Stream Permanence
150	H.2_12	-19.662737	8.50881481	-11.15392	
151	H.2_25	-26.291069	6.13162565	-20.15944	1
152	H.2_50	-6.3189578	0.82274866	-5.496209	1
153	H.2_100	5.32520199	-1.2765988	4.0486031	1
154	H.2_1000	-50.748646	36.6858711	-14.06278	1
155	H.2_2000	-53.285694	35.2416725	-18.04402	1
156	I_0.0	-9.7495403	1.02825272	-8.721287	1
157	I_0.5	-10.148595	0.0453476	-10.10325	
158	I_1.0	-10.598081	-0.6085755	-11.20666	
159	I_1.5	-10.099771	-0.4651048	-10.56488	
160	I_2.0	-10.736832	-0.1722202	-10.90905	
161	I_3.0	-4.7581654	2.27225995	-2.485905	
162	I_6.0	-13.438585	6.48673534	-6.951849	
163	I_9.0	-2.0713935	4.02566862	1.954275	
164	I_12	-33.318485	15.8527184	-17.46577	
165	I_25	-28.805653	19.1133194	-9.692334	1
166	I_50	-2.0958514	1.59533131	-0.50052	1
167	I_100	-15.860663	11.6961536	-4.16451	1
168	J_0.0	-60.883888	54.2730103	-6.61088	1
169	J_0.5	-47.046921	42.6751404	-4.371783	
170	J_1.0	-41.09964	35.7458191	-5.353822	
171	J_1.5	-41.486916	32.0878143	-9.399099	

OID	Name	Curvature	Profile Curve	Plan Curve	Stream Permanence
172	J_2.0	-45.560303	30.5582943	-15.00201	
173	J_3.0	-45.149536	29.5681725	-15.58136	
174	J_6.0	-44.083557	29.2357597	-14.8478	
175	J_9.0	-13.434996	19.5738831	6.1388879	
176	J_12	-24.281134	8.4714222	-15.80971	1
177	J_25	-9.92169	6.54449129	-3.377198	1
178	J_50	-12.572088	10.3040237	-2.268064	1
179	J_100	-33.788837	14.7327452	-19.0561	1
180	IJ_1000	-15.554481	13.294487	-2.259994	1
181	IJ_2000	1.08510959	-4.1536818	-3.068572	1
182	IJ.2_0.5	-22.399097	17.535799	-4.863298	
183	IJ.2_1.0	3.46118665	0.90586555	4.3670521	
184	IJ.2_1.5	3.46118665	0.90586555	4.3670521	
185	IJ.2_2.0	-3.6489177	1.84443605	-1.804482	
186	IJ.2_3.0	-4.8101263	-2.2351727	-7.045299	
187	IJ.2_6.0	-34.827351	20.9812603	-13.84609	
188	IJ.2_9.0	-24.121864	13.4148407	-10.70702	
189	IJ.2_12	-18.840437	4.70863628	-14.1318	1
190	IJ.2_25	-12.109357	6.64420176	-5.465156	1
191	IJ.2_50	-17.169901	14.5027285	-2.667172	1
192	IJ.2_100	-9.1167831	11.6396322	2.5228496	1
193	IJ.2_1000	-17.767048	11.223238	-6.543809	1

OID	Name	Curvature	Profile Curve	Plan Curve	Stream Permanence
194	IJ.2_2000	-33.736599	22.4968491	-11.23975	1

Appendix 13: Continued Data Summary: **drainage area, installation date and field observations, and soil classification for all Gibson Jack sites**.

Table A13.1. Name, Upstream Accumulation Area (UAA in square meters), date that the well was installed, whether or not the location was wet on the date of well installation, and the NRCS soil classification identifier number of the soils mapped at that location (NRCS Web Soil Survey, 2021; see appendix 4).

OID	Name	UAA (m^2)	Install Date	Wet Install	NRCS_Class
1	A_250	243078	7/23/2020	N	563
2	A_100.0	272597	7/23/2020	N	563
3	A_0.0	305260	7/23/2020	N	749
4	A_0.5	305260	7/23/2020	N	749
5	A_1.0	305403	7/23/2020	N	749
6	A_1.5	305403	7/23/2020	N	749
7	A_2.0	305403	7/23/2020	N	749
8	A_3.0	305406	7/23/2020	N	749
9	A_6.0	305911	7/23/2020	N	749
10	A_9.0	306187	7/23/2020	N	749
11	A_12	306991	7/23/2020	Y	749
12	A_25	309233	7/23/2020	Y	749
13	A_50.0	312106	7/24/2020	Y	749
14	A_100.0	320324	7/24/2020	Y	749
15	A_1000	1786838	7/24/2020	Y	749

OID	Name	UAA (m^2)	Install Date	Wet Install	NRCS_Class
16	A_200.0	390325	7/24/2020	Y	749
17	B_250	137771	7/24/2020	N	208
18	B_100	181072	7/24/2020	N	208
19	B_0.0	287686	7/24/2020	N	208
20	B_0.5	287686	7/24/2020	N	208
21	B_1.0	287721	7/24/2020	N	208
22	B_1.5	287721	7/24/2020	N	208
23	B_2.0	287725	7/24/2020	N	208
24	B_3.0	287731	7/24/2020	N	208
25	B_6.0	287818	7/24/2020	N	208
26	B_9.0	289930	7/24/2020	N	208
27	B_12	290018	7/24/2020	N	208
28	B_25	291613	7/24/2020	N	208
29	B_50	293923	7/24/2020	N	208
30	B_100	718777	7/24/2020	N	208
31	B_1000	1786838	7/28/2020	Y	749
32	Spring	24	7/27/2020	Y	208
33	C_0.0	256137	6/13/2020	N	208
34	C_0.5	256153	6/13/2020	N	208
35	C_1.0	256153	6/13/2020	N	208
36	C_1.5	256267	6/13/2020	N	208
37	C_2.0	256267	6/13/2020	N	208

OID	Name	UAA (m^2)	Install Date	Wet Install	NRCS_Class
38	C_3.0	256274	6/13/2020	N	208
39	C_6.0	256281	6/13/2020	N	208
40	C_9.0	256552	6/13/2020	N	208
41	C_12	256564	6/13/2020	N	208
42	C_25	257745	6/13/2020	N	208
43	C_50	324013	6/13/2020	N	208
44	C_100	344105	6/14/2020	N	208
45	C_1000	1651805	6/14/2020	Y	749
46	C_2000	5791734	9/3/2020	Y	749
47	D_0.0	1494368	5/31/2020	N	208
48	D_0.5	1494379	5/31/2020	N	208
49	D_1.0	1494379	5/31/2020	N	208
50	D_1.5	1494379	5/31/2020	N	208
51	D_2.0	1495918	5/31/2020	N	208
52	D_3.0	1495946	5/31/2020	N	208
53	D_6.0	1496188	5/31/2020	N	208
54	D_9.0	1496188	6/12/2020	N	208
55	D_12	1496306	6/12/2020	N	208
56	D_25	1499730	6/12/2020	N	208
57	D_50	1518029	6/12/2020	N	208
58	D_100	1539649	7/17/2020	N	208
59	D_1000	3066489	7/17/2020	Y	307

OID	Name	UAA (m^2)	Install Date	Wet Install	NRCS_Class
60	D_2000	5481711	9/3/2020	Y	749
61	D.2_0.5	5481720	9/3/2020	Y	749
62	D.2_1.0	5481720	9/3/2020	Y	749
63	D.2_1.5	5481720	9/3/2020	Y	749
64	D.2_2.0	5481721	9/3/2020	Y	749
65	D.2_3.0	5481721	9/3/2020	Y	749
66	D.2_6.0	5485035	9/3/2020	Y	749
67	D.2_9.0	5485084	9/3/2020	Y	749
68	D.2_12	5485117	9/3/2020	Y	749
69	D.2_25	5485734	9/3/2020	Y	749
70	D.2_50	5499047	9/3/2020	Y	749
71	D.2_100	5546291	9/3/2020	Y	749
72	D.2_1000	7122091	9/3/2020	Y	749
73	D.2_2000	11793008	9/3/2020	Y	749
74	D.3_0.5	11793031	9/19/2020	Y	749
75	D.3_1.0	11793031	9/19/2020	Y	749
76	D.3_1.5	11793031	9/19/2020	Y	749
77	D.3_2.0	11793032	9/19/2020	Y	749
78	D.3_3.0	11793032	9/19/2020	Y	749
79	D.3_6.0	11793130	9/19/2020	Y	749
80	D.3_9.0	11793141	9/19/2020	Y	749
81	D.3_12	11793167	9/19/2020	Y	749

OID	Name	UAA (m^2)	Install Date	Wet Install	NRCS_Class
82	D.3_25	11793386	9/19/2020	Y	749
83	D.3_50	11793386	9/19/2020	Y	72
84	D.3_100	11810932	9/19/2020	Y	72
85	D.3_1000	13726864	9/19/2020	Y	386
86	D.3_2000	16406518	9/19/2020	Y	307
87	E_0.0	629588	6/20/2020	N	3002
88	E_0.5	630078	6/20/2020	N	3002
89	E_1.0	630078	6/20/2020	N	3002
90	E_1.5	631288	6/20/2020	N	3002
91	E_2.0	631288	6/20/2020	N	3002
92	E_3.0	631411	6/20/2020	N	3002
93	E_6.0	631426	6/20/2020	N	3002
94	E_9.0	636368	6/20/2020	N	3002
95	E_12	636488	6/20/2020	N	3002
96	E_25	644109	6/20/2020	N	3002
97	E_50	686844	6/20/2020	N	3002
98	E_100	719415	6/20/2020	N	3002
99	E_1000	3192522	6/20/2020	Y	307
100	E_2000	5719471	7/21/2020	Y	749
101	F_0.0	223280	7/21/2020	Y	79
102	F_0.5	223280	7/21/2020	Y	79
103	F_1.0	223286	7/21/2020	Y	79

OID	Name	UAA (m^2)	Install Date	Wet Install	NRCS_Class
104	F_1.5	223286	7/21/2020	Y	79
105	F_2.0	223300	7/21/2020	Y	79
106	F_3.0	223300	7/21/2020	Y	79
107	F_6.0	223416	7/21/2020	Y	79
108	F_9.0	223465	7/21/2020	Y	79
109	F_12	223799	7/21/2020	Y	79
110	F_25	471464	7/21/2020	Y	79
111	F_50	492000	7/21/2020	Y	79
112	F_100	531468	7/21/2020	Y	79
113	F_1000	935139	7/21/2020	Y	3002
114	F_2000	7831356	7/21/2020	Y	67
115	G_0.0	366300	8/22/2020	N	79
116	G_0.5	366300	8/22/2020	N	79
117	G_1.0	366300	8/22/2020	N	79
118	G_1.5	366790	8/22/2020	N	79
119	G_2.0	366790	8/22/2020	N	79
120	G_3.0	366897	8/22/2020	N	79
121	G_6.0	366911	8/22/2020	N	79
122	G_9.0	366955	8/22/2020	N	79
123	G_12	366975	8/22/2020	N	79
124	G_25	370468	8/22/2020	N	79
125	G_50	372002	8/22/2020	N	79

OID	Name	UAA (m^2)	Install Date	Wet Install	NRCS_Class
126	G_100	387123	8/22/2020	N	79
127	G_1000	13418288	8/22/2020	Y	307
128	G_2000	16093004	8/22/2020	Y	307
129	H_0.0	402615	8/13/2020	N	79
130	H_0.5	402832	8/13/2020	N	79
131	H_1.0	402832	8/13/2020	N	79
132	H_1.5	402833	8/13/2020	N	79
133	H_2.0	403677	8/13/2020	N	79
134	H_3.0	403677	8/13/2020	N	79
135	H_6.0	404279	8/13/2020	N	79
136	H_9.0	404357	8/13/2020	N	79
137	H_12	404428	8/13/2020	N	79
138	H_25	406176	8/13/2020	N	79
139	H_50	416917	8/13/2020	N	79
140	H_100	440838	8/13/2020	N	116
141	H_1000	1357203	10/3/2020	N	79
142	H_2000	1658259	10/3/2020	Y	72
143	H.2_0.5	1658586	10/3/2020	Y	72
144	H.2_1.0	1658586	10/3/2020	Y	72
145	H.2_1.5	1658586	10/3/2020	Y	72
146	H.2_2.0	1658608	10/3/2020	Y	72
147	H.2_3.0	1658627	10/3/2020	Y	72

OID	Name	UAA (m^2)	Install Date	Wet Install	NRCS_Class
148	H.2_6.0	1659056	10/3/2020	Y	72
149	H.2_9.0	1659110	10/3/2020	Y	72
150	H.2_12	1659628	10/3/2020	Y	72
151	H.2_25	1660911	10/3/2020	Y	72
152	H.2_50	1663754	10/3/2020	Y	72
153	H.2_100	1667054	10/3/2020	Y	307
154	H.2_1000	16165831	10/3/2020	Y	307
155	H.2_2000	16721163	10/3/2020	Y	307
156	I_0.0	3483814	7/25/2020	Y	67
157	I_0.5	3483814	7/25/2020	Y	67
158	I_1.0	3483818	7/25/2020	Y	67
159	I_1.5	3483818	7/25/2020	Y	67
160	I_2.0	3486086	7/25/2020	Y	67
161	I_3.0	3486087	7/25/2020	Y	67
162	I_6.0	3488994	7/25/2020	Y	67
163	I_9.0	3489030	7/25/2020	Y	67
164	I_12	3492747	7/25/2020	Y	67
165	I_25	3499680	7/25/2020	Y	67
166	I_50	3508121	7/25/2020	Y	67
167	I_100	3530315	7/25/2020	Y	67
168	J_0.0	7923836	8/7/2020	Y	67
169	J_0.5	7923836	8/7/2020	Y	67

OID	Name	UAA (m^2)	Install Date	Wet Install	NRCS_Class
170	J_1.0	7923842	8/7/2020	Y	67
171	J_1.5	7923842	8/7/2020	Y	67
172	J_2.0	7923984	8/7/2020	Y	67
173	J_3.0	7923984	8/7/2020	Y	67
174	J_6.0	7924026	8/7/2020	Y	67
175	J_9.0	7924015	8/7/2020	Y	67
176	J_12	7924872	8/7/2020	Y	67
177	J_25	7925157	8/7/2020	Y	67
178	J_50	7933514	8/7/2020	Y	67
179	J_100	7940158	8/7/2020	Y	67
180	IJ_1000	13417363	10/17/2020	Y	307
181	IJ_2000	15431497	10/17/2020	Y	307
182	IJ.2_0.5	15431497	10/17/2020	Y	307
183	IJ.2_1.0	15431497	10/17/2020	Y	307
184	IJ.2_1.5	16045685	10/17/2020	Y	307
185	IJ.2_2.0	16045685	10/17/2020	Y	307
186	IJ.2_3.0	16045687	10/17/2020	Y	307
187	IJ.2_6.0	16047205	10/17/2020	Y	307
188	IJ.2_9.0	16047236	10/17/2020	Y	307
189	IJ.2_12	16048479	10/17/2020	Y	307
190	IJ.2_25	16049112	10/17/2020	Y	307
191	IJ.2_50	16090346	10/17/2020	Y	307

OID	Name	UAA (m^2)	Install Date	Wet Install	NRCS_Class
192	IJ.2_100	16145867	10/17/2020	Y	307
193	IJ.2_1000	16678141	10/17/2020	Y	307
194	IJ.2_2000	19342600	10/17/2020	Y	69

Appendix 14: Site descriptions including field observations for all Gibson Jack sites.

Table A14.1 includes observations of incision, nearby springs, vegetation, and surface sediment characteristics. Note that all points between 0 and 9m are summarized in the 0.0m well of each nest. Throughout, I use LS, SS, QTZ, and SH to refer to limestone, sandstone, quartzite, and shale, respectively.

OID	Name	Site Description
1	A -250	Installation was in a dry spring below incised step. The channel is incised 1 m into the westward thickening hillslope package. Predominantly silt/clay with tan-grey LS/SS gravels to 14cm cobbles. A lot of aspen, aster, mint, yarrow, and lupine. Notes on channel morphology: between this location and A-100:250-200 is comprised of aspen-covered coalesced slumps composed of predominantly silt/clay w little gravel. Incised 0-1.5m deep x 2m wide then transitions to an open flat meadow w no tree cover and no channel after that.
2	A -100.0	The installation location was in the middle of a wide-open flat valley/meadow w no tree cover—lots of lovely wildflowers and sunshine.
3	A 0.0	The installation site is located in a dry spring below incised step where the channel reemerges from the channel-less valley above. The emergent channel quickly incises to 1-1.5 m. Lots of pine, aspen, and other riparian vegetation surrounding the channel. Sediment comprised of predominantly silt/clay with little LS/SS gravel
4	A 0.5	See A 0.0

OID	Name	Site Description
5	A 1.0	See A 0.0
6	A 1.5	See A 0.0
7	A 2.0	See A 0.0
8	A 3.0	See A 0.0
9	A 6.0	See A 0.0
10	A 9.0	See A 0.0
11	A 12	The installation is above a marshy spring in a dry channel incised ~1m into valley fill. Large pine trees and small aspen in the vicinity and lots of wildflowers and riparian vegetation in the area. The channel widens out to 2 meters below installation before another scarp directly above a marshy spring. Surface sediments consist of silty clay with tan-grey LS gravels (<2cm).
12	A_25	Installation is in a fetid-boggy spring (*the bog of eternal stench) with lots of riparian vegetation. Install went 1m into fetid muck before hitting firmer sediments. Sediments description: Knee-deep stinky-boggy muck.
13	A_50.0	Directly below springs and swampy marshy area. 15 CM of hyper saturated muck than firming to what felt like Clay and silt. The channel is broad and flat bottomed, two meters at the bottom gently sloping on both sides and thickly vegetated with pine, big tooth maple, aspen, and lots of riparian grass.
14	A_100.0	.75 m by 1.5 m channel in sunny open valley. Sediments: loess with no gravel in channel or float on trial few trees lots of lush aquatic grasses and

OID	Name	Site Description
		Equestria sedum. Marshy surface water. The channel became incised and discharge increased as I walked towards this location from the last. Predominantly silt/clay with some (5-10%). 5-2cm shaley gravel in the stream bed.
15	A_1000	Anastomosed and channels, 10 to 20% gravel, quartzite and shale, with an occasional 1m boulder. Angular gravels with rounded larger clasts. Densely vegetated with riparian type vegetation.
16	A_200.0	channel becomes less prominent and stream goes intermittent 20 m hello installation. same sides same veggies.
17	B -250	There are about 40% platy SH gravels (< 2 cm) inside an ~ 1X1.5m deep bedrock channel ranging; there are also numerous meter-sized well-rounded QTZ boulders ranging from .75-1m.
18	B -100	20 m down-channel from where the bedrock channel ends. Sediment description: 70% platy SH gravels <4cm. Densely vegetated with lots of ferns and aspen.
19	B 0.0	Wide-open, aspen-filled valley with a dry .5 x.75m wide/deep channel filled with SH/SS gravels (<5cm).
20	B 0.5	See B 0.0
21	B 1.0	See B 0.0
22	B 1.5	See B 0.0
23	B 2.0	See B 0.0
24	B 3.0	See B 0.0, ~ 0.25m step above log below this site

OID	Name	Site Description
25	B 6.0	See B 0.0
26	B 9.0	See B 0.0
27	B 12	The end of the initial series is still in a dry channel incised .25m x 1m in a large open valley with numerous aspen and ferns. Streambed sediments consist of a mix of SH, SS, and QTZ gravels that range from .5-4 cm, with occasional boulders well rounded QTZ cobbles/boulders throughout the series.
28	B 25	Continuation of above except for less gravel. The surrounding valley fill is comprised of silt/clay with <15% platy SH and several well-rounded QTZ boulders (.25-1.5 m).
29	B 50	Located directly below springs in a marshy area with lots of elder/serviceberries. The installation encountered 15 cm of hyper-saturated muck than firming to what felt like silt/clay until TD. The channel is broad and flat bottomed, two meters wide at the bottom, and thickly vegetated with pine and bigtooth maple.
30	B 100	5m downstream from where the spring discharge enters the main channel. There are numerous springs/seeps in the vicinity, and the area is heavily vegetated. The surficial channel sediments are predominantly silt/clay with some sand and occasional SH, LS gravels (< 3 cm).
31	B 1000	Anastomosed channels, 10 to 20% gravel that consists of QTZ, SH, and some LS with an occasional 1 m boulder. Angular gravels and rounded

OID	Name	Site Description
		larger class. The site is densely vegetated with pine, willow, and riparian vegetation.
32	B.Spring	4-m scarp in silt/clay with almost no gravel and spring below. 10 to 20% gravel, QTZ, and SH, with an occasional well-rounded QTZ boulder (<1m). Densely vegetated with pine, aspen, and other riparian vegetation.
33	C 0.0	Dry on installation date. <0.25cm pebbles to 0.6m well-rounded QTZ boulders. Gravels are 70% QTZ and 30 %platy SH. Series is installed in a densely vegetated channel with lots of tall aspen and is .75m wide and 1.25m deep. This is where the moose tried to trample me; Magdatha is her name.
34	C 0.5	See C 0.0
35	C_1.0	See C 0.0
36	C 1.5	See C 0.0
37	C 2.0	See C 0.0
38	C 3.0	See C 0.0
39	C 6.0	See C 0.0
40	C 9.0	See C 0.0
41	C 12	Channel is similarly described above. Predominantly 0.5-5 cm QTZ and SH gravels with some well-rounded QTZ cobbles and boulders.
42	C 25	See start description for sediment classification. Installation is in a thick aspen grove. Channel is ~1m x 1.5m (w/d).

OID	Name	Site Description
43	C 50	Channel is incised laterally into the hillslope (2m scarp) on river right. Sediments are similar to those described above, as is vegetation. Scarp sediments are predominantly silt/clay with some (<5%) sub rounded SH/QTZ
44	C 100	Channel is .5m deep and 1m wide and incised into valley fill. Surficial channel sediments are similar to those described above.
45	C 1000	Wet installation into braided channel system, located was in the southernmost channel. Sediments were predominantly well rounded QTZ gravel to cobbles with some platy SH gravel and occasional well-rounded QTZ boulders
46	C 2000	Wet on the install date. Predominantly gravel (<2cm) in a sandy-silt matrix with some cobbles and occasional boulders (<1.5m) in the vicinity.
47	D 0.0	0.25 to 3 cm platy/ sub-angular pebbles/gravels (90% SH, 10% QTZ) with sandy silt matrix. Dry on install, but 5m above observed surface water on installation date.
48	D 0.5	See D 0.0
49	D 1.0	See D 0.0
50	D 1.5	See D 0.0
51	D 2.0	See D 0.0
52	D 3.0	See D 0.0
53	D 6.0	See D 0.0

OID	Name	Site Description
54	D 9.0	See D 0.0
55	D 12	Sediment and channel description are similarly described above
56	D 25	Located in a wet pool above a small drop formed by accumulated brush and debris/sediments. .5-3cm pebble to gravel with sub rounded QTZ cobbles to boulders
57	D 50	SH outcrop immediately next to the channel. .5cm pebbles to 0.25m cobbles 80%QTZ with 20% SH gravel.
58	D 100	Dry on July 17th wet on installation date. see start for sediment description
59	D 1000	Surficial stream sediments are 90% QTZ, 10% SH,.5-25 cm, pebbles-cobbles, platy to sub angular. Surface water present.
60	D.2 0.0	Wet on the install date. Predominantly gravel (<2cm) in a sandy-silt matrix with some cobbles and occasional boulders (<1.5m) in the vicinity.
61	D.2 0.5	See D.2 0.0
62	D.2 1.0	See D.2 0.0
63	D.2_1.5	See D.2 0.0
64	D.2 2.0	See D.2 0.0
65	D.2 3.0	See D.2 0.0
66	D.2 6.0	See D.2 0.0
67	D.2 9.0	See D.2 0.0
68	D.2 12	Continuation of above. Extremely vegetated and difficult to move around.

OID	Name	Site Description
69	D.2 25	QTZ gravel to boulders suspended in a silty sand matrix. 1x1.5m (w/d) channel. Densely vegetated.
70	D.2 50	It still hasn't changed; seriously bushwhacking here.
71	D.2 100	Same composition as above, but the range is quarter cm to 40 cm. still very vegetated. Install is at the end of a braided channel network with three channels, and this well is in the channel with the most discharge (center).
72	D.2 1000	Sediments composed of QTZ gravel to boulders suspended in a silty sand matrix. Very vegetated, lots of willows.
73	D.3 0.0	Predominantly QTZ gravel to boulders suspended in a silty sand matrix. Chanel is incised 1.25 x 2m into the valley fill.
74	D.3 0.5	See D.3 0.0
75	D.3 1.0	See D.3 0.0
76	D.3 1.5	See D.3 0.0
77	D.3 2.0	See D.3 0.0
78	D.3 3.0	See D.3 0.0
79	D.3 6.0	See D.3 0.0
80	D.3 9.0	See D.3 0.0
81	D.3 12	Mainstem channel 2m wide and .5 m deep and surrounded by riparian vegetation. Streambed sediments are composed of predominantly well rounded QTZ cobbles with some boulders suspended in a gravely, sandy silt.

OID	Name	Site Description
82	D.3 25	Wet installation in the mainstem between two steps and located in a small pool. Mainly mixed gravels composed of 10%LS, 10%SH, and 80%QTZ with lots of well-rounded QTZ -cobbles and small boulders.
83	D.3_50	Located just above a large nettle patch in the mainstem. Highly vegetated and difficult to move around. Sediments are similarly described above however the install location is in a large straight stretch that runs for ~25m.
84	D.3 100	Sediments are the same size and composition as described above; however, some well-rounded boulders (.5-1.5m) are in the vicinity. The channel is half a meter deep and 1.5 m wide with substantial discharge.
85	D.3 1000	Large pool under a drop. Same sediments as above.
86	D.3 2000	Predominantly QTZ cobbles to boulders suspended in 90%QTZ gravel. Well rounded. Lots of riparian vegetation and old-growth aspen/pine.
87	E 0.0	100% QTZ, angular to sub angular, pebbles to boulders (.05-1.5m). Very bouldery, sunny, and hot. This series was complicated to install.
88	E 0.5	See E 0.0
89	E_1.0	See E 0.0
90	E 1.5	See E 0.0
91	E 2.0	See E 0.0
92	E 3.0	See E 0.0
93	E 6.0	See E 0.0
94	E 9.0	See E 0.0

OID	Name	Site Description
95	E 12	Same as above, but I would like to note that I had difficulty installing this well as the drive collar became severely bound in the sediments.
96	E 25	Numerous angular QTZ boulders. .3-.75m suspended in QTZ gravels and silt/clay.
97	E 50	Five meters below surface water spring on installation date. See start for sediment description.
98	E 100	Sediments are similarly described at the start location—still very boulder and challenging to install. The channel corridor is poorly vegetated, sunny, and hot.
99	E 1000	Wet on the install date. 0.5 cm pebbles to .5m cobbles, predominantly pebbles-gravel suspended in a sandy-silt matrix, predominantly QTZ with occasional (10%) SH pebbles.
100	E 2000	Sediments are similarly described at CD 0.0. Predominantly, QTZ clasts that ranged from .5 to 40cm and were suspended in a sandy-silt matrix.
101	F 0.0	Start cluster is located in a thick package of silt/clay with predominantly QTZ pebbles- gravels in the channel with some cobbles-boulders (>0.5m). Some gamble oak and maple in the vicinity, but not very vegetated. Just below a scarp with emergent spring. Very marshy.
102	F 0.5	See F 0.0
103	F 1.0	See F 0.0
104	F 1.5	See F 0.0
105	F 2.0	See F 0.0

OID	Name	Site Description
106	F 3.0	See F 0.0
107	F 6.0	See F 0.0
108	F 9.0	See F 0.0
109	F 12	Channel sediments are comprised of QTZ gravel to cobbles with occasional .5m boulder suspended in silt and clay. Lots of wildflowers, and the stream is well shaded and cool. Installations in this section are going much better than the last because there are not as many boulders.
110	F_ 25	Channel is deeply incised into valley fill (2m). See above for sed/veg description.
111	F_ 50	Sediments are similarly described above. Channel is still profoundly incised (~3m x 2.5m), and there has been an increase in discharge at 25m and again here.
112	F_ 100	Streambed sediments consist of interworked silt/clay and <2cm sub rounded QTZ pebbles. Channel is incised 1.5x1m (w/d) densely vegetated with gamble oak, nettle, and maple.
113	F_1000	The channel heavily vegetated and is incised 1m into valley fill that is composed of inter worked loess with sub angular to angular 90% court site 10% shale pebbles 1 and 1/2 meter boulders. Boulders are all rounded to well-rounded in this area.
114	F_2000	Installation is located in the north fork. Wide valley filled with aspen and pine. Stream seds are predominantly quartzite gravel with occasional 1m boulder. Found a dead moose skull here.

OID	Name	Site Description
115	G_ 0.0	The channel is located in a dense oak/maple grove and varies in depth between .25 to .5 m, with .5m steps at 12m and 18m created by sediment accumulation around downfall within the channel. Sediments are predominantly angular QTZ gravel to sub angular-sub rounded cobbles.
116	G_ 0.5	See G_ 0.0
117	G_ 1.0	See G_ 0.0
118	G_ 1.5	See G_ 0.0
119	G_ 2.0	See G_ 0.0
120	G_ 3.0	See G_ 0.0
121	G_ 6.0	See G_ 0.0
122	G_ 9.0	See G_ 0.0
123	G_ 12	See above for description.
124	G_ 25	Dry channel in a dense maple grove. Incised .25mx.5m with numerous steps caused by downfall.
125	G_ 50	Located about 4 m above a 1 m incision that is 1 m wide the insulation point area where there is very little existence of a channel lots of gravel on the surface. Gravel is predominantly QTZ sub-rounded .5 to 7 cm.
126	G_ 100	Channel is incised 0.5 by .25m deep and located in a broad flat valley. Sediments are comprised of QTZ pebbles to cobbles. Well rounded.

OID	Name	Site Description
127	G_ 1000	Located in mainstem channel in a wooded area with large pines and maple. Sediments comprised of 75% QTZ gravel to boulders and 25%platy SH gravel. Channel is 1.5 m wide and .5m deep
128	G_ 2000	Wet installation in the thickly vegetated main channel. Primarily cobbles suspended in a 75/25 mix of QTZ and SH pebbles to gravel with a sandy silt matrix. Some well-rounded QTZ boulders.
129	H_ 0.0	Start cluster was ridiculously hard to install. Met a resistant layer from ten cm to approximately 40 cm. Incised channel 3 m deep 2.5 m in valley fill deposit 40% clay 10% sand 30% gravel and 10% boulders.
130	H_ 0.5	See H_ 0.0
131	H_ 1.0	See H_ 0.0
132	H_ 1.5	See H_ 0.0
133	H_ 2.0	See H_ 0.0
134	H_ 3.0	See H_ 0.0
135	H_ 6.0	See H_ 0.0
136	H_ 9.0	See H_ 0.0
137	H_ 12	Predominantly QTZ cobbles to boulders suspended in 90%QTZ gravel. Well rounded. Dry install in a sparsely vegetated valley.
138	H_ 25	25 is located just above a significant slump feature. The channel changes from deeply incised to half a meter deep, and then the channel completely disappears 12 m down from here until 5m above 50 .

OID	Name	Site Description
139	H_50	The sediment description is basically the same as above with exception of a higher concentration of loss this installation was very difficult and it took three attempts to reach the target depth. 10 m above installation site is a large step that is full of folders and cobbles. Below this site the channel rapidly becomes deeply incised to 3 to 4 m deep in valley fill deposits.
140	H_ 100	Incised channel (.75m) with AL Consisting of .5 centimeter gravels to .5m boulders well-rounded QTZ
141	H_ 1000	Just below valley fill composed of large boulders <2m in a dense maple grove. Sediments consist of QTZ gravel to boulders suspended in a silty sand matrix
142	H2_ 0.0	Dense maple and oaks with an incised channel .5m deep by .75m wide in alluvial sediments. Lots of boulders. Mostly QTZ pebbles to gravels with numerous well-rounded cobbles-boulders (<2m).
143	H.2_ 0.5	See H.2_ 0.0
144	H.2_ 1.0	See H.2_ 0.0
145	H.2_ 1.5	See H.2_ 0.0
146	H.2_ 2.0	See H.2_ 0.0
147	H.2_ 3.0	See H.2_ 0.0
148	H.2_ 6.0	See H.2_ 0.0
149	H.2_ 9.0	See H.2_ 0.0
150	H.2_ 12	See above for sediment description

OID	Name	Site Description
151	H.2_ 25	Channel is incised into alluvial deposits with boulders up to 1m. See above for sed/veg description.
152	H.2_ 50	Channel and sediments have been continuous since the start of this series.
153	H.2_100	Wet installation in a .5mwide by .25m deep channel that is incised into alluvial deposits consisting of well rounded cobles to boulders suspended in a silty-sand/gravel matrix.
154	H.2_ 1000	Wet installation in the main stem. Sediments consist of well-rounded QTZ /SH (75/25%) pebbles to gravels and QTZ cobbles to boulders (<1.5m) suspended in a silty sand matrix.
155	H.2_ 2000	Well is located just above a prominent drop feature (1m) created by sediment/downfall accumulation—sediments are similarly described above.
156	I_ 0.0	The series starts in a 2x2m pool with lots of debris. 50% LS, 30% SH, and 20% QTZ gravel covered with calcium carbonate. 1-3cm, sub angular-blocky. 12 is 1m below a meter step. m deep and 2 m
157	I_ 0.5	See I_ 0.0
158	I_ 1.0	See I_ 0.0
159	I_ 1.5	See I_ 0.0
160	I_ 2.0	See I_ 0.0
161	I_ 3.0	See I_ 0.0
162	I_ 6.0	See I_ 0.0
163	I_ 9.0	See I_ 0.0

OID	Name	Site Description
164	I_ 12	Located in a massive willow thicket and incised .5m-1.5 wide. Sediments are mostly QTZ gravel-cobbles with some platy SH and LS interspersed. Some cool tufa accumulation in the stream bed gravels.
165	I_ 25	Channel is 1x2m and filled with predominantly 4-20 cm cobbles with some boulders.
166	I_50	See start description for sediment description. The installation was located in a half meter wide by 1 m deep channel that was heavily vegetated with riparian veggies.
167	I_ 100	See start sediment description. Installed in a 1 x 3 pool with lots of tufa accumulation in the gravels and some on some downfall in the stream.
168	J_ 0.0	0 through 25 are all installed inside of a 2-m by 1-meter deep channel in the base of the valley fill that extends across the valley about 20m. Mostly QTZ gravel with some QTZ cobbles in the channel. Driveshaft came out smeared with gray and orange clay.
169	J_ 0.5	See J_ 0.0
170	J_ 1.0	See J_ 0.0
171	J_ 1.5	See J_ 0.0
172	J_ 2.0	See J_ 0.0
173	J_ 3.0	See J_ 0.0
174	J_ 6.0	See J_ 0.0
175	J_ 9.0	See J_ 0.0

OID	Name	Site Description
176	J_ 12	Wet install on the north fork with lots of willows surrounded by pine. Found bear poo here. QTZ cobbles suspended in QTZ pebbles/sandy silt. Channel is .5m wide and .25m deep.
177	J_ 25	Installation is located in a pool that is in an area similarly described as above except for the presence of two ~1.25m well-rounded QTZ boulders that create a pool drop
178	J_ 50	.5m drop above this location, and the well is located in a pool in a large meander. Big pines offer shade for an excellent lunch consisting of peanut butter and serviceberry sandwiches with a side of fruit snacks.
179	J_ 100	Same vegetation as above, but that channel is about 1.5m wide and .25m deep. Sediments are predominantly QTZ cobbles with an occasional boulder suspended in a silt-pebble matrix.
180	IJ_ 1000	Wet installation in the main stem that is located amongst big pines and maples. Chanel is incised ~2m wide and 1m deep with predominantly QTZ cobles to boulders and QTZ, LS, SH gravel in a silty sand matrix.
181	IJ.2_ 0.0	10%SH 15%LS, and 75% QTZ pebble to gravel with well-rounded QTZ cobbles to boulders. The main channel is .5m deep and 1.75m wide and incised into reworked alluvial deposits. Densely vegetated with willows and oak in the adjacent area and large pie
182	IJ.2_ 0.5	See IJ.2_ 0.0
183	IJ.2_ 1.0	See IJ.2_ 0.0
184	IJ.2_ 1.5	See IJ.2_ 0.0

OID	Name	Site Description
185	IJ.2_ 2.0	See IJ.2_ 0.0
186	IJ.2_ 3.0	See IJ.2_ 0.0
187	IJ.2_ 6.0	See IJ.2_ 0.0
188	IJ.2_ 9.0	See IJ.2_ 0.0
189	IJ.2_ 12	See IJ.2_ 0.0
194	IJ.2_ 25	15%SH 20%LS, and 65% QTZ pebble to gravel with well-rounded QTZ cobbles to boulders Located in a small pool between two choke points/drops caused by ~1m boulders deposited in the channel. A densely vegetated area that is situated amongst the willows and berry bushes.
195	IJ.2_ 50	Installed right after a .5m drop. See above for site description.
196	IJ.2_100	Stream channel located in a large meander. Wet on install date, sediments and vegetation is similarly described above.
197	IJ.2_ 1000	This is my favorite of all the locations. I first tested the installation equipment here, and coincidentally this was my second to last well. Lots of cobbles and boulders suspended in silty sand-gravel (10%SH, 20%LS, 70% QTZ). Install is in a 3m wide pool.
198	IJ.2_2000	Densely vegetated area below the road. Chanel is incised 2m wide and .75m deep into reworked alluvial sediments consisting of predominantly QTZ cobbles to boulders. Streambed sediments are mostly QTZ cobbles with a mixed lithology matrix that consists of 10% SH gravel, 20%ls gravel to cobbles, QTZ gravel to boulders.

Appendix 15: Data Analysis Summary: test timing and processing details.

Table A15.1 includes sample name, date, test time, which slug tests were used in chronological order, and processing notes. "Returns" refer to the recovery of water levels in the well to their pre-slug levels, and were typically close to zero. In some cases, slug additions led to persistently higher water levels that initially observed. This may reflect the development of saturated conditions, and only later tests or a second "b" round of slugs were used for analysis.

OID	Name	Date	Time	Tests Used	Processing Notes
1	A_-250	8/15/2020	13:27	34567	All tests had returns under 1cm
2	A_-100.0	8/15/2020	15:15	13467	All tests had returns under 1cm
3	A_0.0	8/11/2020	9:53	134	3 of the tests got within 7 cm of static conditions, others exceeded 13 cm and were excluded.
4	A_0.5	8/11/2020	9:56	2356	4 of the tests got within 7 cm of static conditions, others exceeded 13 cm and were excluded.
5	A_1.0	8/11/2020	10:03	346	3 of the tests got within 10 cm of static conditions, others exceeded 13 cm at end of test and were excluded.
6	A_1.5	8/11/2020	15:58	1236	4 of the tests got within 10 cm of static conditions, others exceeded 13 cm and were excluded.

OID	Name	Date	Time	Tests Used	Processing Notes
7	A_2.0	8/11/2020	16:07	34567	All tests had returns under 1cm
8	A_3.0	8/11/2020	16:50	23456	All tests had returns under 1cm
9	A_6.0	8/11/2020	16:57	567	Reran, used 6B. 4 of the tests got within 14 cm of static conditions, others exceeded 19 cm and were excluded.
10	A_9.0	8/11/2020	17:07	2b,3b,4b,5b,7a	Reran, used tests from both series
11	A_12	8/11/2020	17:08	13567	All tests had returns under 1cm
12	A_25	8/15/2020	17:17	24567	All tests had returns under 1cm
13	A_50.0	8/11/2020	10:33	23567	Reran, used b for analysis
14	A_100.0	8/11/2020	10:34	23456	Reran, used b for analysis
15	A_1000	8/19/2020	19:19	23457	All tests had returns under 1cm
16	A_200.0	7/27/2020	18:34	23456	This location/value is shared with I_0.0
17	B_-250	8/9/2020	12:07	123	3 of the tests got within 2.77 cm of static conditions, others exceeded 10 cm and were excluded.
18	B_100	8/9/2020	11:10	34567	All used tests had returns at 0.5cm or lower.
19	B_0.0	8/9/2020	11:46	23456	All used tests had returns at 3.7 cm or lower.

OID	Name	Date	Time	Tests Used	Processing Notes
20	B_0.5	8/9/2020	11:54	23567	All used tests had returns at 3 cm or lower.
21	B_1.0	8/9/2020	13:08	12356	All used tests had returns at 2.6 cm or lower.
22	B_1.5	8/9/2020	13:15	12345	All used tests had returns at 1.8 cm or lower.
23	B_2.0	8/9/2020	13:20	24567	All used tests had returns at 1.6 cm or lower.
24	B_3.0	8/9/2020	14:08	23456	All used tests had returns at 3.2 cm or lower.
25	B_6.0	8/9/2020	14:14	3456	All used tests had returns at 1.8 cm or lower.
26	B_9.0	8/9/2020	14:22	12345	All used tests had returns at 1.35 cm or lower.
27	B_12	8/9/2020	15:12	12456	All used tests had returns at 4.1 cm or lower.
28	B_25	8/9/2020	15:21	13567	All used tests had returns at 5.7 cm or lower.
29	B_50	8/9/2020	15:30	1235	All used tests had returns at 5.7 cm or lower.
30	B_100	8/9/2020	16:23	23456	These wells are shared with the A series

OID	Name	Date	Time	Tests Used	Processing Notes
31	B_1000	8/19/2020	19:19	23457	4tests came in under 1 cm of full recovery, others excluded.
32	B_Spring	8/9/2020	16:07	23456	All used tests had returns at 4.8 cm or lower.
33	C_0.0	6/15/2020	18:13	1235	All tests came within 1.3 cm
34	C_0.5	6/15/2020	18:16	3457	All tests came within 4.5 cm
35	C_1.0	6/15/2020	18:16	1245	Only 2 tests came within 5cm of static conditions
36	C_1.5	6/15/2020	21:47	1256	All tests came within .6 cm
37	C_2.0	6/15/2020	21:30	123	All tests came within .5 cm
38	C_3.0	6/15/2020	21:33	12345	All tests came within .6 cm
39	C_6.0	6/15/2020	21:53	34567	All tests came within .6 cm
40	C_9.0	6/15/2020	22:33	1236	All tests came within 1 cm
41	C_12	6/15/2020	22:53	345	Only four tests were usable but all came within 1.5 cm so I used them all
42	C_25	6/15/2020	15:45	34567	All tests came within 1 cm
43	C_50	6/15/2020	16:40	125	Only 3 tests came within 1.2 cm of full recovery, all others exceeded 1.3 cm and were excluded from analysis
44	C_100	6/15/2020	16:48	13456	All tests came within 3.63 cm

OID	Name	Date	Time	Tests Used	Processing Notes
45	C_1000	6/19/2020	19:54	1234	All tests came within 1cm of full recovery
46	C_2000	8/1/2020	19:04	12345	This location/value is shared with CD2_0.0
47	D_0.0	7/17/2020	11:41	12	2 tests came within 3 cm of full recovery, all others excluded from analysis
48	D_0.5	7/17/2020	11:53	34	2 tests came within 1.7 cm of full recovery, all others excluded from analysis
49	D_1.0	7/17/2020	12:45	15	2 tests came within 1.7 cm of full recovery, all others exceeded 5 cm and were excluded from analysis
50	D_1.5	7/17/2020	13:22	345	3 tests came within 1.7 cm of full recovery, all others exceeded 10 cm and were excluded from analysis
51	D_2.0	7/17/2020	14:31	57	2 tests came within 2 cm of full recovery, all others exceeded 5cm and were excluded from analysis
52	D_3.0	7/17/2020	14:36	1236	4 tests came within 5 cm of full recovery, all others exceeded 4 cm and were excluded from analysis

OID	Name	Date	Time	Tests Used	Processing Notes
53	D_6.0	7/17/2020	14:42	1235	All 4 had returns under 1cm
54	D_9.0	7/17/2020	15:41	3467	4 tests came within 2 cm of full recovery, all others exceeded 4 cm and were excluded
55	D_12	7/17/2020	15:50	36	Had to return to location to rerun this site. 2 tests came within 0.19 cm of full recovery, all others exceeded 2.14 cm and were excluded from analysis
56	D_25	7/17/2020	21:34	12345	Reran, All tests in group b came within 3.62 cm
57	D_50	7/17/2020	17:24	1234	4 tests came within 2.5 cm of full recovery, all others exceeded 4 cm and were excluded from analysis
58	D_100	7/17/2020	17:15	123456	All 6 had returns under 2cm
59	D _ 1000	7/25/2020	13:13	12345	All 5 had returns under 2cm
60	D2_0.0	8/1/2020	19:04	1235	All used tests came within 1.3 cm
61	D.2_0.5	8/1/2020	18:35	3457	All used tests came within 4.5 cm
62	D.2_1.0	8/1/2020	18:43	1245	All used tests came within 2.5 cm of static conditions
63	D.2_1.5	8/1/2020	18:52	1256	All tests came within .6 cm
64	D.2_2.0	8/1/2020	14:52	123	All tests came within .5 cm

OID	Name	Date	Time	Tests Used	Processing Notes
65	D.2_3.0	8/1/2020	15:38	12345	All tests came within .6 cm
66	D.2_6.0	8/1/2020	19:23	34567	All tests came within .6 cm
67	D.2_9.0	8/1/2020	19:36	1236	All tests came within 1 cm
68	D.2_12	8/1/2020	19:45	1345	Only four tests were usable but all came within 1.5 cm so I used them all
69	D.2_25	8/1/2020	19:52	34567	All tests came within 1 cm
70	D.2_50	8/1/2020	15:55	125	Only 3 tests came within 1.2 cm of full recovery, all others exceeded 1.3 cm and were excluded from analysis
71	D.2_100	8/1/2020	16:11	13456	All tests came within 3.63
72	D.2_1000	8/1/2020	18:11	1234	All tests came within 1cm of full recovery
73	D.2_2000	9/20/2020	10:30	12345	This location/value is shared with CD3_0.0
74	D.3_0.5	9/20/2020	10:29	1234	All four tests came within 3.2cm of full recovery
75	D.3_1.0	9/20/2020	10:39	12345	All 5 tests came within 3.2cm of full recovery
76	D.3_1.5	9/20/2020	10:38	256	3 tests came within 3.5 cm of full recovery, all others exceeded 3.5

OID	Name	Date	Time	Tests Used	Processing Notes
					cm and were excluded from analysis
77	D.3_2.0	9/20/2020	10:46	23	2 tests came in under 10cm, others were excluded.
78	D.3_3.0	9/20/2020	10:47	12567	All 5 tests came within 3.2cm of full recovery
79	D.3_6.0	9/20/2020	10:50	12	2 tests came within 2cm all others were over 5cm and were excluded from analysis.
80	D.3_9.0	9/20/2020	10:53	12347	All tests within 1.5 cm
81	D.3_12	9/20/2020	11:04	3456	4 tests came in under 1 cm of full recovery, others excluded.
82	D.3_25	9/20/2020	11:06	12345	All 5 tests came within 1.2cm of full recovery
83	D.3_50	9/20/2020	11:34	12345	All 5 tests came within 2.6cm of full recovery
84	D.3_100	10/10/2020	11:36	12345	All 5 tests came within 0.7cm of full recovery
85	D.3_1000	11/1/2020	16:18	345	3 tests came within 4.5 cm of full recovery, all others exceeded 4.5 cm and were excluded from analysis

OID	Name	Date	Time	Tests Used	Processing Notes
86	D.3_2000	11/1/2020	16:20	1345	4 tests came within 1.78 cm
87	E_0.0	7/16/2020	12:46	12456	All tests came within 1.88 cm of full returns. All others excluded.
88	E_0.5	7/16/2020	12:59	12356	All tests came within 2.58 cm of full returns.
89	E_1.0	7/16/2020	13:38	1236	All tests came within 5.01 cm of full returns.
90	E_1.5	7/16/2020	16:25	1245	All tests came within 2.37 cm of full returns.
91	E_2.0	7/16/2020	11:06	1234	All tests came within 2.68 cm of full returns.
92	E_3.0	7/16/2020	11:39	1345	All tests came within 1.5 cm of full returns.
93	E_6.0	7/16/2020	11:40	2345	All tests came within 2.25cm of full returns.
94	E_9.0	7/16/2020	13:22	1234	Four tests came within 1.96 cm, all others excluded.
95	E_12	7/16/2020	14:57	12345	All tests came within 2.6. Others excluded
96	E_25	7/16/2020	14:47	124	Three tests came below 6.1cm of full return. Others exceeded 10 cm and were excluded.

OID	Name	Date	Time	Tests Used	Processing Notes
97	E_50	7/16/2020	12:16	2346	Four tests came below 3.5cm of full return. Others exceeded 10 cm and were excluded.
98	E_100	7/16/2020	12:25	1234	Four tests came within 2.88 cm, all others excluded.
99	E_1000	7/16/2020	12:44	1256	Four tests came within 2.88 cm, all others excluded.
100	E_2000	8/1/2020	17:30	156	Three tests came below 1.5cm of full return. Others excluded.
101	F_0.0	7/29/2020	13:43	12467	All tests came within 1 cm of full return.
102	F_0.5	7/29/2020	13:41	12356	All tests came within 1.5. All others exceeded 1.5 and were excluded.
103	F_1.0	7/29/2020	13:38	12345	All tests came within 5.1cm. All others were excluded
104	F_1.5	7/29/2020	13:21	23456	All used tests came within 1cm. All others were excluded
105	F_2.0	7/29/2020	15:02	12345	All tests used came within 1.16 cm of full return
106	F_3.0	7/29/2020	15:10	12356	All tests used came within 1.18 cm of full return

OID	Name	Date	Time	Tests Used	Processing Notes
107	F_6.0	7/29/2020	14:40	34567	All tests used came within 1.46 cm of full return
108	F_9.0	7/29/2020	13:34	34	Two tests ran properly. Both came in under 2 cm
109	F_12	7/29/2020	13:01	234	Three tests came in under 6.9cm of full return. Others exceeded 8cm and were excluded from analysis.
110	F_25	7/29/2020	12:41	23456	All tests came in under 1 cm of fully retarded. Others exceeded 5 cm and thus were excluded.
111	F_50	7/29/2020	12:20	34567	All tests came in under 1 cm of being fully returned. Others exceeded 5 cm and thus were excluded.
112	F_100	7/29/2020	12:07	12345	All tests came in under 2 cm of being fully returned.
113	F_1000	7/29/2020	17:23	23457	All tests used came within 4.03 cm of full return
114	F_2000	7/29/2020	17:00	12345	All tests used came within 4.03 cm of full return

OID	Name	Date	Time	Tests Used	Processing Notes
115	G_0.0	9/20/2020	12:12	23456	All tests within 8 cm of full return but only used those that came in under 3.4 cm.
116	G_0.5	9/20/2020	12:17	14567	All tests within 5 cm of full return but only used those that came in under 3.5 cm.
117	G_1.0	9/20/2020	12:22	12357	All tests within 7 cm of full return but only used those that came in under 5 cm.
118	G_1.5	9/20/2020	12:34	234	All used tests within 2.46 cm but only used those that came back under 2.12 cm
119	G_2.0	9/20/2020	12:58	2345	All used tests came within 4.6 cm of full returns. Used tests under 4.5cm
120	G_3.0	9/20/2020	13:26	12345	All tests came within 2.68 cm of full returns. Used tests under 4.5cm
121	G_6.0	9/20/2020	15:20	234	3 tests came within .78 cm of full returns. Used tests under 3.1 cm

OID	Name	Date	Time	Tests Used	Processing Notes
122	G_9.0	9/20/2020	15:44	12345	All tests within 3.4 cm but only used those that came back under .31
123	G_12	9/20/2020	15:29	2345	All used tests within 2.54 cm
124	G_25	9/20/2020	16:02	12345	All tests within 1.02 cm
125	G_50	9/20/2020	16:03	12456	All tests within 1.15 cm
126	G_100	9/20/2020	16:12	34567	All tests within 2.24 cm
127	G_1000	9/20/2020	13:35	13456	All used test came within 2.25 cm of full recovery.
128	G_2000	9/20/2020	18:11	13467	All tests within .75 cm of full return but only used those that came in under 6.
129	H_0.0	8/22/2020	11:49	1234	Four tests came within 1.24 cm, all others excluded.
130	H_0.5	8/22/2020	10:50	1234	Four tests Came within 2.6 cm , all others excluded.
131	H_1.0	8/22/2020	11:00	12	Two tests came within 2.1 cm, all others excluded.
132	H_1.5	8/22/2020	11:26	1257	Four tests came within 2.88 cm, all others excluded.
133	H_2.0	8/22/2020	12:01	125	Three tests had returns at 3cm or lower.

OID	Name	Date	Time	Tests Used	Processing Notes
134	H_3.0	8/22/2020	12:08	13456	All tests came within 1.8 cm, all others excluded.
135	H_6.0	8/22/2020	12:30	136	Three tests came within 2.9 cm, all others excluded.
136	H_9.0	8/22/2020	13:41	1234	Two tests came in under 16cm and others were above 32cm but I still used them. This site's Ksat estimate is therefore less certain.
137	H_12	8/22/2020	13:34	1235	Four tests came within 2.88 cm, all others excluded.
138	H_25	8/22/2020	13:44	345	Three tests had returns at 1.2cm or lower. Others exceeded 3.5 cm and were excluded
139	H_50	8/22/2020	13:56	12346	All tests came within 1.8 cm from the static conditions, others excluded from analysis.
140	H_100	8/22/2020	14:49	124	Three tests had returns at 2.3cm or lower. Others exceeded 7.2 cm and were excluded
141	H_1000	10-0ct-20	14:53	34567	All tests Came within 1.8 cm, all others excluded.

OID	Name	Date	Time	Tests Used	Processing Notes
142	H_2000	10-0ct-20	15:12	1245	Four tests came within 1.5 cm of full return, others excluded.
143	H.2_0.5	10-0ct-20	9:11	123	Three tests came within 5 cm of full return, others excluded.
144	H.2_1.0	10-0ct-20	9:15	23456	All used tests came in under 1.5 cm of full return to static conditions.
145	H.2_1.5	10-0ct-20	9:16	23456	All used tests came in under 1.3 cm of full return to static conditions.
146	H.2_2.0	10-0ct-20	9:22	23456	All used tests came in under 10 cm of full return to static conditions.
147	H.2_3.0	10-0ct-20	9:22	34567	All used tests came in under 10 cm of full return to static conditions.
148	H.2_6.0	10-0ct-20	9:54	12456	All tests came within .7 cm of full returns.
149	H.2_9.0	10-0ct-20	9:28	12345	All tests came within 1 cm of full returns.
150	H.2_12	10-0ct-20	9:52	23456	All tests came within .6 cm of full returns.
151	H.2_25	10-0ct-20	9:55	12356	All tests came within .8 cm of full returns.
152	H.2_50	10-0ct-20	10:02	12345	All tests came within 2 cm of full returns.

OID	Name	Date	Time	Tests Used	Processing Notes
153	H.2_100	10-0ct-20	10:07	12456	All tests came within .7 cm of full returns.
154	H.2_1000	10-0ct-20	13:13	12346	All tests came within 1.25 cm of full returns.
155	H.2_2000	11/1/2020	4:56	12345	All tests came within 1.25 cm of full returns.
156	I_0.0	9/20/2020	4:41	23456	All used tests came in under .7 cm of full returns
157	I_0.5	9/20/2020	4:46	23456	All used tests came in under .5 cm of full returns
158	I_1.0	9/20/2020	4:51	12345	All used tests came in under 5 cm of full returns
159	I_1.5	9/20/2020	4:59	2345	All used tests came in under 5 cm of full returns
160	I_2.0	9/20/2020	5:15	12345	All used tests came in under 7.4cm of full returns
161	I_3.0	9/20/2020	5:19	1234	All used tests came in under 1 cm of full return.
162	I_6.0	9/20/2020	5:24	12345	All used tests came in under 2.9cm of full returns
163	I_9.0	9/20/2020	5:29	12345	All used tests came in under .9 cm of full returns

OID	Name	Date	Time	Tests Used	Processing Notes
164	I_12	9/20/2020	5:34	1234	All used tests came in under .9 cm of full returns
165	I_25	9/20/2020	5:39	13456	All used tests came in under 1.56 cm of full returns
166	I_50	9/20/2020	5:45	12345	All used tests came in under 1.56 cm of full returns
167	I_100	9/20/2020	5:51	1345	All used tests came in under .9 cm of full returns
168	J_0.0	9/28/2020	15:17	13456	All used tests came in under 1.9 cm of static conditions.
169	J_0.5	9/28/2020	15:13	23456	All used tests came in under 8 cm of static conditions.
170	J_1.0	9/28/2020	15:18	2345	All used tests came in under 1.3 cm of static conditions.
171	J_1.5	9/28/2020	15:21	1234	All used tests came in under 4.2 cm of static conditions.
172	J_2.0	9/28/2020	15:27	12345	All used tests came in under 1.47 cm of static conditions.
173	J_3.0	9/28/2020	15:34	1234	All used tests came in under .8 cm of static conditions.
174	J_6.0	9/28/2020	15:40	1234	All used tests came in under .7 cm of static conditions.

OID	Name	Date	Time	Tests Used	Processing Notes
175	J_9.0	9/28/2020	15:38	12345	All used tests came in under 8 cm of static conditions.
176	J_12	9/28/2020	15:58	13456	All used tests came in under .51 cm of static conditions.
177	J_25	9/28/2020	16:07	1245	All used tests came in under 2.9 cm of static conditions.
178	J_50	9/28/2020	16:12	12345	All used tests came in under 7.8 cm of static conditions.
179	J_100	9/28/2020	16:18	1234	All used tests came in under 1.17 cm of static conditions.
180	IJ_1000	9/28/2020	13:34	1235	All used tests came in under 1.17 cm of static conditions.
181	IJ_2000	11/1/2020	14:08	3456	All used tests came in under 1.4 cm of static conditions. Did not have weather conditions for this time period so I used 79 KPa as the default.
182	IJ.2_0.5	11/1/2020	14:35	12467	All used tests came in under 1cm of static conditions. Did not have weather conditions for this time period so I used 79 KPa as the default.

OID	Name	Date	Time	Tests Used	Processing Notes
183	IJ.2_1.0	11/1/2020	14:52	456	All used tests came in under 1.4cm of static conditions. Did not have weather conditions for this time period so I used 79 KPa as the default.
184	IJ.2_1.5	11/1/2020	15:02	234	All used tests came in under 2.7 cm of static conditions. Did not have weather conditions for this time period so I used 79 KPa as the default.
185	IJ.2_2.0	11/1/2020	15:04	12356	All used tests came in under 2cm of static conditions. Did not have weather conditions for this time period so I used 79 KPa as the defaults.
186	IJ.2_3.0	11/1/2020	15:07	12345	All used tests came in under 1.4 cm of static conditions. Did not have weather conditions for this time period so I used 79 KPa as the default.
187	IJ.2_6.0	11/1/2020	15:11	123	All used tests came in under 1.19 cm of static conditions. Did not

OID	Name	Date	Time	Tests Used	Processing Notes
					have weather conditions for this time period so I used 79 KPa as the default.
188	IJ.2_9.0	11/1/2020	15:15	1234	All used tests came in under 1 cm of static conditions. Did not have weather conditions for this time period so I used 79 KPa as the default.
189	IJ.2_12	11/1/2020	15:28	23456	All used tests came in <1 cm of static conditions. Did not have weather conditions for this time period so I used 79 KPa as the default.
190	IJ.2_25	11/1/2020	15:29	234	All used tests came in <2 cm of static conditions. Did not have weather conditions for this time period so I used 79 KPa as the default.
191	IJ.2_50	11/1/2020	15:37	12345	All used tests came in <1 cm of static conditions. Did not have weather conditions for this time

OID	Name	Date	Time	Tests Used	Processing Notes
					period so I used 79 KPa as the default.
192	IJ.2_100	11/1/2020	15:41	1234	All used tests came in <1 cm of static conditions. Did not have weather conditions for this time period so I used 79 KPa as the default.
193	IJ.2_1000	11/1/2020	15:43	123	All used tests came in under .5 cm of static conditions. Did not have weather conditions for this time period so I used 79 KPa as the default.
194	IJ.2_2000	11/1/2020	14:13	12345	All used tests came in under 1 cm of static conditions. Did not have weather conditions for this time period so I used 79 KPa as the default.

Appendix 16: Brief geologic description of lithologic units found within the study area modified from Rodgers and Othberg (1999).

Map Unit	Name	Age	Description
Qal	Alluvium	Quaternary	Alluvium
Qfg	Fan Gravels	Quaternary	Crudely stratified silty-sand and pebble-to-boulder gravel that is likely of Wisconsin and pre-Wisconsin age.
Ql/Qfgw	Loess Mantled Fan Gravel	Quaternary	Quaternary fan gravels underlying thick packages of Quaternary loess
Qlb	Loess-Mantled Bedrock	Quaternary	Loess-mantled bedrock
Qls	Landslide Deposit	Quaternary	Unstratified landslide deposits.
€b	Bloomington Formation	Middle Cambrian	Thin to thick beds of light to blue-grey limestone with tan silt laminations interbedded by green shales and a quartz arenite sandstone.
€e	Elkhead Limestone	Middle Cambrian	This unit is distinguished by thick-bedded to massive light-to-medium-grey limestone that is devoid of siliciclastic detritus
€g	Gibson Jack Formation	Lower Cambrian	This unit is characterized by olive-green shales/siltstones and thin to medium bedded quartz arenite

Map Unit	Name	Age	Description
€Zc	Camelback Mountain Quartzite	Lower Cambrian/ Late-Proterozoic	Described as a white-to-tan or light grey thick-bedded quartzite underlain by a distinguishable basal conglomerate that contains red chert and red siltstone pebbles. The protolith is described as being a quartz arenite.
Zm	Mutual Formation	Late Proterozoic	Medium to thick-bedded, pink to dark red quartzite and pebble conglomerate with abundant cross-stratification with an interbedded maroon shale/siltstone unit. Protolith is described as being a subarkosic to sublithic arenite.
Zi	Inkom Formation	Late-Proterozoic	Laminated to thinly bedded olive green slate and phyllite with a maroon upper unit comprised of interbedded slates and quartzite.
Zcu	Caddy Canyon Quartzite, Upper Member	Late Proterozoic	Described as being a thick-bedded-to-massive pink-to-purple quartzite that lacks abundant cross-stratification. The protolith is described as being a subarkosic to sublithic arenite.

Appendix 17: Lessons Learned: Informal Advice to Future Graduate Students

"The key to everything is that everything is chopping wood and carrying water, and that if one does everything mindfully, then it is all the same."

-Buddha-

Dear future graduate student, welcome to the department (Go Bengals!!!) and to Dr. Godsey's hydro/sed lab. I hope the following will help to ease your transition into your program. Your story will differ from mine as my path to graduate success was rather bumpy. I'd like to think that you are not reading this during quarantine and that you're not stressing about the wildfire in your study area burning your cache of field gear. However, if you do experience any of these things, or other similar scenarios, take faith in the fact that nobody expects this adventure you're about to undertake to be easy and that your advisor and department care deeply about your success.

Not Just Grad School, but Life in General:

"If you're going through hell, keep going."

-Winston Churchill-

You will consistently be busier than you have likely ever been, and that's a good thing; this is, after all, graduate school. Expect to quickly identify your thresholds and have them constantly pushed, especially your first year. Work ahead and learn to anticipate your advisors' expectations. Immerse yourself in the literature early on and keep an ongoing annotated bibliography that is up to the standards outlined in Geology 6603. Schedule reading time each week, participate in reading groups and learn to contribute to weekly discussions, even when a paper doesn't seem to apply directly to your specific research. You never know what life will throw at you, and there may be times when you need to shift focus to personal matters, but remember that resilience is also a key component to being a successful graduate student.

Take Breaks and Seek Balance:

"Balance is not something you find; it is something you create."

-Jana Kingsford-

Maintaining balance is essential, as one of the biggest problems I faced during my graduate studies was the lack of work-life balance. I sometimes would push until I couldn't anymore and would subsequently burn out and crash. Please make sure you schedule the time to do the things you love and to hang out with friends. Unfortunately, most of my MS was performed under quarantine conditions, and the feeling of isolation was ever-present. On that note, make friends in the department and go to campus/departmental events, so you can still feel as though you have a social life, even when you likely do not.

Campus and Community Resources/ Service to Others:

"We make a living by what we get but make a life by what we give."

-Winston Churchill-

This one took me a while to get started, but you should know from the beginning that ISU has done an excellent job of creating on-campus support for various purposes. For starters, the Counseling and Testing Program (CATS) offers free counseling and student support services. Furthermore, there is a free and no-questions-asked food pantry (Bennie's Pantry) in the basement of the Student Union Building. This latter program will help you financially as you navigate graduate school.

Also, don't be afraid to give back when you can and are able. You may, like me, find yourself needing help, and this may cause feelings of low self-worth. Maybe you care tremendously about the environment or others. Not only is your advisor keen on the concept of service, but many in the department are as well. I found myself striving to give back (sit on the bench that I installed next to the Animal Sciences building and think on this), and at times, I found service to others and my community rewarding and great for mental health. Please remember why we do service projects and do not expect to receive much (if any) recognition. Please do it for yourself, your community, and the environment; your service will be reward enough.

Philosophy and Funding:

It is true that much time and effort is devoted to training and equipping the scientist's mind, but little attention is paid to the techniques of making the best use of it.

-W. I. B. Beveridge-

Before you even think about where your work will fit in with ongoing research, you should read *To Interpret the Earth: Ten Ways to Be Wrong* (Schumm, 1991). Furthermore, consider taking Dr. Baxter's Philosophy of Science course: it was a surprisingly enlightening class that reshaped my perspective on the scientific process. The insight I gleaned from these two sources allowed me to see that ego and science do not mix well and that being wrong and making mistakes is part of the learning process, both in science and in life. Furthermore, finding funding is a critical part of the process, so take it upon yourself to apply to every grant you can think of. GSA and AEG both offer graduate research grants, and you absolutely must apply for the departmental Geslin research and the ISU CERE grant. Also, I recommend activating the email settings for BOSS (Bengal Online Scholarship System) to notify you of upcoming scholarship opportunities/deadlines. Be sure to save your applications in a separate folder on your hard drive, as you will be able to reuse much of your previous applications for future grants and scholarships.

Field Work:

"A heavy pack is better than a heavy heart."

I don't know where you're originally from, but you're Rocky Mountain now: take this opportunity to dive into fieldwork and genuinely get to know your study area. Seriously, just because you are in a Geosciences department doesn't mean you can't learn to identify flora and fauna as well. My field season coincided with some rough times, and I treated my study area like a monastery, and I will forever be grateful for the time I spent in the Gibson Jack watershed. I hope you will soon feel the same way about your site—test gear before going out. If something looks like it may be close to its life expectancy, then figure out a replacement before it breaks. That said, make sure you have reserve funding to replace broken lab gear. Any funding you get should include replacement gear funds as you will likely break/damage gear, and it is unfair to past, current, and future lab mates as we all either needed this gear or will need it for our research, and it is not just up to Doc G to find you a replacement. Not only will fieldwork take longer than expected, but basically everything else will as well. Plan for this, especially in the field where you will be counted on to keep working even when exhausted. Plan extra days so that you are not constantly behind and try hard to work ahead. Communicate your research/field plans and locations with your advisor, and never head into the wilds alone unless someone knows where you will be working that day and when to expect your safe return.

First Aid/Wilderness Safety:

"Aim above morality. Be not simply good, be good for something."

-Henry David Thoreau-

I am frequently surprised by the lack of preparation on behalf of colleagues and friends when heading into the bush, and sometimes, we happen to forget things when heading into the backcountry. Make sure your first aid kit contains (at least!) an ACE Bandage, absorbent pads, pain relievers, a whistle, and a lighter. Take a wilderness first aid course or at least watch some videos before going out into the field. Also, consider keeping emergency food such as a Cliff Bar or other granola-type snacks. Furthermore, always carry foul weather gear when in the backcountry. These are the Idaho Rockies, and weather will quickly change and often unexpectedly. Even seasoned outdoors people get caught by surprise in this regard, and more than once, I had to hustle to the parking lot because I was utterly saturated with springtime rain and shivering. To emphasize this fact, on June 11th, 2020, it was 67 degrees in Gibson Jack before temps dropped to around freezing, and it began to snow. Remember this for you and plan on potentially being a first responder for others while venturing into the bush.

Wildlife and Music:

I hope this header gave you a mental image of me cutting loose with some sweet Michael Jackson dance moves in a dance-off with a skunk, black bear, and a moose. Sadly, this never happened, but I spent a lot of time solo in my study area, and believe it or not, there were wild animals that did not appreciate my presence, especially when startled. I was charged by a moose and had to dodge skunk spray similarly to that scene in the Matrix. I later found these scenarios to be easily avoidable by announcing my presence to the wilds with the sweet serenades that issue forth from my bluetooth speaker. Seriously, expect to encounter wildlife in your study area, even in places as heavily visited as Gibson Jack.

Data Management:

"No data, no degree."

I don't need to explain the importance of processing data daily and backing it up in multiple locations, but even as I was working on draft four of this chapter, my computer crashed, and I lost half a day's work because I didn't save that morning. Worse yet, I knew a person who lost two years of course/fieldwork because she only had her data saved in one place! Think about this and how horrible it would be to put the next two years into your research only to lose everything because you did not back it up. Update figures and tables as you go, save documents frequently and keep your files organized enough that others will be able to find your data if the need arises (your advisor expects this).

Playing Well With Others:

"No act of kindness, no matter how small, is ever wasted."

–Aesop-

Be an ambassador for yourself, your science, your lab, and the university, not only on campus but in the field as well. Take the time to learn to describe what you are doing to a curious layperson that you may come across. Try to maintain a simple level of grooming even during your extended excursions into the bush. I met many people during my field campaign, and many of them had direct relationships with the university and our advisor. During the ensuing conversations, I would remain as professional as possible as I realized quickly that, even in the backcountry, my actions and demeanor represent my university, department, and lab. This also extends to on-campus relations as you may find yourself in a position where you need to collaborate with someone you don't necessarily click with or don't know well. I encourage you to these opportunities to expand the demographics of your social circle and make new friends.

Lastly,

May your trails be crooked, winding, lonesome, leading to the most amazing view. May your mountains rise into and above the clouds.

-Edward Abbey-

Enjoy the time you have here; it will be over quicker than you think.